

**A THEORETICAL STUDY OF FRACTURE OF
PIEZOELECTRIC SOLIDS**

by

Steven Xilin Xu

A Thesis
submitted to the Faculty of Graduate Studies
in partial fulfillment of the requirements
for the Degree of

DOCTOR OF PHILOSOPHY

Department of Civil & Geological Engineering
University of Manitoba

© March, 2001



**National Library
of Canada**

**Acquisitions and
Bibliographic Services**

395 Wellington Street
Ottawa ON K1A 0N4
Canada

**Bibliothèque nationale
du Canada**

**Acquisitions et
services bibliographiques**

395, rue Wellington
Ottawa ON K1A 0N4
Canada

Your file Votre référence

Our file Notre référence

The author has granted a non-exclusive licence allowing the National Library of Canada to reproduce, loan, distribute or sell copies of this thesis in microform, paper or electronic formats.

The author retains ownership of the copyright in this thesis. Neither the thesis nor substantial extracts from it may be printed or otherwise reproduced without the author's permission.

L'auteur a accordé une licence non exclusive permettant à la Bibliothèque nationale du Canada de reproduire, prêter, distribuer ou vendre des copies de cette thèse sous la forme de microfiche/film, de reproduction sur papier ou sur format électronique.

L'auteur conserve la propriété du droit d'auteur qui protège cette thèse. Ni la thèse ni des extraits substantiels de celle-ci ne doivent être imprimés ou autrement reproduits sans son autorisation.

0-612-57517-9

Canada

**THE UNIVERSITY OF MANITOBA
FACULTY OF GRADUATE STUDIES

COPYRIGHT PERMISSION PAGE**

A Theoretical Study of Fracture of Piezoelectric Solids

BY

Steven Xilin Xu

**A Thesis/Practicum submitted to the Faculty of Graduate Studies of The University
of Manitoba in partial fulfillment of the requirements of the degree
of
Doctor of Philosophy**

STEVEN XILIN XU © 2001

Permission has been granted to the Library of The University of Manitoba to lend or sell copies of this thesis/practicum, to the National Library of Canada to microfilm this thesis/practicum and to lend or sell copies of the film, and to Dissertations Abstracts International to publish an abstract of this thesis/practicum.

The author reserves other publication rights, and neither this thesis/practicum nor extensive extracts from it may be printed or otherwise reproduced without the author's written permission.

Abstract

The emerging technologies of smart materials and structures have found increasing applications in diverse branches of engineering such as civil, aerospace, mechanical, and manufacturing engineering. Piezoelectric materials are ideal candidates for functional (smart) materials, and have been a primary focus of attention in the realization of smart (adaptive) structure systems. The use of piezoelectric materials, however, carries a price, due to the fact that piezoelectric materials are very brittle and susceptible to fracture. The future development of adaptive structures strongly depends on better understanding of the fracture mechanism of piezoelectric materials. Therefore, this thesis presents a theoretical study of fracture mechanics of piezoelectric materials. Based on the literature review, a selected set of basic problems related to linear fracture mechanics of plane piezoelectric media are examined.

A comprehensive study of a plane piezoelectric medium with an arbitrarily oriented elliptical void and a straight crack is presented first. A set of complete analytical solutions for electroelastic fields around the void and at the crack tip are derived for different types of electric boundary conditions. It is found that solutions based on the special cases of defect orientation, *i.e.* defects parallel or perpendicular to the poling direction, cannot be always considered as the critical case. A significant influence of crack orientation on the stress distribution at crack-tip is observed when a crack is under electrical loading or combined loading with larger electric to mechanical load ratio. The influence of an applied electric displacement normal to an impermeable crack is analogous to that of an applied electric field tangential to a conducting crack. It is shown that the Hao and Shen type electric boundary conditions reduce to impermeable or permeable boundary conditions under practical situations. A recently reported solution for exact boundary conditions is actually the previously known solution for a permeable crack.

The branched cracks are then studied as the logical extension of straight cracks. It is found that branch closure happens for certain cases of branch length, branch angle and

loading condition. The ranges of branch angles within which a branch is open are much larger for mechanical loading than for electric loading. It is shown that the asymptotic electroelastic fields at a branch tip have complex dependence on branch length, branch angle, crack orientation and the type of loading. The influence of applied electric loading is found to be more complicated and significant than mechanical loading. Numerical results indicate that asymmetrically branched crack will not simultaneously grow under remote tension.

The issue of fracture criteria is examined next. A new stress-based criterion and two energy-based criteria are proposed to predict crack propagation in piezoelectrics. The salient features of proposed criteria are the consideration of fracture toughness anisotropy and the removal of self-similar crack extension assumption. It is shown that distinctly different propagation directions are predicted if isotropic fracture toughness is used. The criteria of modified hoop stress intensity factor and modified strain energy release rate suggest that, even in a symmetric case (loading and geometry), a crack may branch off from a straight path, which qualitatively agrees with available experimental findings.

Finally, a general method of obtaining electroelastic singularities in piezoelectric wedges and composite piezoelectric wedges/junctions is successfully developed as a precursor to the study of fracture of multi-material systems. It is found that electric boundary conditions have a significant effect on the order of singularities for piezoelectric wedges. The singularities of piezoelectric half planes and semi-infinite cracks are found to be invariant with respect to the direction of polarization. Bi-material systems of two piezoelectrics have stronger singularities when compared to piezoelectric - conductor/composite systems. The presence of a crack or a debonded interface results in a higher order singularity for two and three material systems.

Acknowledgments

First and foremost, the author wishes to express his profound gratitude to his advisor, Professor R.K.N.D. Rajapakse. Throughout the course of this thesis work, Professor Rajapakse provided the author with invaluable guidance and advise. The author is also indebted to Professor Rajapakse for providing financial support through a NSERC research grant and listening to his personal concerns.

Grateful acknowledgments are conveyed to Professor A.H. Shah and Professor R. Jayaraman for serving on the thesis advisory committee. Sincere thanks are conveyed to Professor E. Lajtai for being on the examining committee. Special thanks are conveyed to Professor D. Gross (TH Darmstadt, Germany) for devoting his time to serve as the external examiner. Their valuable comments and suggestions are greatly appreciated.

The University of Manitoba Graduate Fellowship, Gordon P. Osler Graduate Scholarship, Edward R. Toporeck Graduate Fellowship and UMSU Scholarship awarded through the University of Manitoba are acknowledged.

Similar to all other working environments, higher education provides the opportunity to make friends and learn from colleagues, professional staff, and other acquaintance. The author benefited and learnt from: Dr. R. Chandrakeerthy, Dr. D. Chen, Mr. M. Hagos, Ms. S. Morris, Ms. L. Parsons, Ms. B. Phillips, Mr. B. Robert, Dr. D. Schonwetter, Mr. X. Zeng, Dr. Y. Zhou, Dr. W. Zhuang. The author looks forward to a lifelong friendship with them.

Last but not the least, the author wishes to express his gratitude to his parents and his wife for their understanding, encouragement and support during the course of his Ph.D program.

Contents

Abstract	ii
Acknowledgments	iv
List of Tables	viii
List of Figures	ix
List of Symbols	xii
1 Introduction	1
1.1 General	1
1.2 Literature review	3
1.3 Objectives and scope	8
2 Arbitrarily Oriented Voids and Straight Cracks	9
2.1 Infinite Plane with an Elliptical Void	9
2.1.1 Basic equations	9
2.1.2 Impermeable void	13
2.1.3 Permeable void	14
2.2 Impermeable crack	17
2.3 Conducting crack	20
2.4 Other crack boundary conditions	22
2.5 Numerical results and discussion	27
2.5.1 Electroelastic fields around a void	27
2.5.2 Impermeable crack	31
2.5.3 Conducting crack	36
2.5.4 Hao and Shen type crack	38

2.6	Conclusions	46
3	Branched Cracks	48
3.1	Dislocation modeling	48
3.2	Branched crack	52
3.3	Bifurcated crack	57
3.4	Numerical results and discussion	61
3.4.1	A branched crack	61
3.4.2	A bifurcated crack	70
3.5	Conclusion	74
4	Fracture Criteria	78
4.1	Fracture toughness anisotropy	78
4.2	A stress-based criterion	80
4.3	Angular distribution of energy release rates	84
4.4	Energy-based criteria	88
4.5	Conclusion	92
5	Singularities in Piezoelectric Wedges	98
5.1	Governing equations	98
5.2	Characteristic equations	101
5.2.1	Piezoelectric wedges	102
5.2.2	Piezoelectrics – conductor/composite wedges and junctions	102
5.2.3	Two piezoelectric material wedge	103
5.2.4	Multi-material system	104
5.3	Special cases of half plane and crack	104
5.4	Numerical results and discussion	105
5.4.1	Piezoelectric wedges	106
5.4.2	Piezoelectric – conductor wedges and junctions	112
5.4.3	Piezoelectric – graphite/epoxy wedges and junctions:	115
5.4.4	Piezoelectric bi-material systems:	115
5.4.5	Three material systems	118
5.5	Conclusions	118

6	Conclusions and Recommendations	121
6.1	Major Findings	121
6.2	Recommendations for future work	124
	Reference	125
A	Material properties	131
B	Constants Associated with Branched Cracks	133

List of Tables

2.1	Critical value of load ratio R for crack closure under combined tension and negative electric field for an impermeable crack.	36
2.2	Critical value of load ratio R for crack closure under combined tension and positive electric field for a conducting crack.	38
2.3	Normal electric displacement on crack faces based on eqn (2.69) ($\beta = 0$).	39
2.4	Energy release rates based on eqn (2.69) for a crack in PZT-4 ($\beta = 0, E_z^\infty=0$).	40
3.1	Comparison of field intensity factors at branch tip in PZT-4 for the special case of a branched crack ($\beta = 0, L/a = 10^{-6}$).	63
3.2	Range of branch angles (deg) for an open branch in PZT-4.	64
3.3	Comparison of stress intensity factors at the tip of a symmetrically branched crack in an isotropic elastic solid under remote tension ($L_1 = L_2 = 2a, \omega_1 = -\omega_2 = \omega$).	70
3.4	Comparison of stress intensity factor ratios at the tip of an asymmetrically branched crack in an isotropic elastic solid under remote tension ($L_1/a = 0.8, L_2/a = 0.4$).	71
4.1	Comparison of energy release rates calculated by eqns (4.17) and (4.18) in PZT-4 and PZT-5H ($\sigma_{zz}^\infty = 100N/m^2, \beta = 30^\circ$).	87
4.2	Comparison of energy release rates $G(\omega)/G(0^\circ)$ in orthotropic elastic solid.	87
5.1	Admissible basic boundary conditions on edge surfaces.	101
5.2	Comparison of roots λ for isotropic bi-material wedges (Figure 5.2).	108
5.3	Order of singularities for a right angle wedge, half plane and crack ($\beta = 0$).	109

List of Figures

1.1	Illustration of piezoelectric effect in a cylinder of PZT material (<i>APC International Ltd.: Piezoelectric Ceramics and Application Notes</i>).	2
1.2	Composite wedges and junctions encountered in adaptive structures.	7
2.1	Arbitrarily oriented elliptical void in a piezoelectric plane.	10
2.2	Arbitrarily oriented crack in a piezoelectric plane.	17
2.3	Electroelastic field around the boundary of an arbitrarily oriented elliptical hole (impermeable boundary) in PZT-4 due to remote tension.	28
2.4	Maximum values of hoop stress and electric displacement at the boundary of an elliptical void (impermeable boundary) in PZT-4.	30
2.5	Variation of crack tip hoop stresses under remote tension in PZT-4 (impermeable crack).	31
2.6	Variation of crack tip hoop stresses under remote electric field in PZT-4 (impermeable crack).	32
2.7	Variation of crack tip hoop stresses for combined remote tension and positive electric field in PZT-4 (impermeable crack).	34
2.8	Variation of crack tip hoop stresses for combined remote tension and negative electric field in PZT-4 (impermeable crack).	35
2.9	Variation of crack tip hoop stresses under remote electric field in PZT-4 (conducting crack).	37
2.10	Variation of electric displacement intensity factor with electric field in PZT-4 under tensile stress $\sigma_{zz}^{\infty} = 0.6MPa$ for different crack models.	41
2.11	Variation of strain energy release rate with electric field in PZT-4 under tensile stress $\sigma_{zz}^{\infty} = 0.6MPa$ for different crack models.	42
2.12	Variation of total energy release rate with electric field in PZT-4 under tensile stress $\sigma_{zz}^{\infty} = 0.6MPa$ for different crack models.	44

2.13	Variation of crack tip hoop stresses in PZT-4 under applied positive electric field for different crack models.	45
3.1	Crack configuration.	49
3.2	Superposition scheme for a branched crack.	53
3.3	Superposition scheme for a bifurcated crack.	58
3.4	Comparison of stress intensity factors at the tip of a branched crack in an orthotropic elastic solid under remote tension.	62
3.5	Normalized stress/electric intensity factors at the tip of a branched crack in PZT-4 due to remote tension for crack orientation $\beta = 0$ and different branch length L/a	65
3.6	Normalized stress/electric intensity factors at the tip of a branched crack in PZT-4 due to positive electric displacement for crack orientation $\beta = 0$ and different branch length L/a	66
3.7	Variation of branch tip hoop stress intensity factors under remote tension for different branch angles and crack orientations (branch length $L/a = 0.01$).	68
3.8	Variation of branch tip hoop stress intensity factors under positive electric field for different branch angles and crack orientations (branch length $L/a = 0.01$).	69
3.9	Stress intensity factors at the tips of an asymmetrically branched crack in PZT-4 under remote tension for different branch length ratios ($L_2/a = 0.1$, $\omega_1 = 30$, $\omega_2 = 0$ in Figure 3.1b).	72
3.10	Stress intensity factors at the tips of an asymmetrically branched crack in PZT-4 under positive electric field for different branch length ratios ($L_2/a = 0.1$, $\omega_1 = 30$, $\omega_2 = 0$ in Figure 3.1b).	73
3.11	Stress intensity factors at the tips of an asymmetrically branched crack in PZT-4 under remote tension for different branch length ratios ($L_2/a = 0.1$, $\omega_1 = 30$, $\omega_2 = -15$ in Figure 3.1b).	75
3.12	Stress intensity factors at the tips of an asymmetrically branched crack in PZT-4 under positive electric field for different branch length ratios ($L_2/a = 0.1$, $\omega_1 = 30$, $\omega_2 = -15$ in Figure 3.1b).	76
4.1	Illustration of fracture toughness anisotropy in piezoelectrics.	79
4.2	Variation of modified hoop stress intensity factor under remote tension loading for different crack orientation angles.	82

4.3	Variation of modified hoop stress intensity factor under positive electric field loading for different crack orientation angles.	83
4.4	Variation of modified strain energy release rate and modified hoop stress intensity factor at crack tip in PZT-4 under remote tensile stress $\sigma_{zz}^{\infty} = 0.6MPa$. 90	90
4.5	Variation of modified energy release rates and modified hoop stress intensity factor at crack tip in PZT-4 under positive electric field $E_z^{\infty} = 12KV/m$	91
4.6	Variation of modified strain energy release rate at crack tip in PZT-4 under applied tensile stress $\sigma_{zz}^{\infty} = 0.6MPa$ or electric field $E_z^{\infty} = \pm 12KV/m$	93
4.7	Variation of modified strain energy release rate at crack tip in PZT-4 under applied tensile stress $\sigma_{zz}^{\infty} = 0.6MPa$ or electric field $E_z^{\infty} = \pm 60KV/m$	94
4.8	Variation of modified total energy release rate at crack tip in PZT-4 under applied tensile stress $\sigma_{zz}^{\infty} = 0.6MPa$ or electric field $E_z^{\infty} = \pm 12KV/m$	95
4.9	Variation of modified total energy release rate at crack tip in PZT-4 under applied tensile stress $\sigma_{zz}^{\infty} = 0.6MPa$ or electric field $E_z^{\infty} = \pm 60KV/m$	96
5.1	A piezoelectric wedge.	99
5.2	A bi-material system.	103
5.3	Variation of the order of singularity with the wedge angle.	107
5.4	Variation of the order of singularity with the polarization angle for traction free and electrically open wedges.	111
5.5	Variation of the order of singularity with the polarization angle for right angle wedges.	111
5.6	Variation of the order of singularity for PZT-4 – aluminum (nickel) wedges.	113
5.7	Variation of the order of singularity for PZT-4 – aluminum (nickel) junctions.	114
5.8	Variation of the order of singularity for PZT-4 – graphite/epoxy systems.	116
5.9	Variation of the order of singularity for PZT-4 – PZT-5 junctions with debonded interface.	117
5.10	Variation of the order of singularity for three material systems with a crack in piezoelectrics.	119

List of Symbols

a	major axis of an elliptical void or half length of a crack
a_{ij}	two-dimensional elastic constants
$\mathbf{B}(B_1, B_2, B_3)$	extended Burgers vector
b	minor axis of an elliptical void
$b_i(x)$	densities of distributed dislocations
b_{ij}	two-dimensional piezoelectric constants
$[c]$	matrix of elastic constants
D_i	electric displacement vector
D_i^v	electric displacement inside the void
D_i^∞	far field electric displacement
d_{ij}	two-dimensional dielectric constants
$[e]$	matrix of piezoelectric constants
E_i	electric field vector
E_i^v	electric field inside the void
E_i^∞	far field electric field
$F(x, z)$	stress function
$[g]$	matrix of piezoelectric constants
G	total energy release rate
G_c	fracture toughness in terms of energy release rate
G^E	electric energy release rate
G^M	mechanical (strain) energy release rate
H	modified total energy release rate
H^M	modified strain energy release rate
K_0	fracture toughness in directions parallel to the poling direction
K_{90}	fracture toughness in directions perpendicular to the poling direction
K_c	fracture toughness in terms of stress intensity factor

K_D	electric displacement intensity factor
$K_{D\omega}$	hoop electric displacement intensity factor
K_E	electric field intensity factor
$K_{r\omega}$	shear stress intensity factor
$K_{\omega\omega}$	hoop stress intensity factor
K_I	Mode I stress intensity factor
K_{II}	Mode II stress intensity factor
K^*	modified hoop stress intensity factor
$\mathbf{n}(n_x, n_z)$	outward unit normal
$[s]$	matrix of elastic constants
u_i	displacement vector
β	angle of polarization orientation
$[\beta]$	matrix of dielectric constants
ϵ_{ij}	strain tensor
Δu_i	crack opening displacements
$[\epsilon]$	matrix of dielectric constants
ϵ_0	dielectric permittivity of vacuum
ϵ_v	dielectric permittivity of the medium inside the void
λ	root of characteristic equation (5.12)
$\lambda - 2$	order of electroelastic singularity
μ_n	root of characteristic equation (2.6)
σ_{ij}	stress tensor
σ_{ij}^∞	far field stress field
ϕ	electric potential
ϕ^v	electric potential inside the void
$\Psi(x, z)$	electric displacement function
ω	branch angle
ω_i	branch angles

Chapter 1

Introduction

1.1 General

Smart materials and structures have found increasing applications in diverse branches of engineering (*e.g.* civil, aerospace, mechanical, and manufacturing engineering). Actuators and sensors made of functional (smart) materials are integrated with structural materials in smart structures, and the resultant structures are able to adaptively respond to changes of external or internal parameters analogously to biological systems (Tani, *et al*, 1998). Popular materials being used for sensors and actuators are piezoelectric materials, magnetostrictive materials, shape memory alloys, and optical fibers. Among all these materials, piezoelectric materials are most widely used because of their fast electromechanical response and low power requirements (Jain and Sirkis, 1994).

There are two basic phenomena which enable piezoelectric materials to qualify as functional (smart) materials (Figure 1.1). The first phenomenon is known as the direct piezoelectric effect which implies that the application of mechanical force or pressure to a piezoelectric material produces an electrical charge or voltage (Figures 1.1b and 1.1c). On the other hand, the application of an electrical charge or voltage to the material induces strain or displacement, which is known as converse piezoelectric effect (Figures 1.1d - 1.1f). The direct and converse piezoelectric effects form the basis for employing piezoelectric materials as sensors and actuators, respectively.

Tani *et al* (1998) and Sunar and Rao (1999) presented extensive reviews on piezoelectric materials and their broad applications in the emerging field of smart structures. For example, in aerospace applications, piezoelectric actuators have been used to manipulate the

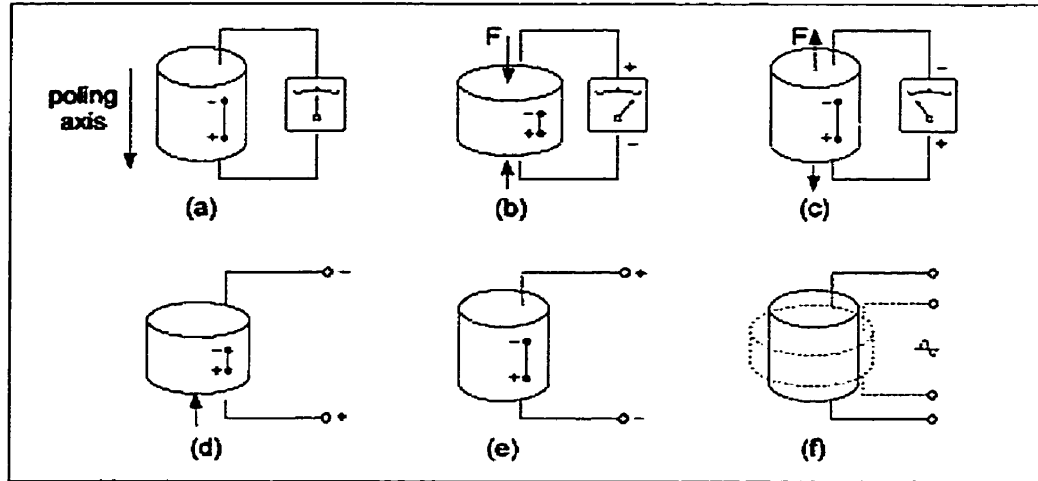


Figure 1.1: Illustration of piezoelectric effect in a cylinder of PZT material (*APC International Ltd.: Piezoelectric Ceramics and Application Notes*).

blade twists of the helicopter rotors (Chen and Chopra, 1997). In civil infrastructure, the vibration control of a steel building using large piezoelectric actuators has been demonstrated (Kamada, *et al*, 1997).

The major concern about using piezoelectric materials is their brittleness and susceptibility to fracture. These materials may experience mechanical failure or dielectric breakdown under complex electromechanical loading. Commercially available piezoceramics such as lead zirconate titanate (PZT) are very brittle. The unavoidable presence of defects during manufacturing processes increases the likelihood of failure of piezoceramic elements. There is evidence that the service performance of piezoceramics is hampered by defects or anomalies such as voids and cracks. Park *et al* (1998) experimentally demonstrated that damage initiates and grows around internal void-like defects. Barsoum (1997) reported that fatigue degradation is caused by the presence of cracks. The structural integrity of piezoelectric ceramics is becoming increasingly important as their use is extended to new frontiers. Comprehensive studies about better understanding of fracture behavior and quantitative prediction of possible crack extension are imperative for the reliable application of piezoelectric materials in adaptive structures technology. Therefore, this thesis aims at studying some basic fracture mechanics problems involving piezoelectric materials.

A concise review of literature related to the fracture of piezoelectric ceramics is presented in the ensuing section in order to define the objectives and the scope of the present study.

1.2 Literature review

Voids and Straight cracks

The study of electroelastic fields around defects in piezoelectric ceramics has been quite extensive in the past decade. By assuming an electrically impermeable boundary, Sosa (1990) studied stress concentration around an elliptical hole by extending Lekhnitskii's complex potential functions (Lekhnitskii, 1963). Numerical results were presented to show the piezoelectric effect and the dependence of stress and electric fields on defect geometry and applied loading. Sosa and Khutoryansky (1996) revisited an identical problem by removing the assumption of an impermeable boundary. There are also several recent studies (e.g. Park and Carman, 1997; Zhang *et al*, 1998; Gao and Fan, 1999) dealing with elliptic voids. A major restriction of these studies is the assumption that the defect axis is either parallel or perpendicular to the poling direction. In view of the great likelihood that defects are arbitrarily oriented, it is important to develop solutions for such general cases to gain more insight.

A number of researchers examined the problem of impermeable cracks in plane piezoelectrics. Sosa (1992) obtained the crack solution by reducing the solution for an elliptical void. Sosa (1992) and Suo *et al* (1992) added an electric intensity factor to the well-known elastic stress intensity factors. Pak (1992) and Suo *et al* (1992) used the energy release rate to study crack problems. Park and Sun (1995a) employed Stroh formalism (Stroh, 1962) to derive electroelastic fields around a horizontal centre crack. Park and Sun (1995b) performed compact tension tests and reported that a positive field along the poling direction reduces the fracture load, and a negative one increases it. Using the Vickers indentation, Singh and Wang (1995) observed experimental results contrary to the findings of Park and Sun (1995b). They found that crack propagation is inhibited under a positive applied electric field, and is enhanced under a negative field. In a series of papers, Kumar and Singh (1996, 1997a, 1997b) employed the finite element method to study crack problems and compared their results with the experimental results of Singh and Wang (1995). No consensus has been reached on the role of an applied electric field. The condition that the crack plane is perpendicular to the poling direction is exclusively used in the above studies.

Conflicting views on electric boundary conditions for cracks containing air or vacuum are also observed in the literature. Polovinkina and Ulitko (1978) and Mikhailov and Parton (1990) used a permeable crack model, which assumes the continuity of electric potential and the normal component of electrical displacement across the crack faces. Suo *et al* (1992)

argued that this condition is not realistic, as there is an electric potential drop across the crack. Deeg (1980) proposed an impermeable crack model, *i.e.*, the vanishing of normal electric displacement on the crack faces. Pak (1990) provided arguments for the validity of Deeg's model. Dunn (1994), Zhang and Tong (1996) and Zhang *et al* (1998) examined the crack face boundary conditions by studying an elliptical void. By taking the limits of a void, Zhang and Tong (1996) and Zhang *et al* (1998) discussed the effects of crack geometry and permittivity. They found that different limits of governing variables result in different crack face conditions. Hao and Shen (1994) proposed a new electric boundary condition by considering the electric permeability of air or vacuum in a crack. Gao and Fan (1999) claimed that the solution for a plane crack under exact electric boundary conditions is obtained by reducing the solution for a permeable void.

Apparently, coordinated experimental studies are needed to understand the real electric boundary conditions on crack faces and to clarify the role of an applied electric field. It is noted that past theoretical studies exclusively assumed that a crack is perpendicular/parallel to the poling direction or has impermeable crack faces. In addition, the electric boundary conditions proposed by Hao and Shen (1994) have not been closely examined. Also, it is questionable that the crack solution reported by Gao and Fan (1999) is exact.

Fracture criteria

Criteria of crack propagation are fundamentally important in the study of fracture mechanics. For linear isotropic elastic materials, fracture criteria of maximum stress intensity factor, maximum hoop stress and maximum energy release rate result in quite similar fracture predictions. However, these criteria do not predict similar crack propagation paths in anisotropic materials (Azhdari and Nemat-Nasser, 1998). The prediction of crack propagation in piezoelectric materials is more complicated due to the coupling between mechanical and electrical fields.

According to the conventional field intensity factors (Suo *et al*, 1992), the mechanical and electrical fields are completely decoupled. Experimental studies indicate a dependence of piezoelectric fracture on applied electric field (Park and Sun, 1995b; Singh and Wang, 1995), implying that the fracture criterion of stress intensity factor is not feasible for piezoelectrics. Some efforts have been made to seek appropriate fracture criteria for impermeable cracks in piezoelectrics. The criterion of total energy release rate was employed by Pak (1992), whereas the criterion of mechanical (strain) energy release rate was proposed by Park and Sun (1995b). The assumption of self-similar crack propagation was used in the above studies.

However, a crack may deviate from the straight path in piezoelectric solids due to material anisotropy. Using the double torsion testing technique, McHenry and Koepke (1983) reported that cracks in symmetric piezoceramic specimen deviate from straight paths under symmetric electric loading. In an attempt to explain experimental observations of crack branching (McHenry and Koepke, 1983), Kumar and Singh (1996) employed the criterion of the maximum hoop stress to examine the crack propagation. In another attempt, Kumar and Singh (1997a, 1997b) used the finite element method to calculate the angular distribution of the energy release rate, and applied the criterion of maximum energy release rate to predict crack propagation. Their results of energy release rate distribution, however, are not accurate, and there is a discrepancy between their finite element solutions and the analytical solutions reported in the literature (Pak, 1992). Accurate solution for angular distribution of energy release rates has not appeared in the literature.

It is noted that the above studies only considered the case that the poling direction is perpendicular to the crack. Furthermore, the assumption of isotropic fracture toughness in piezoelectric materials was exclusively used. However, this assumption is not true. Due to their anisotropic material properties, the fracture toughness in piezoelectrics is expected to be orientation dependent, which is confirmed by experimental data (Calderon-Moreno, *et al*, 1997; Pisarenko, *et al*, 1985; Chen, *et al*, 1999).

Branched cracks

The phenomenon of crack branching is an important aspect of fracture mechanics (Miller and Stock, 1989; Karihaloo and Anderson, 1998). Branched cracks are commonly encountered in the fracture of brittle materials. Crack branching may be caused by anti-symmetric loading, anisotropic material properties, voids, impurities *etc*. Polarized ceramics have anisotropic mechanical and electric properties. McHenry and Koepke (1983) reported the phenomenon of crack branching in piezoelectric ceramics based on their experimental study. Lynch *et al* (1995) observed that an impermeable crack would branch and have a feathered appearance in a piezoceramic sample. Although crack branching in elastic materials has been extensively investigated (Obata, *et al*, 1989; Azhdari and Nemat-Nasser, 1996; *etc*), no studies have considered branched cracks in piezoelectric solids except for a recent study by Zhu and Yang (1999).

Zhu and Yang (1999) theoretically examined a branched crack in a piezoelectric plane by employing the Stroh formalism combined with dislocation modeling. The electroelastic field at the branch tip was investigated in terms of field intensity factors under remote mechanical

or electric loading. Their formulation was validated by checking possible closure of the main crack. Considering a crack with an infinitesimal branch, they discussed the possible directions of crack branching based on the assumption of isotropic fracture toughness. The numerical results showed that a crack tends to propagate along the self-similar line under a tensile stress and a positive electric loading. However, their analysis is restricted to the special case of a crack normal to the poling direction. The possible closure of the crack branch was not examined, implying invalidity of some of their results. Moreover, the assumption of isotropic fracture toughness is not true for piezoelectrics as stated above.

Singularities in multi-material systems

An adaptive structure generally has several composite wedges and material junctions involving piezoelectric materials (Figure 1.2). In practical applications, piezoelectric sensors or actuators are embedded in or bonded to a parent structure. In addition, commonly used piezoceramic stack actuators also involve some of the material junctions shown in Figure 1.2. A complete study of fracture of multi-material systems is beyond the scope of this study. However, the knowledge of singularities at multi-material junctions/wedges is essential in the application of linear fracture mechanics to such systems and composites. A precise understanding of electroelastic singularities at corners of composite piezoelectric wedges and junctions is valuable to the optimum design and failure analysis of piezoceramic actuators and adaptive structures. Furthermore, the knowledge of the order of singularity can be useful in the development of special crack-tip elements for analysis of fracture of bi-material actuator systems.

In the case of piezoelectric media, both stress and electric fields at a sharp corner may be singular. This implies that either local mechanical failure due to stress concentration or dielectric failure due to electric field concentration could take place at a sharp corner. A review of literature reveals that a comprehensive analytical and numerical study of electroelastic singularities in composite piezoelectric wedges has not yet been reported while there have been extensive studies on elastic wedge problems (*e.g.* Williams 1952, 1956; Bogy 1968, 1970; Hein and Erdogan, 1971; Dempsey and Sinclair 1979; Delale, 1984; Mantič *et al* 1997 and others). The only studies that have addressed related problems are presented by Sosa and Pak (1990) and Kuo and Barnett (1991). These studies examined electroelastic singularities at the tip of planar cracks perpendicular to the direction of polarization in homogeneous piezoelectrics and bi-material systems.

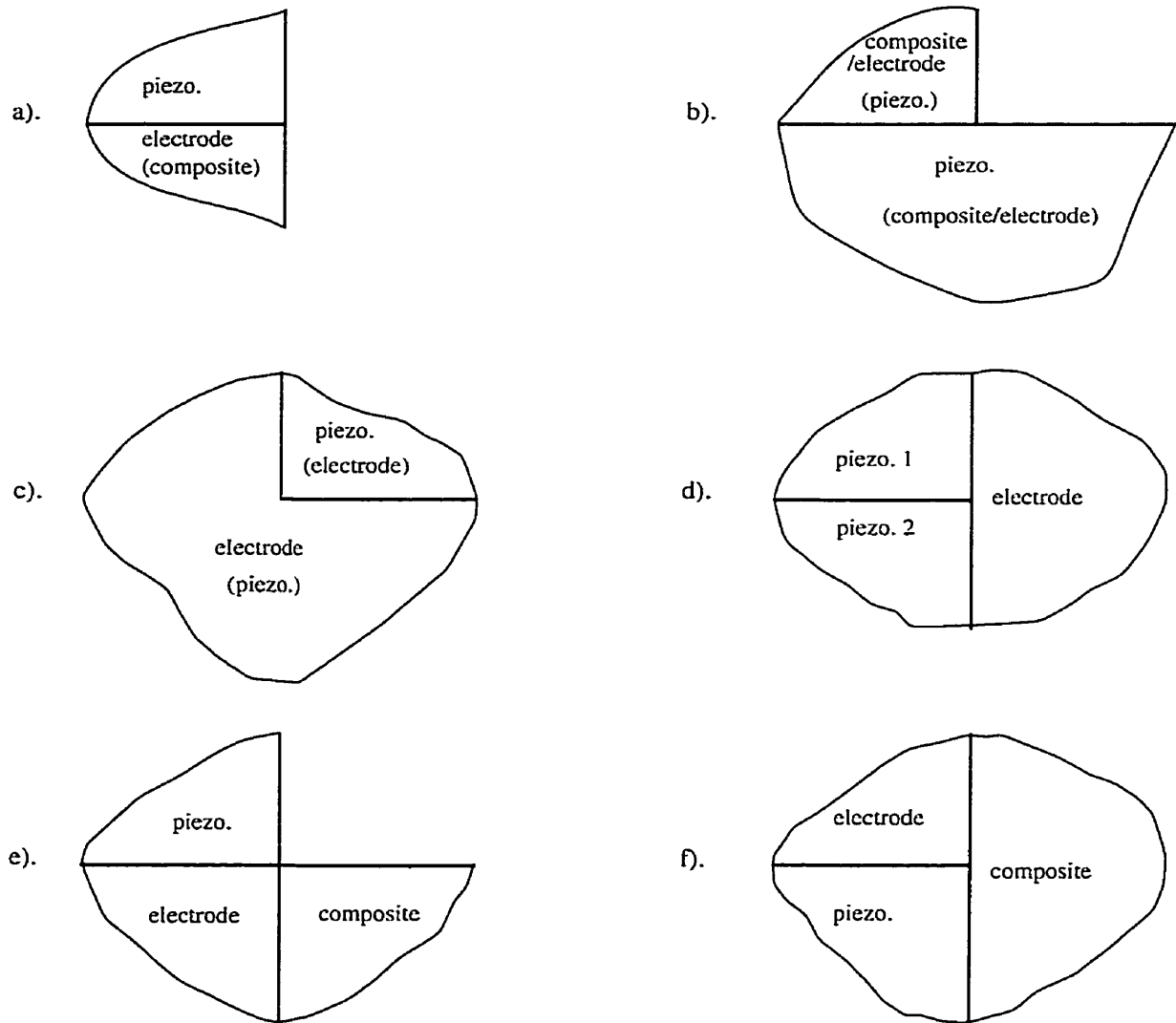


Figure 1.2: Composite wedges and junctions encountered in adaptive structures.

1.3 Objectives and scope

Based on the above literature review, it is clear that there are still a number of areas related to linear fracture mechanics of piezoelectricity which require further attention. Topics such as the effect of void orientation and singularities in composite piezoelectric wedges have not been considered in the literature. Little knowledge exists on the dependence of fracture parameters on crack orientation and electric boundary conditions. Past studies also show conflicting observations on some key issues. For example, entirely distinct conclusions, supported by both theoretical and experimental studies, have been reported regarding the effect of applied electrical field on crack propagation. So far, no consensus has been reached on the electric boundary conditions on the crack faces. Previous studies on branched cracks and fracture criteria employed irrational assumptions or simplifications. Therefore, there exists a necessity to examine several key issues related to fracture of piezoelectrics.

A theoretical study of piezoelectric materials is presented in this thesis with four main objectives. First, a comprehensive study of an arbitrarily oriented elliptical void and a straight crack is carried out. Analytical solutions are developed for different types of void and crack boundary conditions. The effects of defect orientation and electric boundary condition are closely examined. Secondly, the problem of an arbitrarily oriented branched crack is studied. The influence of the deviated branch is investigated. The condition for an open crack is taken into consideration. Thirdly, the issue of fracture criteria for piezoelectric materials is investigated. The commonly used assumption of self-similar crack extension is relaxed, and the fracture toughness anisotropy is taken into consideration. Finally, the electroelastic singularities at the corner of composite piezoelectric wedges are examined. The singularity analysis may appear, at first glance, to be somewhat independent, but the result of this analysis is actually used in the analysis of branched crack problems. More important, the knowledge of singularities is essential when constructing analytical solutions for composite piezoelectric systems and in the development of special crack-tip elements for finite and boundary element methods.

Chapter 2

Arbitrarily Oriented Voids and Straight Cracks

2.1 Infinite Plane with an Elliptical Void

2.1.1 Basic equations

Depending on the choice of variables, two sets of constitutive equations are frequently used in the literature for piezoelectrics. With stress $\{\sigma\}$ and electric displacement $\{D\}$ as independent variables, the constitutive equations are

$$\{\epsilon\} = [s]\{\sigma\} + [g]^T\{D\}; \quad \{E\} = -[g]\{\sigma\} + [\beta]\{D\} \quad (2.1)$$

where $\{\epsilon\}$, $\{E\}$ denote strain and electric field vectors, respectively. $[s]$, $[g]$ and $[\beta]$ are matrices denoting the elastic constants, piezoelectric constants and dielectric constants, respectively. The superscript T denotes transpose of a matrix.

Alternatively, with strain and electric field as the independent variables,

$$\{\sigma\} = [c]\{\epsilon\} - [e]^T\{E\}; \quad \{D\} = [e]\{\epsilon\} + [\epsilon]\{E\} \quad (2.2)$$

where $[c]$, $[e]$ and $[\epsilon]$ are matrices representing the elastic constants, piezoelectric constants and dielectric constants, respectively.

Note that eqns (2.1) and (2.2) are dependent, and the material constants in these two equations are related to each other. A majority of piezoelectric materials used in commercial applications are either hexagonally symmetric crystals or polarized ceramics. The properties of three piezoceramics used in this thesis are given in the Appendix A.

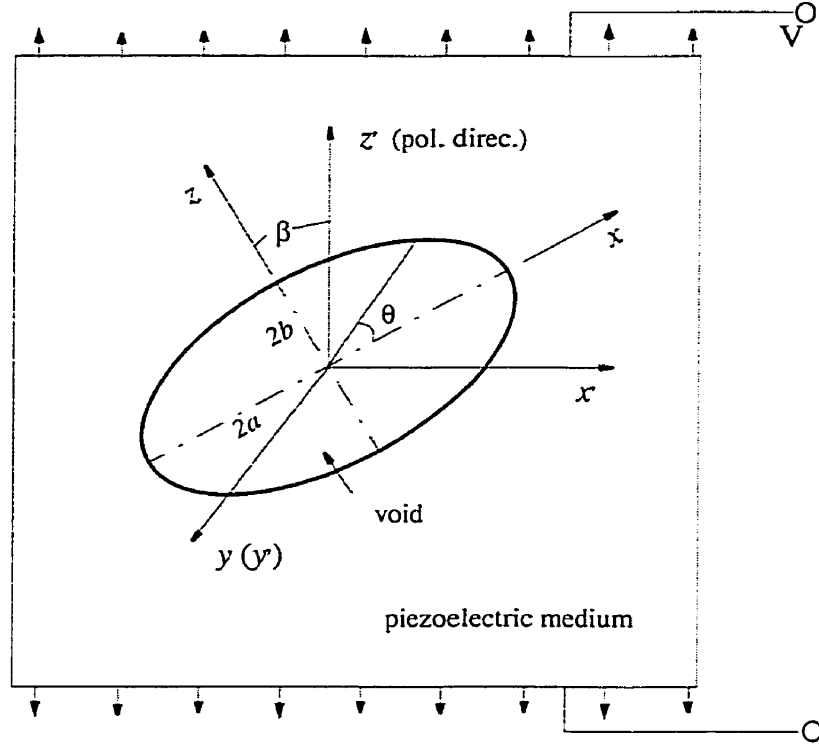


Figure 2.1: Arbitrarily oriented elliptical void in a piezoelectric plane.

Consider an arbitrarily oriented elliptical void in a piezoceramic plane, as shown in Figure 2.1. The poling direction (z' -axis of the coordinate system $x'z'$) makes angle β with one axis of the void (z -axis of the system xz), and β is measured from the z' axis in the counter-clockwise direction. Far field mechanical and electric loading are denoted by $\sigma_{x'x'}^\infty$, $\sigma_{z'z'}^\infty$, $\sigma_{x'z'}^\infty$ and $D_{x'}^\infty$, $D_{z'}^\infty$ (or $E_{x'}^\infty$, $E_{z'}^\infty$), respectively. Alternatively, the loading can be expressed as σ_{xx}^∞ , σ_{zz}^∞ , σ_{xz}^∞ and D_x^∞ , D_z^∞ (or E_x^∞ , E_z^∞) under the xz system. In the special case of $\beta = 0$, the problem has been well studied (Sosa, 1991, *etc.*).

The constitutive equations of piezoceramics polarized along the z' -axis are identical to piezocrystals with hexagonal symmetry about the same axis. Assuming plane stress ($\sigma_{y'y'} = 0, D_{y'} = 0$) or plane strain ($\epsilon_{y'y'} = 0, E_{y'} = 0$) conditions and

using the eqn (2.1), the following constitutive equations can be obtained.

$$\begin{aligned}
\epsilon_{xx} &= a_{11}\sigma_{xx} + a_{12}\sigma_{zz} + a_{13}\sigma_{xz} + b_{11}D_x + b_{21}D_z \\
\epsilon_{zz} &= a_{12}\sigma_{xx} + a_{22}\sigma_{zz} + a_{23}\sigma_{xz} + b_{12}D_x + b_{22}D_z \\
2\epsilon_{xz} &= a_{13}\sigma_{xx} + a_{23}\sigma_{zz} + a_{33}\sigma_{xz} + b_{13}D_x + b_{23}D_z \\
E_x &= -b_{11}\sigma_{xx} - b_{12}\sigma_{zz} - b_{13}\sigma_{xz} + d_{11}D_x + d_{12}D_z \\
E_z &= -b_{21}\sigma_{xx} - b_{22}\sigma_{zz} - b_{23}\sigma_{xz} + d_{12}D_x + d_{22}D_z
\end{aligned} \tag{2.3}$$

where coefficients a_{ij} , b_{ij} and d_{ij} are two-dimensional elastic, piezoelectric and dielectric constants, respectively. These coefficients are functions of defect orientation angle β , and are different for plane stress and plane strain cases. The invariable property of potential energy is used to derive the above relations.

Now extend Lekhnitskii's formalism (Lekhnitskii, 1963) for elastic solids to piezoelectric solids by introducing the following potential function representation.

$$\begin{aligned}
\sigma_{xx} &= \frac{\partial^2 F}{\partial z^2}; & \sigma_{zz} &= \frac{\partial^2 F}{\partial x^2}; & \sigma_{xz} &= -\frac{\partial^2 F}{\partial x \partial z}; \\
D_x &= \frac{\partial \Psi}{\partial z}; & D_z &= -\frac{\partial \Psi}{\partial x}
\end{aligned} \tag{2.4}$$

It can be shown that the equilibrium and Maxwell's equations are automatically satisfied. The above potential function representation can be considered as an extension of Lekhnitskii's representation for elastic solids. Using the strain and electric field compatibility equations for piezoelectric solids, the following sixth-order differential equation can be derived.

$$D_1 D_2 D_3 D_4 D_5 D_6 F = 0 \tag{2.5}$$

where $D_n = \frac{\partial}{\partial z} - \mu_n \frac{\partial}{\partial x}$, and $\mu_n (n = 1, \dots, 6)$ are the roots of the characteristic equation

$$l_1(\mu)l_3(\mu) + l_2^2(\mu) = 0 \tag{2.6}$$

with

$$\begin{aligned}
l_1 &= d_{11}\mu^2 - 2d_{12}\mu + d_{22}; & l_2 &= b_{11}\mu^3 - (b_{21} + b_{13})\mu^2 + (b_{12} + b_{23})\mu - b_{22} \\
l_3 &= a_{11}\mu^4 - 2a_{13}\mu^3 + (2a_{12} + a_{33})\mu^2 - 2a_{23}\mu + a_{22}
\end{aligned}$$

The roots (μ) of eqn (2.6) can be shown to be complex with three conjugate pairs, and are generally distinct. Note that eqn (2.6) breaks down if no coupling exists between

mechanical and electrical fields. Instead, a second degree equation $l_1(\mu) = 0$ and a fourth degree equation $l_3(\mu) = 0$ can be obtained for electrostatics and elasticity, respectively. For piezoelectric materials, functions $l_1(\mu)$, $l_2(\mu)$ and $l_3(\mu)$ generally have non-zero values. If μ' are the roots of the characteristic equation corresponding to a defect oriented along the z' -axis (*i.e.* $\beta = 0$), it can be shown that the following relationship exists between μ and μ' .

$$\mu = \frac{\mu' \cos \beta - \sin \beta}{\cos \beta + \mu' \sin \beta} \quad (2.7)$$

Some useful properties of roots of eqn (2.6) are implied from eqn (2.7), *e.g.* two identical roots corresponding to a particular defect orientation will remain identical for any arbitrary orientation.

Let μ_1 , μ_2 and μ_3 be the roots with positive imaginary parts. The general solutions for complex functions $F(x, z)$ and $\Psi(x, z)$ in eqn (2.4) can be expressed as

$$F(x, z) = 2Re \sum_{n=1}^3 F_n(z_n); \quad \Psi(x, z) = 2Re \sum_{n=1}^3 \delta_n \frac{\partial F_n(z_n)}{\partial z_n} \quad (2.8)$$

where Re denotes the real part of a complex valued quantity, $z_n = x + \mu_n z$, and $\delta_n = l_2(\mu_n)/l_1(\mu_n)$.

With the aid of the basic relations in linear piezoelectricity (Parton and Kudryavtsev, 1988), the general solutions for plane piezoelectric problems excluding the corresponding rigid body terms can be obtained as

$$\begin{aligned} u_x &= 2Re \sum_{n=1}^3 p_n \varphi_n(z_n); & u_z &= 2Re \sum_{n=1}^3 q_n \varphi_n(z_n); & \phi &= 2Re \sum_{n=1}^3 s_n \varphi_n(z_n) \\ \sigma_{xx} &= 2Re \sum_{n=1}^3 \mu_n^2 \varphi_n'(z_n); & \sigma_{zz} &= 2Re \sum_{n=1}^3 \varphi_n'(z_n); & \sigma_{xz} &= -2Re \sum_{n=1}^3 \mu_n \varphi_n'(z_n) \\ D_x &= 2Re \sum_{n=1}^3 \delta_n \mu_n \varphi_n'(z_n); & D_z &= -2Re \sum_{n=1}^3 \delta_n \varphi_n'(z_n) \\ E_x &= -2Re \sum_{n=1}^3 s_n \varphi_n'(z_n); & E_z &= -2Re \sum_{n=1}^3 t_n \varphi_n'(z_n) \end{aligned} \quad (2.9)$$

where complex function $\varphi_n(z_n) = F_n'(z_n)$ with a prime (') denoting differentiation with respect to the corresponding argument, and the complex variables p_n , q_n , s_n and t_n are

given below.

$$\begin{aligned}
p_n &= a_{11}\mu_n^2 + a_{12} - a_{13}\mu_n + \delta_n(b_{11}\mu_n - b_{21}) \\
q_n &= (a_{12}\mu_n^2 + a_{22} - a_{23}\mu_n + \delta_n b_{12}\mu_n - \delta_n b_{22})/\mu_n \\
s_n &= b_{11}\mu_n^2 + b_{12} - b_{13}\mu_n - \delta_n(d_{11}\mu_n - d_{12}) \\
t_n &= b_{21}\mu_n^2 + b_{22} - b_{23}\mu_n - \delta_n(d_{12}\mu_n - d_{22})
\end{aligned} \tag{2.10}$$

The general solutions given by eqn (2.9) are essential to the formulation of subsequent problems considered in this thesis.

2.1.2 Impermeable void

Assume traction free and electrically impermeable conditions on the boundary of the void in Figure 2.1. Therefore,

$$\sigma_{ij}n_j = 0; \quad D_i n_i = 0 \quad (i, j = x, z) \tag{2.11}$$

where \mathbf{n} (n_x, n_z) denote the outward unit normal of the void boundary.

The task now is to determine the three unknown complex functions $\varphi_n(z_n)$ ($n = 1, 2, 3$) in eqn (2.9) by considering the void boundary conditions given by eqn (2.11) and remote uniform mechanical and electric loading conditions.

Construct the complex function φ_n ($n = 1, 2, 3$) in the form of

$$\varphi_n(z_n) = c_n z_n + \varphi_n^0(z_n); \quad \text{with} \quad \varphi_n^0(z_n) = \sum_{k=0}^{\infty} \frac{a_k^{(n)}}{z_n^k} \tag{2.12}$$

where c_n are complex constants, and $\varphi_n^0(z_n)$ are holomorphic functions up to infinity with complex constants $a_k^{(n)}$.

With the aid of functions given below, which map the exterior of an ellipse in the z_n plane into the exterior of an unit circle in the ξ_n plane (Lekhnitskii, 1963),

$$z_n = \frac{a - i\mu_n b}{2} \xi_n + \frac{a + i\mu_n b}{2} \frac{1}{\xi_n} \tag{2.13}$$

the functions $\varphi_n^0(z_n)$ and the constants c_n can be obtained by applying the relevant boundary conditions.

Omitting details, the final results are

$$\varphi_n^0(z_n) = \frac{z_n - \sqrt{z_n^2 - (a^2 + \mu_n^2 b^2)}}{a + i\mu_n b} (\Lambda_{n1} Q_1 + \Lambda_{n2} Q_2 + \Lambda_{n3} Q_3); \quad (n = 1, 2, 3) \tag{2.14}$$

where

$$\begin{pmatrix} \Lambda_{11} & \Lambda_{12} & \Lambda_{13} \\ \Lambda_{21} & \Lambda_{22} & \Lambda_{23} \\ \Lambda_{31} & \Lambda_{32} & \Lambda_{33} \end{pmatrix} = \frac{1}{\Delta} \begin{pmatrix} \mu_2\delta_3 - \mu_3\delta_2 & \delta_2 - \delta_3 & \mu_3 - \mu_2 \\ \mu_3\delta_1 - \mu_1\delta_3 & \delta_3 - \delta_1 & \mu_1 - \mu_3 \\ \mu_1\delta_2 - \mu_2\delta_1 & \delta_1 - \delta_2 & \mu_2 - \mu_1 \end{pmatrix} \quad (2.15)$$

$$\Delta = \mu_1(\delta_2 - \delta_3) + \mu_2(\delta_3 - \delta_1) + \mu_3(\delta_1 - \delta_2) \quad (2.16)$$

$$Q_1 = -\frac{a\sigma_{zz}^\infty}{2} + i\frac{b\sigma_{xz}^\infty}{2}; \quad Q_2 = \frac{a\sigma_{xz}^\infty}{2} - i\frac{b\sigma_{zz}^\infty}{2}; \quad Q_3 = \frac{aD_z^\infty}{2} - i\frac{bD_x^\infty}{2} \quad (2.17)$$

The complex constants c_n ($n = 1, 2, 3$) can be determined by solving the following equation system.

$$\begin{aligned} -\sum_{n=1}^3 a\text{Re}\{c_n\} + ib\text{Re}\{c_n\mu_n\} &= Q_1; & -\sum_{n=1}^3 a\text{Re}\{c_n\mu_n\} + ib\text{Re}\{c_n\mu_n^2\} &= Q_2 \\ -\sum_{n=1}^3 a\text{Re}\{c_n\delta_n\} + ib\text{Re}\{c_n\delta_n\mu_n\} &= Q_3 \end{aligned} \quad (2.18)$$

Note that only five independent equations exist in the eqn (2.18), and one of the six unknowns in c_n is set to zero by excluding the corresponding rigid body terms.

Complex functions $\varphi_n(z_n)$, $\varphi'(z_n)$ are now completely determined as

$$\varphi_n(z_n) = c_n z_n + (\Lambda_{n1}Q_1 + \Lambda_{n2}Q_2 + \Lambda_{n3}Q_3) \frac{z_n - \sqrt{z_n^2 - (a^2 + \mu_n^2 b^2)}}{a + i\mu_n b} \quad (2.19)$$

$$\varphi'(z_n) = c_n + (\Lambda_{n1}Q_1 + \Lambda_{n2}Q_2 + \Lambda_{n3}Q_3) \frac{1}{a + i\mu_n b} \left\{ 1 - \frac{z_n}{\sqrt{z_n^2 - (a^2 + \mu_n^2 b^2)}} \right\} \quad (2.20)$$

The substitution of eqns (2.19) and (2.20) into (2.9) yields the complete solutions for electroelastic fields around an arbitrarily oriented elliptical void with the impermeable boundary. The closed form solutions derived here are functions of defect orientation (β), defect geometry (a, b), far-field loading and material properties (a_{ij} , b_{ij} and d_{ij}). The solution given by Sosa (Sosa, 1991) can be recovered by letting $\beta = 0$.

2.1.3 Permeable void

Removing the assumption of an impermeable void boundary, the exact solution for an arbitrarily oriented elliptical void (Figure 2.1) is derived in this subsection. To this end, the medium inside the void must be taken into consideration, and a two-domain problem needs to be solved. The homogeneous domain inside the void may be vacuum or air. The void is free of electric charges, and no free charges exist on the piezoelectric-void interface.

The dielectric medium (air or vacuum) inside the void is governed by Maxwell's equation, electric constitutive equations and electric field-potential relations. Let ϵ_v denote the dielectric permittivity of the medium inside the void, then,

$$D_{i,i}^v = 0; \quad D_i^v = \epsilon_v E_i^v; \quad E_i^v = -\phi_{,i}^v \quad (2.21)$$

where a superscript v is used to denote quantities associated with the void.

The general solutions for a dielectric medium governed by eqn (2.21) can be expressed as,

$$\begin{aligned} \phi^v &= 2Im[\psi(z_v)] \\ D_x^v &= -2\epsilon_v Im[\psi'(z_v)]; \quad D_z^v = -2\epsilon_v Re[\psi'(z_v)] \\ E_x^v &= -2Im[\psi'(z_v)]; \quad E_z^v = -2Re[\psi'(z_v)] \end{aligned} \quad (2.22)$$

where $\psi(z_v)$ is a complex function with $z_v = x + iz$, Im denotes the imaginary part of a complex-valued quantity.

The following equations hold on the void boundary (*i.e.* piezoelectric-void interface).

$$\sigma_{xx}n_x + \sigma_{xz}n_z = 0; \quad \sigma_{xz}n_x + \sigma_{zz}n_z = 0 \quad (2.23)$$

$$D_n = D_n^v; \quad \phi = \phi^v \quad (2.24)$$

Note that the continuity requirement of the electric potential is equivalent to that of the tangential component of the electric field(Bottcher, 1973).

The potential functions $\varphi_n(z_n)$ ($n = 1, 2, 3$) in eqn (2.9) and $\psi(z_v)$ in eqn (2.22) are determined such that the prescribed boundary conditions are satisfied. The derivation can be carried out by following Sosa and Khutoryansky (1996) who considered the special case of $\beta = 0$.

Alternatively, Chen and Lai (1997) showed that the electroelastic field inside a plane inhomogeneity is uniform under uniform far-field loading. Let uniform electric fields and electric displacements inside the void are denoted by E_x^0, E_z^0 and D_x^0, D_z^0 , respectively. Eqn (2.24) can be rewritten as

$$D_n = D_x^0 n_x + D_z^0 n_z; \quad \phi = -E_x^0 x - E_z^0 z \quad (2.25)$$

The problem now reduces to determining the three unknown complex functions $\varphi_n(z_n)$ and two constants D_x^0, D_z^0 (or E_x^0, E_z^0). Construct φ_n in the form of eqn (2.12) and apply the mapping functions of eqn (2.13). The complex functions $\varphi_n^0(z_n)$, complex constants

c_n , and constants D_x^0 and D_z^0 can be obtained by applying far-field loading conditions and interface conditions given by eqns (2.23) and (2.25).

Details of the derivation are omitted for brevity. The results for complex functions $\varphi_n(z_n)$ and $\varphi'(z_n)$ are given below.

$$\varphi_n(z_n) = \bar{c}_n z_n + (\Lambda_{n1} Q_1 + \Lambda_{n2} Q_2 + \Lambda_{n3} \bar{Q}_3) \frac{z_n - \sqrt{z_n^2 - (a^2 + \mu_n^2 b^2)}}{a + i\mu_n b} \quad (2.26)$$

$$\varphi'(z_n) = \bar{c}_n + (\Lambda_{n1} Q_1 + \Lambda_{n2} Q_2 + \Lambda_{n3} \bar{Q}_3) \frac{1}{a + i\mu_n b} \left\{ 1 - \frac{z_n}{\sqrt{z_n^2 - (a^2 + \mu_n^2 b^2)}} \right\} \quad (2.27)$$

where Λ_{nj} ($n, j = 1, 2, 3$), Q_1, Q_2 are defined in eqns (2.15)-(2.17), and \bar{Q}_3 is

$$\bar{Q}_3 = \frac{a(D_z^\infty - D_z^0)}{2} - i \frac{b(D_x^\infty - D_x^0)}{2} \quad (2.28)$$

The complex constants \bar{c}_n ($n = 1, 2, 3$) are determined from the following equation system.

$$\begin{aligned} - \sum_{n=1}^3 a \operatorname{Re}\{\bar{c}_n\} + ib \operatorname{Re}\{\bar{c}_n \mu_n\} &= Q_1; & - \sum_{n=1}^3 a \operatorname{Re}\{\bar{c}_n \mu_n\} + ib \operatorname{Re}\{\bar{c}_n \mu_n^2\} &= Q_2 \\ - \sum_{n=1}^3 a \operatorname{Re}\{\bar{c}_n \delta_n\} + ib \operatorname{Re}\{\bar{c}_n \delta_n \mu_n\} &= \bar{Q}_3 \end{aligned} \quad (2.29)$$

As in the case of eqn (2.18), one of the six unknowns in \bar{c}_n is set to zero by excluding the corresponding rigid body terms.

Electric displacements D_x^0 and D_z^0 are determined from,

$$\begin{aligned} a \operatorname{Re}\{A_1\} D_z^0 + (b \operatorname{Im}\{A_1\} + a/\varepsilon_v) D_x^0 &= 2 \operatorname{Re}\{A_2\} + a E_x^\infty + a \operatorname{Re}\{A_1\} D_z^\infty + b \operatorname{Im}\{A_1\} D_x^\infty \\ (a \operatorname{Im}\{A_1\} - b/\varepsilon_v) D_z^0 - b \operatorname{Re}\{A_1\} D_x^0 &= 2 \operatorname{Im}\{A_2\} + b E_z^\infty + a \operatorname{Im}\{A_1\} D_z^\infty - b \operatorname{Re}\{A_1\} D_x^\infty \end{aligned} \quad (2.30)$$

where

$$A_1 = - \sum_{n=1}^3 s_n \Lambda_{n3}; \quad A_2 = - \sum_{n=1}^3 s_n (\Lambda_{n1} Q_1 + \Lambda_{n2} Q_2)$$

Substitution of eqns (2.26) and (2.27) into eqn (2.9) yields the complete solution for electroelastic fields outside a permeable void. With D_x^0 and D_z^0 known, the electroelastic solution within the void is also completely known.

For the special case of an impermeable void boundary, $\varepsilon_v = 0$ leads to the vanishing of D_z^v and D_x^v (or D_z^0 and D_x^0) based on eqn (2.22). Therefore, $\bar{Q}_3 = Q_3$ and $\bar{c}_n = c_n$ according to eqns (2.28) and (2.29), and the solution for an impermeable void is recovered.

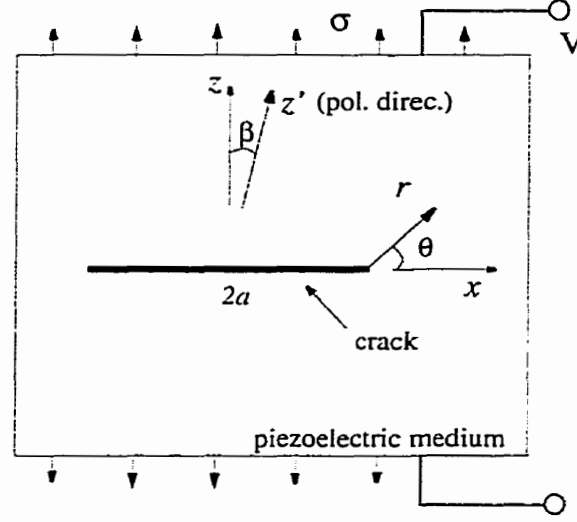


Figure 2.2: Arbitrarily oriented crack in a piezoelectric plane.

2.2 Impermeable crack

Assume the crack faces in Figure 2.2 are electrically impermeable. Therefore,

$$\sigma_{zz} = 0; \quad \sigma_{xz} = 0; \quad D_z = 0; \quad (-a \leq x \leq a) \quad (2.31)$$

The case for an impermeable crack can be obtained by letting b of an impermeable void approach zero. Using eqns (2.17), (2.19) and (2.20), complex functions $\varphi_n(z_n)$, $\varphi'_n(z_n)$ reduce to

$$\varphi_n(z_n) = c_n z_n + \frac{1}{2} (-\Lambda_{n1} \sigma_{zz}^\infty + \Lambda_{n2} \sigma_{xz}^\infty + \Lambda_{n3} D_z^\infty) (z_n - \sqrt{z_n^2 - a^2}) \quad (2.32)$$

$$\varphi'_n(z_n) = c_n + \frac{1}{2} (-\Lambda_{n1} \sigma_{zz}^\infty + \Lambda_{n2} \sigma_{xz}^\infty + \Lambda_{n3} D_z^\infty) \left(1 - \frac{z_n}{\sqrt{z_n^2 - a^2}}\right) \quad (2.33)$$

It is interesting to note that loading components σ_{xx}^∞ and D_x^∞ are not present in above equations. Electroelastic fields in a cracked plane can be obtained by substituting eqns (2.32), (2.33) into eqn (2.9). Crack opening displacements (COD) are defined as the jump in the displacements along the crack line ($z = 0$). It can be shown that crack opening displacements Δu_x and Δu_z are

$$\begin{aligned} \Delta u_x &= 2\sqrt{a^2 - x^2} \operatorname{Im} \sum_{n=1}^3 p_n (-\Lambda_{n1} \sigma_{zz}^\infty + \Lambda_{n2} \sigma_{xz}^\infty + \Lambda_{n3} D_z^\infty) \\ \Delta u_z &= 2\sqrt{a^2 - x^2} \operatorname{Im} \sum_{n=1}^3 q_n (-\Lambda_{n1} \sigma_{zz}^\infty + \Lambda_{n2} \sigma_{xz}^\infty + \Lambda_{n3} D_z^\infty) \end{aligned} \quad (2.34)$$

To ensure that a crack remains open, the z -component of opening displacements should not be negative. Thus,

$$\text{Im} \sum_{n=1}^3 q_n (-\Lambda_{n1} \sigma_{zz}^{\infty} + \Lambda_{n2} \sigma_{xz}^{\infty} + \Lambda_{n3} D_z^{\infty}) \geq 0 \quad (2.35)$$

In fracture mechanics applications, the electromechanical fields in the vicinity of the crack tip are of primary interest. Introduce a polar coordinate system (r, θ) with the origin at the right crack tip, as shown in Figure 2.2. Then,

$$z_n = a + r(\cos \theta + \mu_n \sin \theta) \quad \text{with } r > 0 \quad (2.36)$$

By assuming that r is small in comparison with the half crack length a , the following explicit analytical solutions for crack tip asymptotic fields can be obtained.

$$\begin{aligned} u_x(r, \theta) &= \sqrt{2r} \text{Re} \sum_{n=1}^3 p_n h_n \sqrt{\cos \theta + \mu_n \sin \theta}; & u_z(r, \theta) &= \sqrt{2r} \text{Re} \sum_{n=1}^3 q_n h_n \sqrt{\cos \theta + \mu_n \sin \theta} \\ \phi(r, \theta) &= \sqrt{2r} \text{Re} \sum_{n=1}^3 s_n h_n \sqrt{\cos \theta + \mu_n \sin \theta} \\ \sigma_{xx}(r, \theta) &= \frac{1}{\sqrt{2r}} \text{Re} \sum_{n=1}^3 \frac{h_n \mu_n^2}{\sqrt{\cos \theta + \mu_n \sin \theta}}; & \sigma_{zz}(r, \theta) &= \frac{1}{\sqrt{2r}} \text{Re} \sum_{n=1}^3 \frac{h_n}{\sqrt{\cos \theta + \mu_n \sin \theta}} \\ \sigma_{xz}(r, \theta) &= -\frac{1}{\sqrt{2r}} \text{Re} \sum_{n=1}^3 \frac{h_n \mu_n}{\sqrt{\cos \theta + \mu_n \sin \theta}} \\ D_x(r, \theta) &= \frac{1}{\sqrt{2r}} \text{Re} \sum_{n=1}^3 \frac{h_n \mu_n \delta_n}{\sqrt{\cos \theta + \mu_n \sin \theta}}; & D_z(r, \theta) &= -\frac{1}{\sqrt{2r}} \text{Re} \sum_{n=1}^3 \frac{h_n \delta_n}{\sqrt{\cos \theta + \mu_n \sin \theta}} \\ E_x(r, \theta) &= -\frac{1}{\sqrt{2r}} \text{Re} \sum_{n=1}^3 \frac{h_n s_n}{\sqrt{\cos \theta + \mu_n \sin \theta}}; & E_z(r, \theta) &= -\frac{1}{\sqrt{2r}} \text{Re} \sum_{n=1}^3 \frac{h_n t_n}{\sqrt{\cos \theta + \mu_n \sin \theta}} \end{aligned} \quad (2.37)$$

where

$$h_n = \sqrt{a} (\Lambda_{n1} \sigma_{zz}^{\infty} - \Lambda_{n2} \sigma_{xz}^{\infty} - \Lambda_{n3} D_z^{\infty}); \quad n = 1, 2, 3 \quad (2.38)$$

Eqn (2.37) implies that classical inverse square root type singularity exists for stresses and electric displacements at the tip of an impermeable crack irrespective of the orientation angle β .

If the remote electric loading are electric fields instead of electric displacements, D_z^∞ in crack solutions given by eqns (2.32)-(2.38) is replaced by,

$$D_z^\infty = \frac{1}{d_{11}d_{22} - d_{12}^2} [d_{11}E_z^\infty - d_{12}E_x^\infty + (b_{21}d_{11} - b_{11}d_{12})\sigma_{xx}^\infty + (b_{22}d_{11} - b_{12}d_{12})\sigma_{zz}^\infty + (b_{23}d_{11} - b_{13}d_{12})\sigma_{xz}^\infty] \quad (2.39)$$

Eqn (2.39) indicates that loading σ_{xx}^∞ and E_x^∞ may have an effect on the crack solution.

Along the self-similar plane of the crack ($\theta = 0$), the normal and shear components of stresses and normal electric displacement are decoupled and

$$\sigma_{zz}(r, 0) = \frac{\sqrt{a}}{\sqrt{2r}}\sigma_{zz}^\infty; \quad \sigma_{xz}(r, 0) = \frac{\sqrt{a}}{\sqrt{2r}}\sigma_{xz}^\infty; \quad D_z(r, 0) = \frac{\sqrt{a}}{\sqrt{2r}}D_z^\infty \quad (2.40)$$

The conventional intensity factors (Suo *et al.*, 1992) defined at the crack tip are

$$K_I = \sqrt{\pi a} \sigma_{zz}^\infty; \quad K_{II} = \sqrt{\pi a} \sigma_{xz}^\infty; \quad K_D = \sqrt{\pi a} D_z^\infty \quad (2.41)$$

Crack tip hoop stress is another important parameter in fracture mechanics. It can be shown that,

$$\sigma_{\theta\theta}(r, \theta) = \frac{1}{\sqrt{2r}} \operatorname{Re} \sum_{n=1}^3 h_n (\cos \theta + \mu_n \sin \theta)^{3/2} \quad (2.42)$$

Assuming self-similar crack propagation, the energy release rate can be obtained by extending Irwin's concept of crack closure integral for elastic problems (Irwin, 1957). For piezoelectric crack problems, mechanical (strain) energy and electrical energy co-exist due to the coupling between electric and elastic fields, and the sum of these two energies is the total energy. Suppose a crack extends by a small amount δa , the total energy release rate by the crack closure integral can be expressed in the following form using the polar coordinate system shown in Fig. 2.2.

$$G = \lim_{\delta a \rightarrow 0} \frac{1}{2\delta a} \int_0^{\delta a} \{ \sigma_{iz}(x, 0) u_i(\delta a - x, \pm\pi) + D_z(x, 0) \phi(\delta a - x, \pm\pi) \} dx \quad (2.43)$$

where $i = x, z$ for mode II and I respectively; x is defined along the crack front; $u_i(\delta a - x, \pm\pi) \equiv u_i(\delta a - x, \pi) - u_i(\delta a - x, -\pi)$ denotes displacement jump; $\sigma_{iz}(x, 0)$ denote stress components near the crack tip; $D_z(x, 0)$ denotes the electric displacement component near the crack tip; $\phi(\delta a - x, \pm\pi)$ denotes electric potential jump across the crack.

The first part of the integral in eqn (2.43) corresponds to the mechanical (strain) energy release rate G^M , and the second part to the electric energy release rate G^E . The total energy release rate $G = G^M + G^E$.

In the case of far-field uniform stresses and electric displacements (σ_{xx}^∞ , σ_{zz}^∞ , σ_{xz}^∞ and D_x^∞ , D_z^∞), it can be shown that

$$\begin{aligned}
G^M &= \frac{\pi a}{2} \left[-Im \sum_{n=1}^3 q_n \Lambda_{n1} (\sigma_{zz}^\infty)^2 + Im \sum_{n=1}^3 p_n \Lambda_{n2} (\sigma_{xz}^\infty)^2 + Im \sum_{n=1}^3 (q_n \Lambda_{n2} - p_n \Lambda_{n1}) \sigma_{zz}^\infty \sigma_{xz}^\infty \right. \\
&\quad \left. + Im \sum_{n=1}^3 p_n \Lambda_{n3} \sigma_{xz}^\infty D_z^\infty + Im \sum_{n=1}^3 q_n \Lambda_{n3} \sigma_{zz}^\infty D_z^\infty \right] \\
G^E &= \frac{\pi a}{2} \left[-Im \sum_{n=1}^3 s_n \Lambda_{n1} \sigma_{zz}^\infty D_z^\infty + Im \sum_{n=1}^3 s_n \Lambda_{n2} \sigma_{xz}^\infty D_z^\infty + Im \sum_{n=1}^3 s_n \Lambda_{n3} (D_z^\infty)^2 \right] \quad (2.44)
\end{aligned}$$

For the special case of poling direction perpendicular to the crack surface ($\beta = 0$), Pak (1992) obtained the expression of G_I for PZT-5H. Park and Sun (1995b) presented the expressions of G_I^M for PZT-4. It can be shown that using the material properties given in the Appendix A and setting $\beta = 0$, eqn (2.44) reduces to

$$\begin{aligned}
G_I^M(\sigma_{zz}^\infty, D_z^\infty) &= \frac{\pi a}{2} [1.749 \times 10^{-11} (\sigma_{zz}^\infty)^2 + 2.214 \times 10^{-2} \sigma_{zz}^\infty D_z^\infty] \\
G_I^M(\sigma_{zz}^\infty, E_z^\infty) &= \frac{\pi a}{2} [2.280 \times 10^{-11} (\sigma_{zz}^\infty)^2 + 2.221 \times 10^{-10} \sigma_{zz}^\infty E_z^\infty] \quad (2.45)
\end{aligned}$$

for PZT-4 and the total energy release rate

$$\begin{aligned}
G_I(\sigma_{zz}^\infty, D_z^\infty) &= \frac{a}{8} [2.020 \times 10^{-10} (\sigma_{zz}^\infty)^2 + 2 \times 1.605 \times 10^{-1} \sigma_{zz}^\infty D_z^\infty - 5.749 \times 10^8 (D_z^\infty)^2] \\
G_I(\sigma_{zz}^\infty, E_z^\infty) &= \frac{a}{8} [2.462 \times 10^{-10} (\sigma_{zz}^\infty)^2 + 2 \times 4.840 \times 10^{-11} \sigma_{zz}^\infty E_z^\infty - 2.416 \times 10^{-7} (E_z^\infty)^2] \quad (2.46)
\end{aligned}$$

for PZT-5H. Eqns (2.45) and (2.46) are identical (up to the numerical accuracy) to those given by Park and Sun (1995b) and Pak (1992), respectively.

2.3 Conducting crack

A conducting crack model is suitable when a conducting species migrates on the crack surfaces. Assume the crack faces in Figure 2.2 are conducting, which is

$$\sigma_{zz} = 0; \quad \sigma_{xz} = 0; \quad E_x = 0; \quad (-a \leq x \leq a) \quad (2.47)$$

The solution for a conducting crack can be obtained in a manner similar to the case of an impermeable crack. A void with the conducting boundary is solved first, and the crack solution can then be obtained by letting b approach zero in the void solution. It is found

that the loading component E_z^∞ has no influence on a conducting crack. Neglecting the details for brevity, the final solutions are summarized below.

Crack opening displacements Δu_x and Δu_z are

$$\begin{aligned}\Delta u_x &= 2\sqrt{a^2 - x^2} \operatorname{Im} \sum_{n=1}^3 p_n (-\bar{\Lambda}_{n1} \sigma_{zz}^\infty + \bar{\Lambda}_{n2} \sigma_{xz}^\infty + \bar{\Lambda}_{n3} E_x^\infty) \\ \Delta u_z &= 2\sqrt{a^2 - x^2} \operatorname{Im} \sum_{n=1}^3 q_n (-\bar{\Lambda}_{n1} \sigma_{zz}^\infty + \bar{\Lambda}_{n2} \sigma_{xz}^\infty + \bar{\Lambda}_{n3} E_x^\infty)\end{aligned}\quad (2.48)$$

where

$$\begin{pmatrix} \bar{\Lambda}_{11} & \bar{\Lambda}_{12} & \bar{\Lambda}_{13} \\ \bar{\Lambda}_{21} & \bar{\Lambda}_{22} & \bar{\Lambda}_{23} \\ \bar{\Lambda}_{31} & \bar{\Lambda}_{32} & \bar{\Lambda}_{33} \end{pmatrix} = \frac{1}{\bar{\Delta}} \begin{pmatrix} \mu_2 s_3 - \mu_3 s_2 & s_2 - s_3 & \mu_3 - \mu_2 \\ \mu_3 s_1 - \mu_1 s_3 & s_3 - s_1 & \mu_1 - \mu_3 \\ \mu_1 s_2 - \mu_2 s_1 & s_1 - s_2 & \mu_2 - \mu_1 \end{pmatrix}\quad (2.49)$$

$$\bar{\Delta} = \mu_1(s_2 - s_3) + \mu_2(s_3 - s_1) + \mu_3(s_1 - s_2)\quad (2.50)$$

To ensure that cracks remain open,

$$\operatorname{Im} \sum_{n=1}^3 q_n (-\bar{\Lambda}_{n1} \sigma_{zz}^\infty + \bar{\Lambda}_{n2} \sigma_{xz}^\infty + \bar{\Lambda}_{n3} E_x^\infty) \geq 0\quad (2.51)$$

The conventional intensity factors defined at the crack tip are

$$K_I = \sqrt{\pi a} \sigma_{zz}^\infty; \quad K_{II} = \sqrt{\pi a} \sigma_{xz}^\infty; \quad K_E = \sqrt{\pi a} E_x^\infty\quad (2.52)$$

Using the polar coordinate system (r, θ) in Fig. 2.2, crack tip fields are expressed as,

$$\begin{aligned}\{u_x, u_z, \phi\}^T &= \sqrt{2r} \operatorname{Re} \sum_{n=1}^3 \{p_n, q_n, s_n\}^T \bar{h}_n \sqrt{\cos \theta + \mu_n \sin \theta} \\ \{\sigma_{xx}, \sigma_{zz}, \sigma_{xz}\}^T &= \frac{1}{\sqrt{2r}} \operatorname{Re} \sum_{n=1}^3 \{\mu_n^2, 1, -\mu_n\}^T \frac{\bar{h}_n}{\sqrt{\cos \theta + \mu_n \sin \theta}} \\ \{D_x, D_z\}^T &= \frac{1}{\sqrt{2r}} \operatorname{Re} \sum_{n=1}^3 \{\delta_n \mu_n, -\delta_n\}^T \frac{\bar{h}_n}{\sqrt{\cos \theta + \mu_n \sin \theta}} \\ \{E_x, E_z\}^T &= -\frac{1}{\sqrt{2r}} \operatorname{Re} \sum_{n=1}^3 \{s_n, t_n\}^T \frac{\bar{h}_n}{\sqrt{\cos \theta + \mu_n \sin \theta}}\end{aligned}\quad (2.53)$$

where

$$\bar{h}_n = \sqrt{a} (\bar{\Lambda}_{n1} \sigma_{zz}^\infty - \bar{\Lambda}_{n2} \sigma_{xz}^\infty - \bar{\Lambda}_{n3} E_x^\infty); \quad n = 1, 2, 3\quad (2.54)$$

The expression of crack tip hoop stress is found to be identical to eqn (2.42), except that h_n should be replaced by \bar{h}_n . Assuming self-similar crack propagation, the total energy release rate can be expressed in the following form.

$$G = \lim_{\delta a \rightarrow 0} \frac{1}{2\delta a} \int_0^{\delta a} \{\sigma_{iz}(x, 0)u_i(\delta a - x, \pm\pi) + \phi(x, 0)D_z(\delta a - x, \pm\pi)\} dx \quad (2.55)$$

where variables δa etc are defined under eqn (2.43).

In the case of far-field uniform stresses and electric displacements (σ_{xx}^∞ , σ_{zz}^∞ , σ_{xz}^∞ and E_x^∞ , E_z^∞),

$$\begin{aligned} G^M &= \frac{\pi a}{2} \left[-Im \sum_{n=1}^3 q_n \bar{\Lambda}_{n1} (\sigma_{zz}^\infty)^2 + Im \sum_{n=1}^3 p_n \bar{\Lambda}_{n2} (\sigma_{xz}^\infty)^2 + Im \sum_{n=1}^3 (q_n \bar{\Lambda}_{n2} - p_n \bar{\Lambda}_{n1}) \sigma_{zz}^\infty \sigma_{xz}^\infty \right. \\ &\quad \left. + Im \sum_{n=1}^3 p_n \bar{\Lambda}_{n3} \sigma_{xz}^\infty E_x^\infty + Im \sum_{n=1}^3 q_n \bar{\Lambda}_{n3} \sigma_{zz}^\infty E_x^\infty \right] \\ G^E &= \frac{\pi a}{2} \left[-Im \sum_{n=1}^3 \delta_n \bar{\Lambda}_{n1} \sigma_{zz}^\infty E_x^\infty + Im \sum_{n=1}^3 \delta_n \bar{\Lambda}_{n2} \sigma_{xz}^\infty E_x^\infty + Im \sum_{n=1}^3 \delta_n \bar{\Lambda}_{n3} (E_x^\infty)^2 \right] \end{aligned} \quad (2.56)$$

For the special case of poling direction perpendicular to the crack surface ($\beta = 0$), Zhang *et al* (1998) obtained the expression of G for PZT-4 (PZT-4a in the Appendix A). It can be shown that using the material properties given in the Appendix A and setting $\beta = 0$, eqn (2.56) reduces to

$$G = a[3.629 \times 10^{-11} (\sigma_{zz}^\infty)^2 + 3.40 \times 10^{-11} (\sigma_{xz}^\infty)^2 + 6.758 \times 10^{-10} \sigma_{xz}^\infty E_x^\infty + 1.197 \times 10^{-8} (E_x^\infty)^2] \quad (2.57)$$

Eqn (2.57) is identical (up to the numerical accuracy) to the result given by Zhang *et al* (1998) where the term $\sigma_{xz}^\infty E_x^\infty$ was neglected.

2.4 Other crack boundary conditions

For cracks containing air or vacuum in piezoelectrics, the permeable crack model (Polovinkina and Ulitko, 1978) and the Hao & Shen type crack model (Hao and Shen, 1994) are also used in the literature besides the impermeable crack model. No agreement has been reached so far on the nature of the crack boundary conditions. The solutions for an impermeable crack and a conducting crack have been derived by reducing the solutions for an impermeable void and a conducting void, respectively. The exact void solution has been obtained in subsection 2.2.3 by considering a permeable void boundary. A logical question is: can the exact crack solution be obtained by reducing the exact void solution?

In this section, the application of reducing the permeable void solution to the crack solution is examined first. A unified formulation for cracks containing air or vacuum, which accounts for three existing types of crack boundary conditions, is then developed.

It is a common practice to deduce the solution for a crack from a void solution by setting $b = 0$. Following this practice, setting $b = 0$ in eqns (2.26)-(2.30) for a permeable void yields

$$\varphi_n(z_n) = c_n z_n - \frac{1}{2\sqrt{a}} [\Lambda_{n1} \sigma_{zz}^\infty - \Lambda_{n2} \sigma_{xz}^\infty - \Lambda_{n3} (D_z^\infty - D_z^0)] (z_n - \sqrt{z_n^2 - a^2}) \quad (2.58)$$

$$D_z^0 = \frac{Im \sum_{n=1}^3 s_n (-\Lambda_{n1} \sigma_{zz}^\infty + \Lambda_{n2} \sigma_{xz}^\infty)}{Im \sum_{n=1}^3 s_n \Lambda_{n3}} + D_z^\infty \quad (2.59)$$

Eqns (2.58), (2.59) based on the permeable void solution indicate that remote electric loading has no influence on the crack problems. For the special case of $\beta = 0$, Gao and Fan (1999) made the same observation by setting $b = 0$ in their permeable void solution. They concluded that such a solution is exact with respect to electric boundary conditions and should be used when solving fracture problems in piezoelectric materials.

The applicability of above reduction, however, should be examined. In the case of a void with impermeable or conducting boundary, such a reduction is reliable since the crack boundary conditions are consistent with the void boundary conditions. When dealing with a permeable void, such a reduction has to be carefully applied. When letting $b = 0$, the medium inside the void physically vanishes, and the original two-domain problem (void case) becomes an one-domain problem (crack case). Consequently, the following continuities of electrical potential and normal electric displacement across the crack faces are automatically established.

$$D_z^+ = D_z^-; \quad \phi^+ = \phi^- \quad (2.60)$$

where the superscripts $+$ and $-$ indicate the upper and lower crack surfaces, respectively.

Cracks described by eqn (2.60) are referred to as permeable cracks in literature. This type of crack face electric conditions was initially proposed by Polovinkina and Ulitko (1978). In fact, eqn (2.60) implies that a crack has no impact on the electric field. Therefore, in contrary to Gao and Fan's (1999) conclusion, the crack solution given by eqns (2.58) and (2.59) is not the solution for exact electric boundary conditions. It yields the already known solution for a permeable crack as shown in the sequel.

Zhang and Tong (1996) presented an interesting discussion on reducing void solutions to crack solutions. They introduced two dimensionless parameters (functions of crack geometry and permittivity) to examine different limiting processes. It was found that permeable

cracks and impermeable cracks correspond to two different limiting cases. Such a scheme, however, is not utilized here. This section aims at closely examining three existing crack models including a permeable crack, an impermeable crack and a Hao and Shen type crack.

Deeg (1980), Pak (1992) and Suo *et al* (1992) assumed that crack faces are impermeable, *i.e.*

$$D_z^+ = D_z^- = 0 \quad (2.61)$$

Hao and Shen (1994) argued that neither eqns (2.60) nor (2.61) could avoid being one-sided. By considering the electrical permeability of air or vacuum in a crack, they proposed the following electric conditions on crack faces.

$$D_z^+ = D_z^-; \quad D_z^+(u_2^+ - u_2^-) = \epsilon_v(\phi^- - \phi^+) \quad (2.62)$$

For the special case of $\epsilon_v = 0$, *i.e.* a medium having zero permittivity, eqn (2.62) reduces to the conditions for an impermeable crack. If potential jump ($\phi^+ - \phi^-$) is zero, eqn (2.62) reduces to the case of a permeable crack. The influence of crack face conditions expressed by eqn (2.62) on fracture parameters is not clear from the analysis given by Hao and Shen (1994). Limited numerical results given by them shed little insight into the effects of eqn (2.62).

A unified formulation that accounts for different electric boundary conditions [eqns(2.60) - (2.62)] is developed in the ensuing part of this section for an arbitrarily oriented crack containing air or vacuum. This new solution allows the theoretical treatment of cracks in piezoelectrics by using a single analysis. The three types of electric boundary conditions commonly assume that the normal electric displacement is continuous across the crack faces. The electric field has been shown uniform (special case of an elliptical void) under uniform loading (Chen and Lai, 1997). Therefore,

$$D_z^+ = D_z^- = D_z^0 \quad (2.63)$$

where D_z^0 is a constant.

Following relations can be obtained by using eqns (2.9), (2.63) and vanishing tractions on crack faces.

$$\begin{aligned} 2Re \sum_{n=1}^3 \varphi_n(x) &= 0; & 2Re \sum_{n=1}^3 \mu_n \varphi_n(x) &= 0 \\ 2Re \sum_{n=1}^3 \delta_n \varphi_n(x) &= -D_z^0 x \end{aligned} \quad (2.64)$$

where x is along the crack line ($-a \leq x \leq a$), and the complex functions φ_n ($n = 1, 2, 3$) are in the form of eqn (2.12).

Applying the mapping of eqn (2.13), $\varphi_n(z_n)$ identical to eqn (2.58) are obtained. Crack tip fields can be expressed by using the polar coordinate system (r, θ) in Fig. 2.2 as,

$$\begin{aligned} \{u_x, u_z, \phi\}^T &= \sqrt{2r} \operatorname{Re} \sum_{n=1}^3 \{p_n, q_n, s_n\}^T \hat{h}_n \sqrt{\cos \theta + \mu_n \sin \theta} \\ \{\sigma_{xx}, \sigma_{zz}, \sigma_{xz}\}^T &= \frac{1}{\sqrt{2r}} \operatorname{Re} \sum_{n=1}^3 \{\mu_n^2, 1, -\mu_n\}^T \frac{\hat{h}_n}{\sqrt{\cos \theta + \mu_n \sin \theta}} \\ \{D_x, D_z\}^T &= \frac{1}{\sqrt{2r}} \operatorname{Re} \sum_{n=1}^3 \{\delta_n \mu_n, -\delta_n\}^T \frac{\hat{h}_n}{\sqrt{\cos \theta + \mu_n \sin \theta}} \\ \{E_x, E_z\}^T &= -\frac{1}{\sqrt{2r}} \operatorname{Re} \sum_{n=1}^3 \{s_n, t_n\}^T \frac{\hat{h}_n}{\sqrt{\cos \theta + \mu_n \sin \theta}} \end{aligned} \quad (2.65)$$

where

$$\hat{h}_n = \sqrt{a} [\Lambda_{n1} \sigma_{zz}^\infty - \Lambda_{n2} \sigma_{xz}^\infty - \Lambda_{n3} (D_z^\infty - D_z^0)]; \quad n = 1, 2, 3 \quad (2.66)$$

Eqn (2.65) implies that classical inverse square root type singularity exists for stresses and electric displacements irrespective of the crack orientation angle and the type of electric boundary conditions.

Crack opening displacements (COD) and the jump of electric potential along the crack line ($-a \leq x \leq a$) can be obtained as,

$$\begin{aligned} u_x^+ - u_x^- &= -2\sqrt{a^2 - x^2} \operatorname{Im} \sum_{n=1}^3 p_n [\Lambda_{n1} \sigma_{zz}^\infty - \Lambda_{n2} \sigma_{xz}^\infty - \Lambda_{n3} (D_z^\infty - D_z^0)] \\ u_z^+ - u_z^- &= -2\sqrt{a^2 - x^2} \operatorname{Im} \sum_{n=1}^3 q_n [\Lambda_{n1} \sigma_{zz}^\infty - \Lambda_{n2} \sigma_{xz}^\infty - \Lambda_{n3} (D_z^\infty - D_z^0)] \\ \phi^+ - \phi^- &= -2\sqrt{a^2 - x^2} \operatorname{Im} \sum_{n=1}^3 s_n [\Lambda_{n1} \sigma_{zz}^\infty - \Lambda_{n2} \sigma_{xz}^\infty - \Lambda_{n3} (D_z^\infty - D_z^0)] \end{aligned} \quad (2.67)$$

To ensure that cracks remain open,

$$\operatorname{Im} \sum_{n=1}^3 q_n (-\Lambda_{n1} \sigma_{zz}^\infty + \Lambda_{n2} \sigma_{xz}^\infty + \Lambda_{n3} (D_z^\infty - D_z^0)) \geq 0 \quad (2.68)$$

The problem now reduces to determining the constant D_z^0 . An additional condition other than eqn (2.63) must be considered. Apparently, this condition comes from eqns

(2.60), (2.61) and (2.62) for permeable, impermeable and the Hao & Shen type cracks, respectively.

For an impermeable crack, substituting $D_z^0 = 0$ into eqn (2.65) yields the complete electroelastic fields.

For a permeable crack (eqn (2.60)), D_z^0 is obtained by vanishing of the electric potential jump expressed by eqn (2.67). The result is identical to D_z^0 given by eqn (2.59). Therefore, the exact solution claimed by Gao and Fan (1999) is indeed the solution for a permeable crack.

For a Hao & Shen type crack, the following solution for D_z^0 can be obtained by using eqns (2.62) and (2.67).

$$D_z^0 = -\varepsilon_v \frac{Im \sum_{n=1}^3 s_n [\Lambda_{n1} \sigma_{zz}^\infty - \Lambda_{n2} \sigma_{xz}^\infty - \Lambda_{n3} (D_z^\infty - D_z^0)]}{Im \sum_{n=1}^3 q_n [\Lambda_{n1} \sigma_{zz}^\infty - \Lambda_{n2} \sigma_{xz}^\infty - \Lambda_{n3} (D_z^\infty - D_z^0)]} \quad (2.69)$$

Eqns (2.59) and (2.69) show that, in contrast to vanishing D_z^0 for impermeable cracks, permeable and the Hao and Shen type cracks generally result in non-zero crack face electric displacements. Both far field mechanical and electric loading may contribute to D_z^0 . Note that eqn (2.69) is a quadratic of D_z^0 (except $\varepsilon_v = 0$), and two real or complex roots may exist. On the other hand, D_z^0 should be uniquely determined for a given piezoelectric material and applied loading. This issue was not discussed by Hao and Shen (1994).

Stress intensity factors K_I , K_{II} and electric displacement intensity factor K_D can be expressed as,

$$K_I = \sqrt{\pi a} \sigma_{zz}^\infty; \quad K_{II} = \sqrt{\pi a} \sigma_{xz}^\infty; \quad K_D = \sqrt{\pi a} (D_z^\infty - D_z^0) \quad (2.70)$$

Eqn (2.70) shows that K_I and K_{II} are identical for the three types of electric boundary conditions, but K_D is different.

Crack tip hoop stress is found to have the same expression as eqn (2.42), except that h_n should be replaced by \hat{h}_n . Energy release rate on the crack line ($\theta = 0$) can be obtained by using crack closure integral. In the case of far-field uniform stresses and electric

displacements ($\sigma_{xx}^\infty, \sigma_{zz}^\infty, \sigma_{xz}^\infty$ and D_x^∞, D_z^∞),

$$\begin{aligned}
G^M &= \frac{\pi a}{2} \left[-Im \sum_{n=1}^3 q_n \Lambda_{n1} (\sigma_{zz}^\infty)^2 + Im \sum_{n=1}^3 p_n \Lambda_{n2} (\sigma_{xz}^\infty)^2 + Im \sum_{n=1}^3 (q_n \Lambda_{n2} - p_n \Lambda_{n1}) \sigma_{zz}^\infty \sigma_{xz}^\infty \right. \\
&\quad \left. + Im \sum_{n=1}^3 p_n \Lambda_{n3} \sigma_{xz}^\infty (D_z^\infty - D_z^0) + Im \sum_{n=1}^3 q_n \Lambda_{n3} \sigma_{zz}^\infty (D_z^\infty - D_z^0) \right] \\
G^E &= \frac{\pi a}{2} \left[-Im \sum_{n=1}^3 s_n \Lambda_{n1} \sigma_{zz}^\infty (D_z^\infty - D_z^0) + Im \sum_{n=1}^3 s_n \Lambda_{n2} \sigma_{xz}^\infty (D_z^\infty - D_z^0) \right. \\
&\quad \left. + Im \sum_{n=1}^3 s_n \Lambda_{n3} (D_z^\infty - D_z^0)^2 \right] \tag{2.71}
\end{aligned}$$

2.5 Numerical results and discussion

In this section, coupled stress and electric fields around an arbitrarily oriented elliptical void and at a crack tip are computed using the closed form solutions derived earlier. Plane strain conditions are used. The condition of crack closure (eqn (2.35), eqn (2.51) or eqn (2.68)) is checked during the computation. The effect of crack orientation and electric boundary condition on fracture parameters such as hoop stress and energy release rates is discussed. The role of an applied electric field is examined. PZT-4 and PZT-5H (material properties are given in Appendix A) are used in the numerical study.

2.5.1 Electroelastic fields around a void

Consider an elliptical void with electrically impermeable boundary and geometry ratio $a/b = 2$ (Figure 2.1). Figure 2.3 shows the electroelastic field around the boundary of the void due to remote tension $\sigma_{z'z'}$. The results for two void orientations ($\beta = 0^\circ$ and 30°) are shown. In the absence of any other known solutions for an arbitrarily oriented elliptical void, the analytical solutions obtained in this Chapter are compared with the boundary element based solutions (Xu and Rajapakse, 1998). Thirty-two quadratic boundary elements were used in the boundary element analysis. The boundary element solutions agree closely with the analytical solutions. In the case of $\beta = 0^\circ$, the hoop stresses show symmetry with respect to the x and z -axes, whereas the electric displacements are symmetric with respect to the x -axis and antisymmetric with respect to the z -axis. For $\beta = 30^\circ$, the hoop stresses and electric displacements are no longer symmetric or antisymmetric about the void axes, and show a significant dependence on the orientation angle β for all values of θ . Quite often it has been considered that the critical values of field variables occur when the defects are

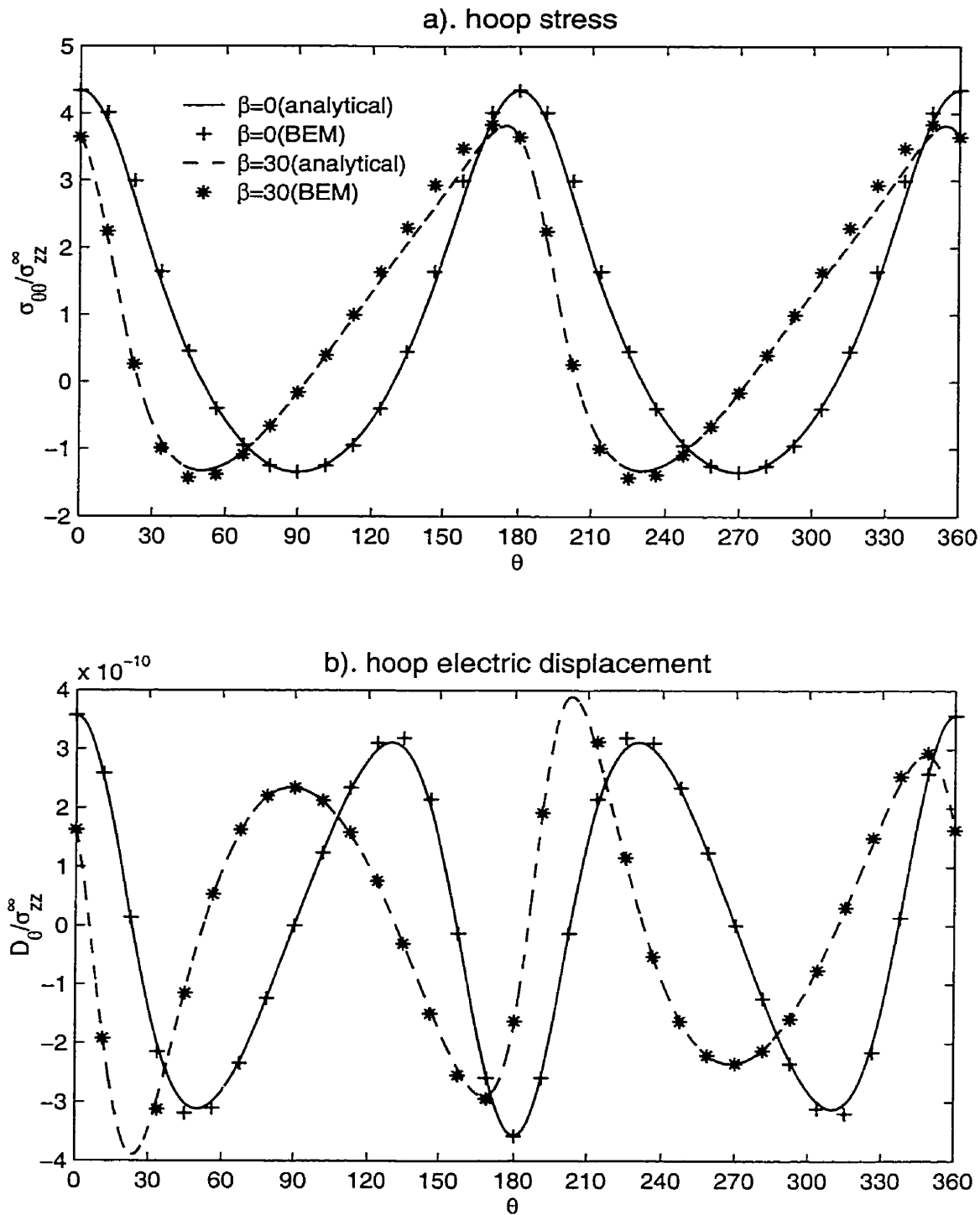


Figure 2.3: Electroelastic field around the boundary of an arbitrarily oriented elliptical hole (impermeable boundary) in PZT-4 due to remote tension.

either parallel or perpendicular to the direction of polarization ($\beta = 0^\circ$ or 90°). Results shown in Fig. 2.3 suggest that this may not be always the case. For example, the maximum value of normalized electric displacement corresponding to $\beta = 30^\circ$ is 9.2% higher than the corresponding value for $\beta = 0^\circ$, and is 66.4% higher than the maximum value for $\beta = 90^\circ$.

Taking advantage of obtained explicit solutions, the critical values of field variables for an arbitrarily oriented elliptical void under applied electromechanical loading can be readily searched using a simple computer program. To further examine the dependence of void orientation on the electroelastic fields, Figure 2.4 presents the maximum values of hoop stress (tensile) and hoop electric displacement around the boundary of an elliptical void with $a/b = 2$ for different β , under remote mechanical and electric loading. Results are shown only for the range of $\beta \in [0^\circ, 90^\circ]$, due to symmetry of the field variables with respect to the orientation angle. A strong influence of void orientation on the maximum field variables is noted. In the case of remote tension in the z' -direction, the largest value of hoop stress occurs at $\theta = 0^\circ$ when $\beta = 0^\circ$, and the maximum value of hoop stress decreases with increasing β . However, the largest value of electric displacement occurs at $\beta = 40^\circ$, which is 11.2% higher than the value corresponding to $\beta = 0^\circ$. In the case of remote electric loading along the negative z' -axis, the largest value of hoop stress occurs at $\beta = 33^\circ$, which is 26.6% higher than the value for $\beta = 0^\circ$. The largest values of maximum hoop stress under negative electric loading is slightly higher than the corresponding value under positive electric loading. In addition, the maximum hoop stresses remain nearly constant for $30^\circ < \beta < 90^\circ$ under positive electric loading. In contrast, the maximum values of hoop electric displacement are identical for both positive and negative electric loadings, and show dependence on β that is similar to the trend of the hoop stresses under remote tension. The significance of void orientation angle β is clearly confirmed by the results shown in Fig. 2.4.

Now consider an elliptical void with permeable boundary. The medium within the void is vacuum with $\varepsilon_v = \varepsilon_0 = 8.85 \times 10^{-12} C^2/Nm^2$. Remote mechanical or electric loading are applied along z' -axis. The maximum stress concentration factors on the void boundary are computed for the case $\beta = 0^\circ$ and various values of geometry ratio a/b . The results corresponding to the impermeable void boundary are also computed for the purpose of comparison. It is found that permeable voids and impermeable voids have virtually identical results under pure mechanical loading. In the case of electrical loading, results of permeable voids and impermeable voids are quite close when a/b is less than 100. However, the two results are significantly different when a/b is larger than 1000. Therefore, if the geometry ratio of a vacuum void is larger than 1000, the permeable void model should be

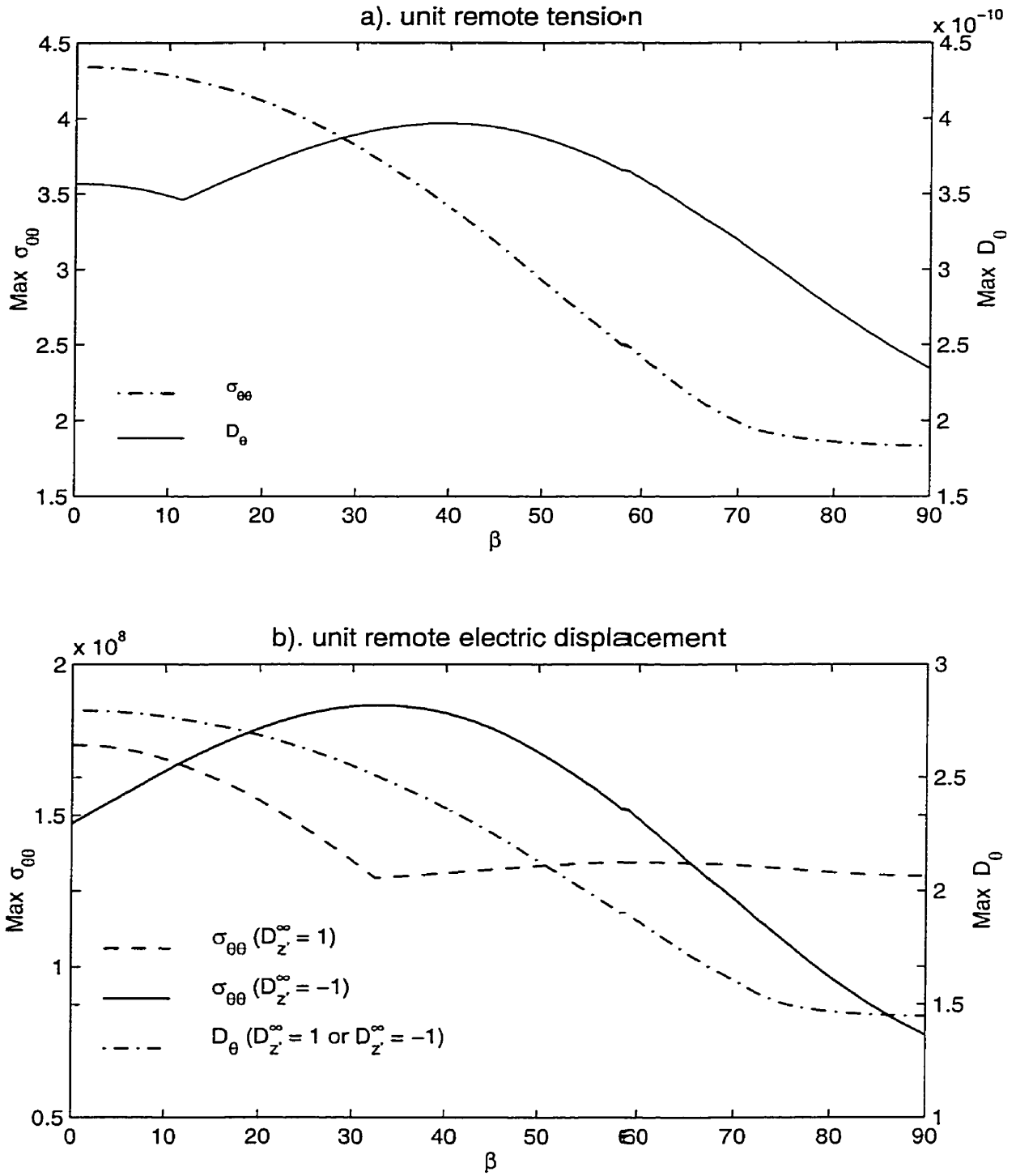


Figure 2.4: Maximum values of hoop stress and electric displacement at the boundary of an elliptical void (impermeable boundary) in PZT-4.

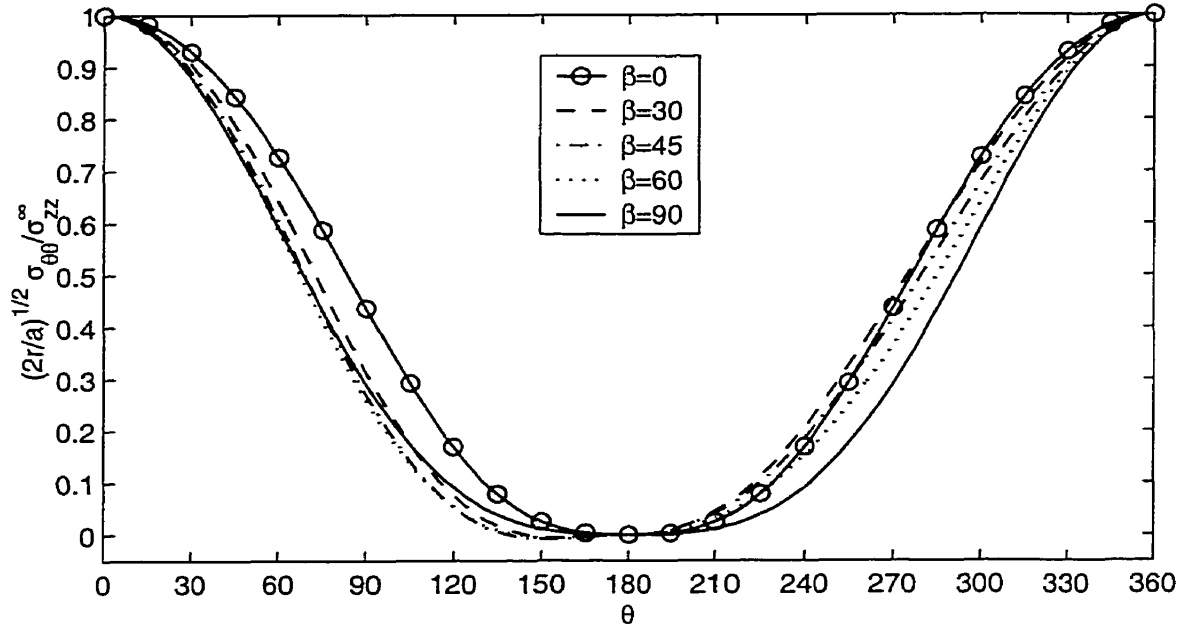


Figure 2.5: Variation of crack tip hoop stresses under remote tension in PZT-4 (impermeable crack).

used for accurate simulation. The case of $\beta \neq 0^\circ$ is also considered, and a similar conclusion is reached. Note that Dunn (1994) drew a similar conclusion for antiplane piezoelectric problems ($\beta = 0^\circ$ or 90°) using the equivalent inclusion method.

2.5.2 Impermeable crack

Assume the crack boundary in Figure 2.2 is electrically impermeable. Figures 2.5 - 2.8 present the distributions of crack tip hoop stress under applied mechanical or electrical loading.

Consider the case of pure tensile stress σ_{zz}^∞ applied along the z -axis first. Variation of normalized hoop stresses $\sqrt{2r/a}\sigma_{\theta\theta}/\sigma_{zz}^\infty$ (a is the half crack length, r is the radial distance from the crack tip) with angle θ are shown in Figure 2.5. Under symmetric loading, the orientation angles $\beta = \alpha$, $\beta = -\alpha$ and $\beta = 180^\circ - \alpha$ (α is arbitrary) yield identical stress fields. Therefore, only $\beta \in [0^\circ, 90^\circ]$ need be considered in the numerical study. Five different orientation angles, $\beta = 0^\circ, 30^\circ, 45^\circ, 60^\circ, 90^\circ$ are considered in the figure. Hoop stress profiles at the crack tip show negligible dependence on orientation angle β . Critical hoop stresses are always observed at $\theta = 0^\circ$ for all values of β . This implies that, under a pure tensile stress, based on maximum hoop stress criterion a crack propagates along the self-similar

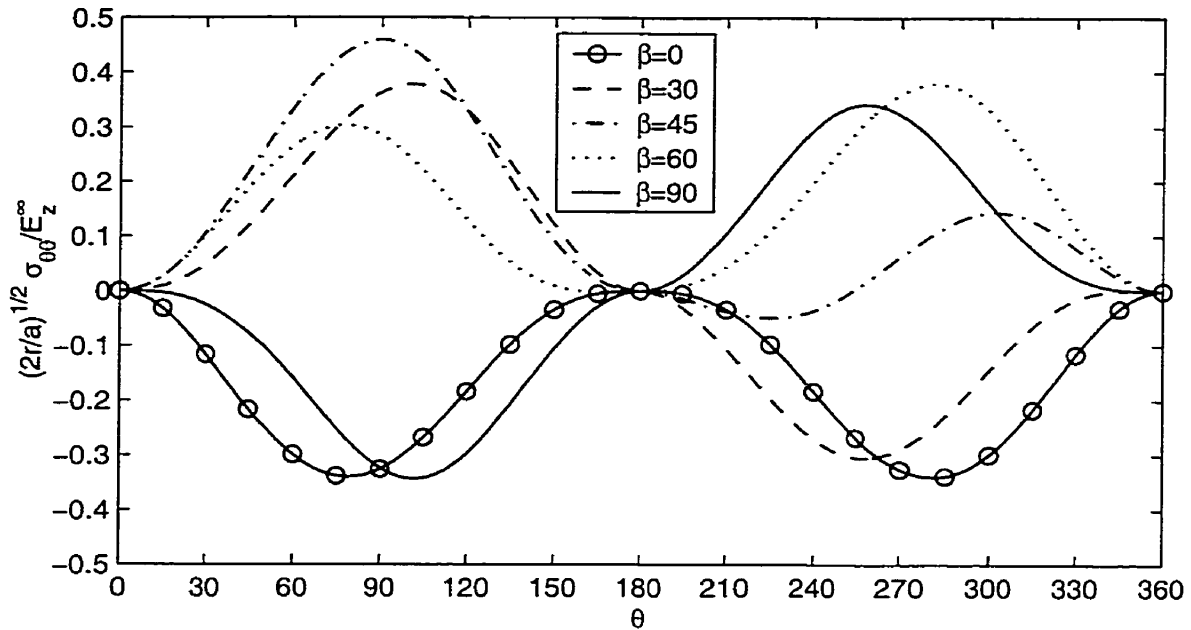


Figure 2.6: Variation of crack tip hoop stresses under remote electric field in PZT-4 (impermeable crack).

plane regardless of its orientation. Hoop stress is symmetrical with respect to the crack face ($\theta = 0$) only in the case of $\beta = 0^\circ$.

Figure 2.6 shows the variation of normalized hoop stresses $\sqrt{2r/a}\sigma_{\theta\theta}/E_z^\infty$ under a pure positive electric field E_z^∞ along the z -axis. The requirement of crack opening displacement given by eqn (2.35) is found to be satisfied for all β for this loading case. It is found that hoop stress distribution depends significantly on the crack orientation. Only the case of $\beta = 0^\circ$ induces symmetrical hoop stresses with respect to the crack face. Compressive hoop stresses are observed for all θ when $\beta = 0^\circ$, implying no crack propagation based on the criterion of maximum hoop stress. However, for $\beta = 90^\circ$ hoop stresses are tensile for $\theta \in [180^\circ, 360^\circ]$. Tensile crack tip stresses are also observed for all values of θ when $\beta = 60^\circ$. Compressive hoop stresses are noted for $\beta = 30^\circ$ in the range $\theta \in [180^\circ, 360^\circ]$, and for $\beta = 45^\circ$ in the range $\theta \in [180^\circ, 253^\circ]$. The critical hoop stresses occur at $\theta = 100.7^\circ, 90^\circ, 281.2^\circ, 258.2^\circ$ for $\beta = 30^\circ, 45^\circ, 60^\circ$ and 90° , respectively. Note that none of these critical hoop stresses occur at $\theta = 0^\circ$, implying that the crack does not extend along a straight line based on the maximum stress criterion. Among all critical values for different orientations, $\beta = 45^\circ$ has a maximum normalized value of 0.4595. Therefore, the most critical case does not correspond to a crack normal to polarization. If the applied electric

field is negative, the stresses are given by Fig. 2.6 with an opposite sign. A crack with $\beta = 60^\circ$ induces compressive hoop stresses for all values of θ . The critical hoop stresses occur at $\theta = 78.8^\circ(281.2^\circ)$, 257.8° , 225.3° and 101.8° for $\beta = 0^\circ$, 30° , 45° and 90° , respectively. Note that the critical hoop stresses for $\beta = 45^\circ$ is very small (only 0.0489). A maximum critical value of 0.3426 is obtained for $\beta = 90^\circ$. The crack opening displacement (COD) defined by eqn (2.35) indicates that crack closure occurs for a negative electric field for all β except $\beta = 90^\circ$. Therefore, under pure electric loading, arbitrarily oriented impermeable cracks may propagate along different planes or close depending on the crack orientation and the direction of applied electric field.

Figure 2.7 shows the variation of normalized hoop stress at the crack tip under combined tension and positive electric field. Three different electric to mechanical load ratios ($R = E_z^\infty / \sigma_{zz}^\infty \text{ Vm/N}$), *i.e.* $R = 0.2, 1.0, 5.0$, are considered. For all values of β and R , eqn (2.35) is satisfied. Symmetric hoop stresses about the crack face are observed only in the case of $\beta = 0^\circ$ for all values of R . For small values of R (0.2), the hoop stress profile is similar to the Fig. 2.5 and critical stresses are noted along the crack plane. The stress distribution has negligible dependence on the orientation angle β . For a unit value of load ratio ($R = 1.0$), a strong influence of crack orientation on the hoop stress distribution is observed. However, the effect on critical values of hoop stresses is still weak. The maximum normalized hoop stress is 1.0 for $\beta = 0^\circ, 30^\circ$ and 90° at $\theta = 0^\circ$. Slightly higher values of hoop stresses are found for $\beta = 45^\circ$ and 60° at $\theta \neq 0^\circ$ (1.0004 at $\theta = 17.3^\circ$ for $\beta = 45^\circ$, 1.009 at $\theta = 323.6^\circ$ for $\beta = 60^\circ$). Compressive hoop stresses are found over a rather limited range of θ for $\beta = 0^\circ, 30^\circ$ and 90° . For larger values of load ratio ($R = 5.0$), a very significant effect of crack orientation is observed similar to that noted in Fig. 2.6. Maximum normalized hoop stress is equal to 1.0 at $\theta = 0^\circ$ for $\beta = 0^\circ$, and much larger critical normalized hoop stresses are found for other values of β at $\theta \neq 0^\circ$, *i.e.* 2.137 for $\beta = 30^\circ$, 2.603 for $\beta = 45^\circ$, 2.394 for $\beta = 60^\circ$, and 1.929 for $\beta = 90^\circ$. Therefore, under combined tension and positive electric field, crack tip fields are controlled by the load ratio R and crack orientation. Once the electric field dominates ($R \gg 1$), the effect is similar to the case of a pure positive electric load.

Consider the same problem as in Figure 2.7 but with a negative electric field. The variation of hoop stress at the crack tip is shown in Figure 2.8. Similar to Figure 2.7, symmetric hoop stresses about the crack face are observed only in the case of $\beta = 0^\circ$. The effect of crack orientation on the hoop stress distribution and critical values of hoop stresses becomes stronger as the load ratio increases. Based on eqn (2.35), it is interesting to note

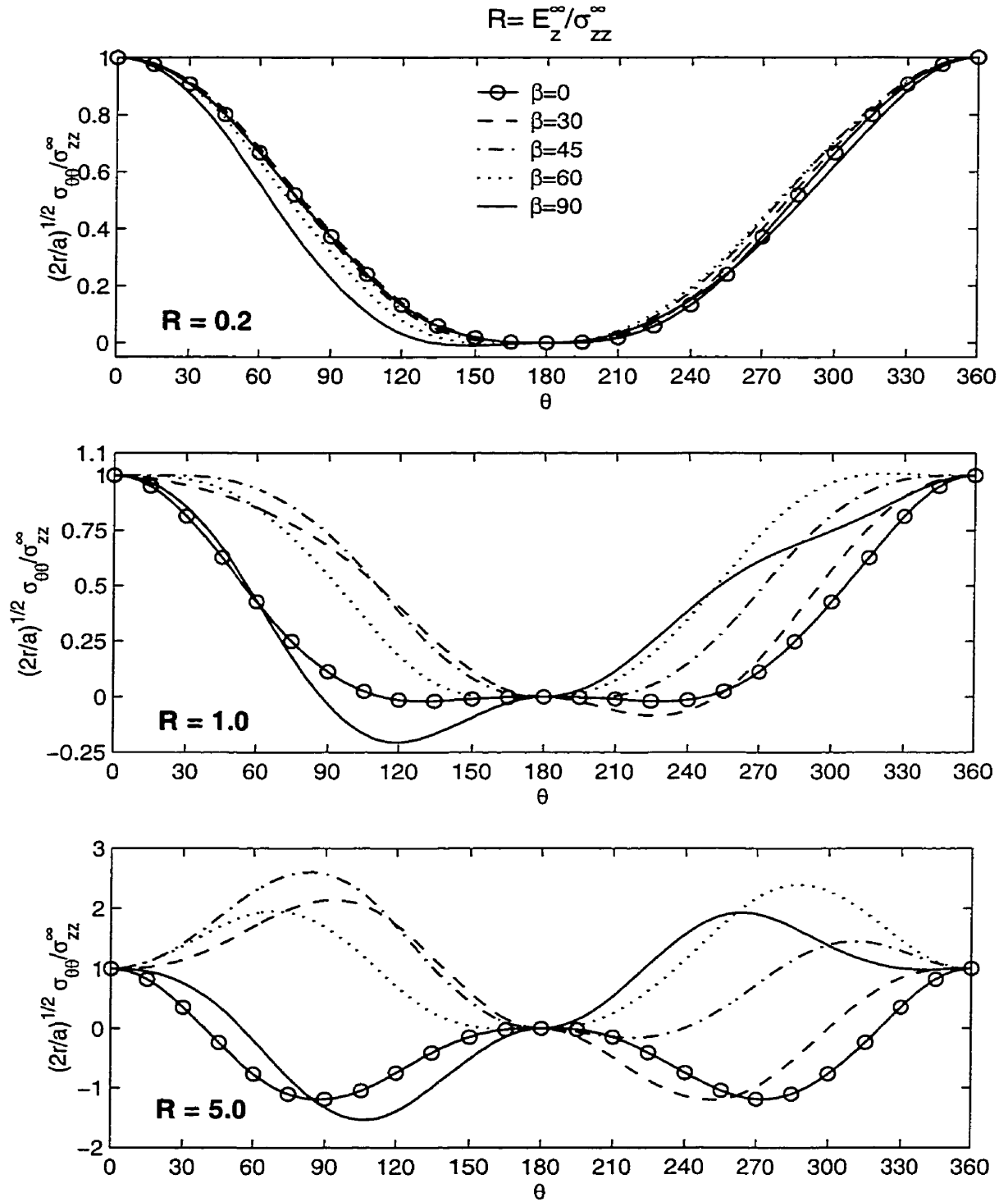


Figure 2.7: Variation of crack tip hoop stresses for combined remote tension and positive electric field in PZT-4 (impermeable crack).

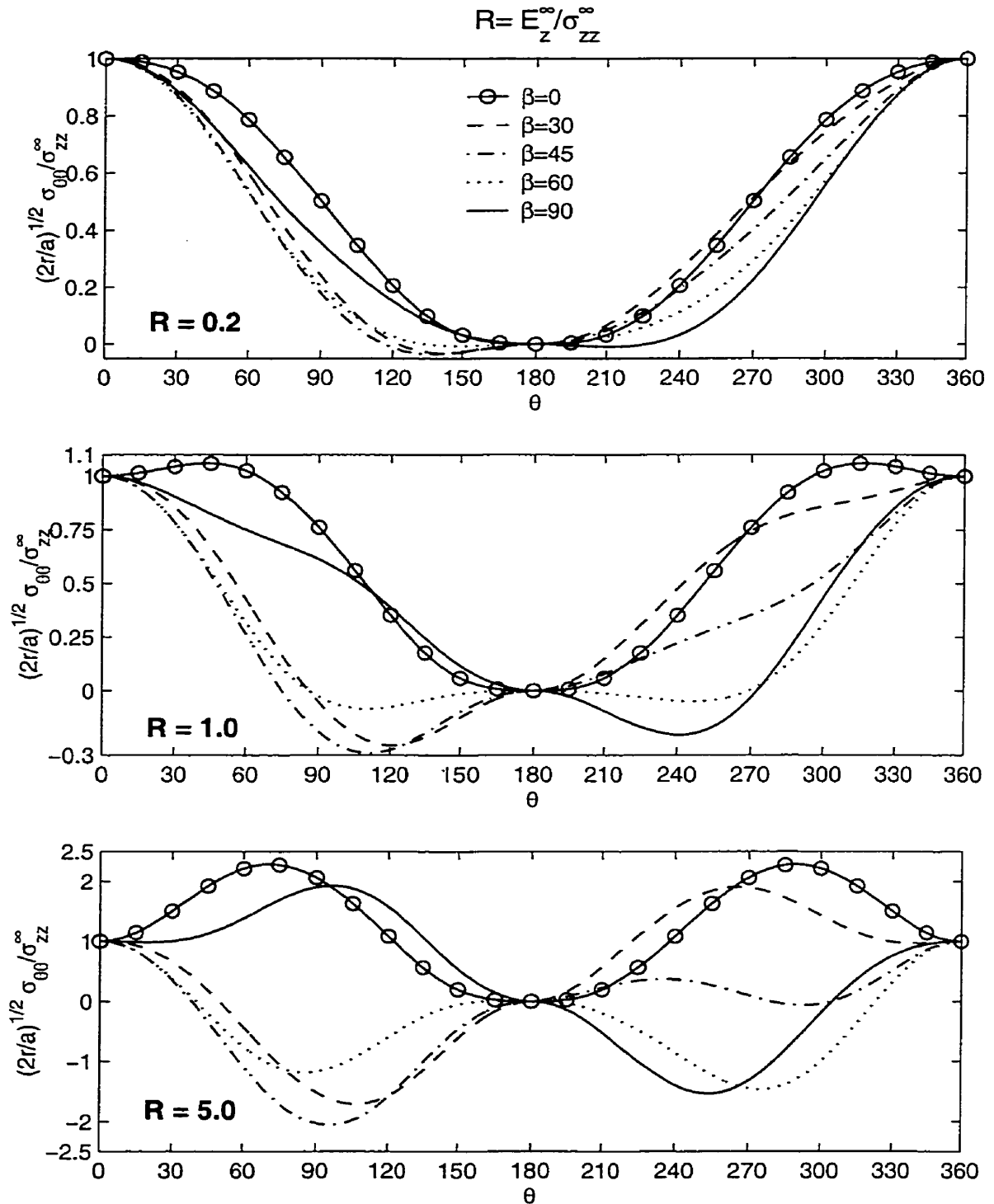


Figure 2.8: Variation of crack tip hoop stresses for combined remote tension and negative electric field in PZT-4 (impermeable crack).

Table 2.1: Critical value of load ratio R for crack closure under combined tension and negative electric field for an impermeable crack.

β (deg)	0	30	45	60	90
PZT-4	0.1026	0.1060	0.1150	0.1420	∞
PZT-5H	0.0747	0.0817	0.0945	0.1258	∞

that the crack closure occurs for all three R values and five β angles in Fig. 2.8 except $\beta = 90^\circ$. A critical value of load ratio R corresponding to crack closure exists for different crack orientations. A crack remains open only if load ratio R is less than the critical value. Table 2.1 shows the critical values of R obtained by using eqn (2.35) for PZT-4 and PZT-5H for combined tension and negative electric field. For both materials, the critical load ratio increases as crack orientation angle β becomes larger. The critical load ratio for PZT-4 is generally larger than that for PZT-5H.

The crack tip hoop stress distributions shown in Figures 2.7 and 2.8 include the results for the special case of $\beta = 0^\circ$ reported in the literature (Pak, 1992; Kumar and Singh, 1996; *etc.*) With the aid of the finite element method, Kumar and Singh (1996) employed the maximum stress criterion to predict the crack propagation in PZT-5H. Their predictions only touched the case of $\beta = 0^\circ$. For the loading conditions of pure tension, pure positive electric field or combined tension and positive electric field, current crack propagation predictions are identical to those of Kumar and Singh (1996). In the case of combined tension and negative electric field, they checked the normal component of crack opening displacements, and found that the crack is open for a very low load ratio ($R = 0.021$) while the crack closure occurs for a high load ratio ($R = 7.692$). This observation is in agreement with Table 2.1. In the case of pure negative field, however, they did not check the COD requirement, and concluded that a negative field enhances crack growth. Obviously, within the framework of linear piezoelectricity, if combined tension and negative electric field close a crack, removing tension surely results in crack closure.

2.5.3 Conducting crack

Now consider the crack faces in Fig 2.2 are electrically conducting. The hoop stress profile at the tip of a conducting crack is examined in this subsection. Five different orientation angles, namely $\beta = 0^\circ, 30^\circ, 45^\circ, 60^\circ, 90^\circ$ are considered.

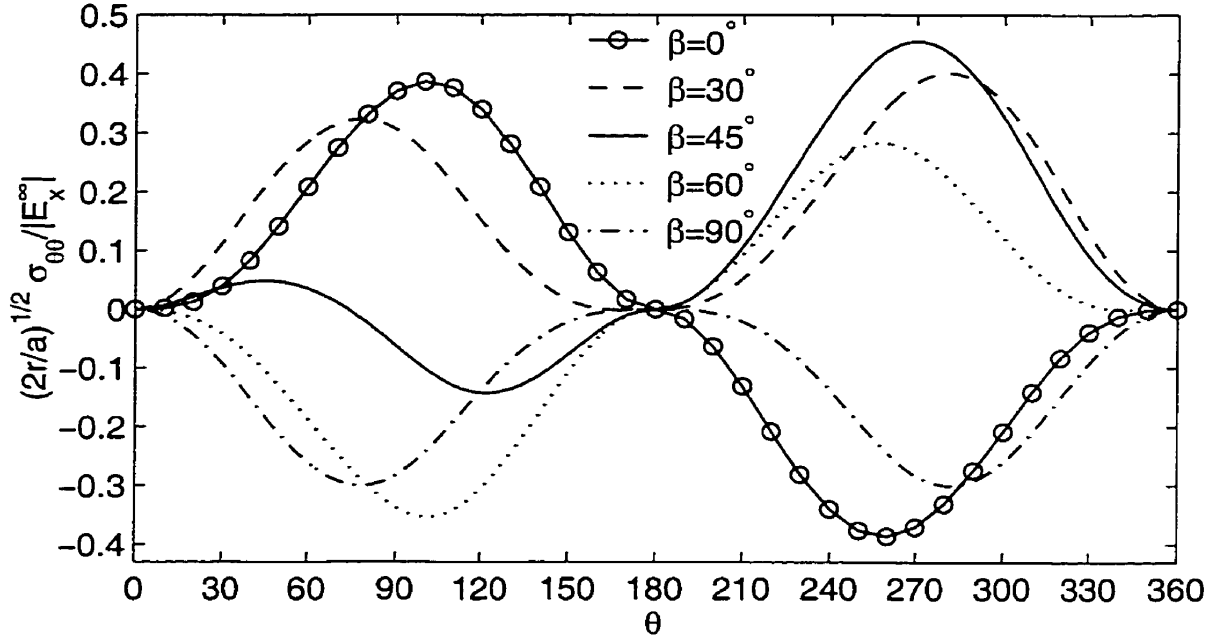


Figure 2.9: Variation of crack tip hoop stresses under remote electric field in PZT-4 (conducting crack).

In the case of a remote tensile stress, hoop stress profiles are found to be identical to those of an impermeable crack (Fig. 2.5), showing little dependence on crack orientation angle β . Under a positive applied electric field E_x^∞ , the crack opening displacement defined by eqn (2.51) indicates that crack closure occurs for all values of β except $\beta = 0$. A crack remains open for all β when a negative electric field E_x^∞ is applied at far field. The variation of normalized hoop stress $\sqrt{2r/a}\sigma_{\theta\theta}/\|E_x^\infty\|$ for this loading case is shown in Figure 2.9. It is found that crack orientation angles have significant effect on the hoop stress distribution. A crack with $\beta = 90^\circ$ induces compressive hoop stresses at the entire area of the crack tip, whereas $\beta = 30^\circ$ induces tensile hoop stresses at entire crack tip. The critical hoop stresses occur at $\theta = 101.2^\circ, 280.8^\circ, 270.0^\circ$ and 257.7° for $\beta = 0^\circ, 30^\circ, 45^\circ$ and 60° , respectively. A maximum critical value of 0.4552 is obtained for $\beta = 45^\circ$. Therefore, based on the maximum hoop stress criterion, the self-similar crack extension is not expected except when $\beta = 90^\circ$. The most critical case does not correspond to a crack normal/parallel to the poling direction, which is similar to the case of an impermeable crack.

The case of combined loading is also examined. The crack tip hoop stress distribution is controlled by the crack orientation and electric to mechanical load ratio ($R = E_x^\infty/\sigma_{zz}^\infty$ Vm/N). Similar to the case of an impermeable crack, when electric field dominates (large

Table 2.2: Critical value of load ratio R for crack closure under combined tension and positive electric field for a conducting crack.

β (deg)	0	30	45	60	90
PZT-4	∞	0.2114	0.1470	0.1181	0.1006
PZT-5H	∞	0.2136	0.1500	0.1216	0.1045

values of load ratio R), the effect is similar to the case of a pure electric field. A crack always remains open under combined tension and negative electric field E_x^∞ . Under combined tension and positive electric field, a critical value of R corresponding to crack closure exists for different crack orientations. A conducting crack remains open only for load ratios that are less than the critical values. The critical values of R obtained by using eqn (2.51) for PZT-4 and PZT-5H are given in Table 2.2. In contrast to the case of an impermeable crack (Table 2.1), the critical load ratio decreases as crack orientation angle β becomes larger for both PZT-4 and PZT-5H. The critical values for PZT-5H are slightly larger than those for PZT-4.

2.5.4 Hao and Shen type crack

Figures 2.10 - 2.13 present numerical results for a Hao and Shen type crack. To gain insight into three existing types of electric boundary conditions (*i.e.*, impermeable, permeable and Hao & Shen type) for cracks containing vacuum, the results for impermeable and permeable cracks are also shown in these figures.

The solution for D_z^0 (normal electric displacement on crack faces) obtained from eqn (2.69) is discussed first. Eqn (2.69) generally has two real or complex roots for D_z^0 , while only a real value is physically admissible. Numerical studies show that the discriminant of eqn (2.69) is positive for all considered cases. Hence two distinct real roots exist. Let root 1 and root 2 denote the roots with positive and negative signs before the discriminant, respectively. Table 2.3 presents the two roots (*i.e.* D_z^0) for a crack perpendicular to the poling direction, under applied stress $\sigma_{zz}^\infty = 1.0MPa$ and different applied electric displacements ($D_z^\infty = 2.0 \times 10^{-4}C/m^2$, 0 and $-2.0 \times 10^{-4}C/m^2$). For PZT-4, the three cases of electric displacement loading result in identical values for root 1 and distinctly different values for root 2. It is unlikely that electric loading has no effect on the crack face electric field under the boundary condition given by eqn (2.62). This suggests that root 1 may not be

Table 2.3: Normal electric displacement on crack faces based on eqn (2.69) ($\beta = 0$).

loading ($\sigma_{zz}^{\infty} = 1.0$ MPa)	PZT-4		PZT-5H	
	D_z^0 (root 1)	D_z^0 (root 2)	D_z^0 (root 1)	D_z^0 (root 2)
$D_z^{\infty} = 2.0 \times 10^{-4}$	3.598×10^{-2}	-5.173×10^{-5}	3.241×10^{-2}	-7.547×10^{-5}
$D_z^{\infty} = 0.0$	3.598×10^{-2}	-2.460×10^{-4}	3.323×10^{-2}	-2.663×10^{-4}
$D_z^{\infty} = -2.0 \times 10^{-4}$	3.598×10^{-2}	-4.403×10^{-4}	3.322×10^{-2}	-4.573×10^{-4}

admissible. The results for PZT-5H are similar to those of PZT-4. Another evidence of admissibility of root 2 comes from Hill's boundary element results (Hill, 1997). Under the same conditions as in Table 2.3, Hill performed iterations based on eqn (2.62) to compute D_z^0 for a penny shaped crack in PZT-4. The final converged values are unique and are closer to root 2 in Table 2.3. Table 2.4 presents the strain energy release rate (G^M) and the total energy release rate (G) for a Hao & Shen type crack in PZT-4 ($\beta = 0$) under pure mechanical loading σ_{zz}^{∞} (MPa). It is found that far field tension (including zero) results in non-positive G^M and negative G corresponding to root 1. Again, this is physically unrealistic. The case of $\beta \neq 0^\circ$ is also examined, and the behavior of roots is similar to that of $\beta = 0$. Therefore, it can be concluded that the admissible root of eqn (2.69) is the one that has a negative sign before the discriminant.

For an open crack, the z -component of crack opening displacements given by eqn (2.68) should not be negative. Obviously, for a given far field tensile stress, permeable cracks (eqn(2.60)) meet this condition regardless of the value of applied electric field. A Hao & Shen type crack is found to be open under an applied electric field or a tensile stress, irrespective of electric field direction and crack orientation. An impermeable crack remains open under a pure positive electric field, and crack closure occurs under a pure negative electric field except $\beta = 90^\circ$. Under combined tension and negative electric field, critical values of load ratio exist for different crack orientations (Table 2.1). A crack remains open only for load ratios that are less than the critical values. The condition of an open crack is satisfied by all cases considered in the ensuing computations.

Figure 2.10 shows K_D/\sqrt{a} (C/m^2) under varying electric field for different electric

Table 2.4: Energy release rates based on eqn (2.69) for a crack in PZT-4 ($\beta = 0$, $E_z^\infty=0$).

loading (MPa)	G^M (root 1)	G^M (root 2)	G (root 1)	G (root 2)
$\sigma_{zz}^\infty = 0.0$	0.0	0.0	-1.677×10^5	0.0
$\sigma_{zz}^\infty = 0.2$	-2.431×10^2	1.451	-1.697×10^5	1.452
$\sigma_{zz}^\infty = 0.5$	-6.078×10^2	9.070	-1.728×10^5	9.070
$\sigma_{zz}^\infty = 0.8$	-9.727×10^2	23.217	-1.759×10^5	23.224
$\sigma_{zz}^\infty = 1.0$	-1.216×10^3	36.274	-1.780×10^5	36.287

boundary conditions and $\sigma_{zz}^\infty = 0.6MPa$. Three crack orientation angles, *i.e.* $\beta = 0^\circ$, 30° and 90° in PZT-4 are considered. As expected, K_D is independent of electric loading for a permeable crack. For impermeable cracks, a relatively weak effect of β on K_D is observed, and K_D varies linearly with E_z^∞ . When $\beta = 0^\circ$ or 30° , the Hao and Shen type cracks and permeable cracks have nearly identical K_D , which are significantly different from K_D of impermeable cracks. When $\beta = 90^\circ$, impermeable cracks and the Hao and Shen type cracks have identical K_D , whereas permeable cracks show vanishing K_D .

In the case of the Hao and Shen type cracks, K_D corresponding to $\beta = 90^\circ$ is significantly different from that for $\beta \neq 90^\circ$. This behavior is due to the quadratic term $Im \sum_{n=1}^3 q_n \Lambda_{n3}$ appearing in eqn (2.69). For PZT-4 when $\beta = 90^\circ$, this term is vanishingly small. For example, the values are 2.214×10^{-2} , 1.918×10^{-2} , 3.845×10^{-3} , 1.932×10^{-4} , -6.720×10^{-18} for $\beta = 0^\circ$, 30° , 80° , 89.5° and 90° respectively. The linear term of eqn (2.69) is generally negative. Since the admissible root is the one that has a negative sign before the discriminant, $D_z^0 \simeq 0$ is obtained for $\beta = 90^\circ$. As a result, the Hao and Shen type cracks based on eqn (2.62) have identical behavior as impermeable cracks. This observation is also confirmed by numerical results for energy release rates and hoop stresses given below.

Figure 2.11 shows the strain energy release rate G^M/a (N/m^2) for PZT-4 under varying electric field and $\sigma_{zz}^\infty = 0.6MPa$. Five values of crack orientation angle, *i.e.* $\beta = 0^\circ$, 30° , 45° , 60° and 90° , are considered. A strong influence of crack orientation on G^M is observed. For all three types of electric boundary conditions, G^M decreases as β becomes larger except

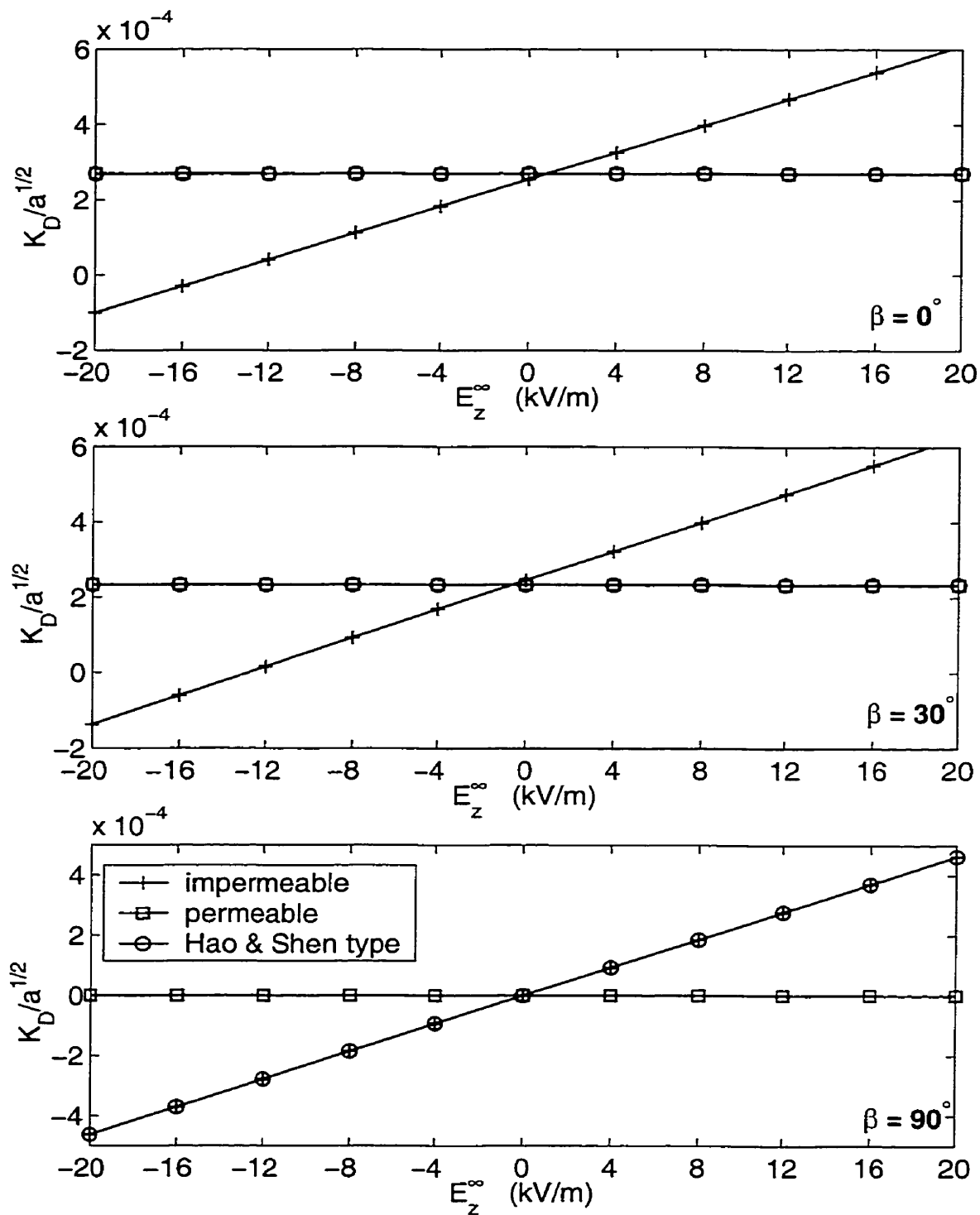


Figure 2.10: Variation of electric displacement intensity factor with electric field in PZT-4 under tensile stress $\sigma_{zz}^\infty = 0.6 \text{ MPa}$ for different crack models.

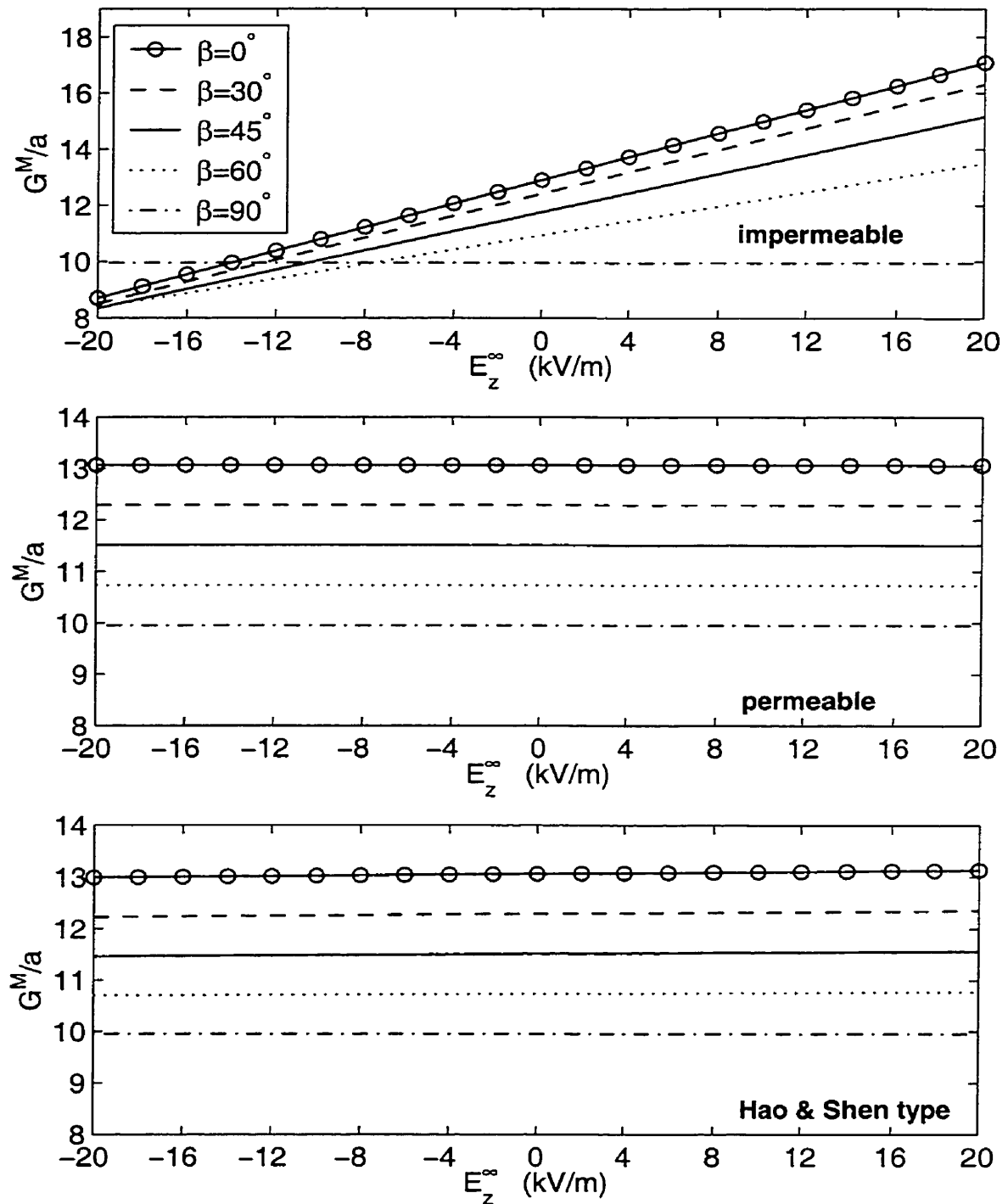


Figure 2.11: Variation of strain energy release rate with electric field in PZT-4 under tensile stress $\sigma_{zz}^\infty = 0.6 \text{ MPa}$ for different crack models.

for an impermeable crack and $E_z^\infty \leq -10kV/m$. When applied loading is pure mechanical ($E_z^\infty = 0$), G^M is independent of electric boundary conditions for any β . As expected, applied electric field has no effect on G^M for a permeable crack. For an impermeable crack, G^M increases with E_z^∞ when $\beta \neq 90^\circ$ and E_z^∞ has no effect on G^M when $\beta = 90^\circ$. The dependence of G^M on E_z^∞ decreases as β increases. Both permeable cracks and the Hao and Shen type cracks have nearly identical G^M values that are practically independent of E_z^∞ . Strain energy release rate of a crack parallel to the poling direction is independent of E_z^∞ and electric boundary conditions.

Total energy release rate G for a permeable crack is identical to G^M shown in Figure 2.11. G/a for impermeable cracks and the Hao and Shen type cracks based on eqn (2.62) are presented in Fig. 2.12. For impermeable cracks, an applied electric field tends to decrease G with increasing β . For the Hao and Shen type cracks, an electric field has no effect on G when $\beta \neq 90^\circ$. Again, the Hao and Shen type cracks and impermeable cracks show virtually identical G values when $\beta = 90^\circ$. Under pure mechanical loading ($E_z^\infty = 0$), G is independent of electric boundary conditions for any β . Total energy release rate is not symmetric with respect to E_z^∞ for impermeable cracks when remote tension is non-zero.

Based on the criterion of strain energy release rate, an increasing β generally increases the fracture load for all three types of electric boundary conditions. An applied electric field has no effect on fracture of impermeable cracks parallel to the poling direction ($\beta = 90^\circ$), and permeable and the Hao and Shen type cracks of arbitrary orientations. When $\beta \neq 90^\circ$, a positive electric field tends to enhance extension of an impermeable crack and a negative one tends to retard it. Applying the criterion of total energy release rate, the fracture load increases with increasing β regardless of electric boundary conditions, which is similar to the behaviour of G^M . For arbitrarily oriented impermeable cracks and the Hao and Shen type cracks parallel to the poling direction, both positive and negative electric fields tend to impede crack growth. For the Hao and Shen type cracks not parallel to the poling direction, an applied electric field has no influence on their fracture behavior.

Hoop stress distribution at a crack tip is also considered. Under pure tensile loading σ_{zz}^∞ , hoop stress profiles are found to be virtually independent of electric boundary conditions and crack orientation angle β . Numerical results are not shown for brevity. Figure 2.13 shows the variation of normalized hoop stress $\sqrt{2r/a}\sigma_{\theta\theta}/E_z^\infty$ (N/Vm) under a pure positive electric field E_z^∞ in PZT-4. For a permeable crack, a pure electric field has no contribution to hoop stress, which is obvious from eqns (2.58) and (2.59). For an impermeable crack, hoop stress distribution depends significantly on β . Again, a Hao and Shen type crack has practically

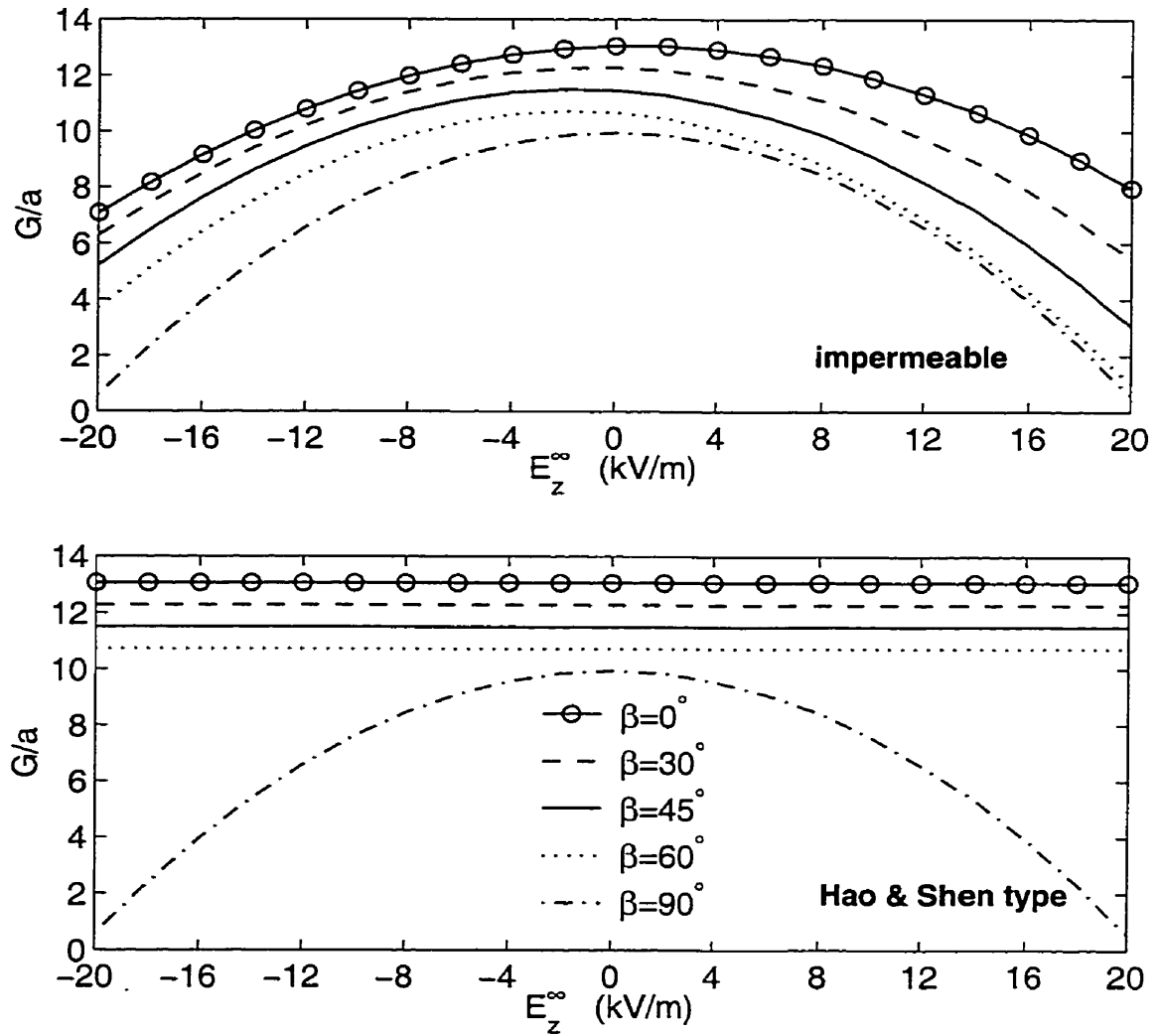


Figure 2.12: Variation of total energy release rate with electric field in PZT-4 under tensile stress $\sigma_{zz}^\infty = 0.6 \text{ MPa}$ for different crack models.

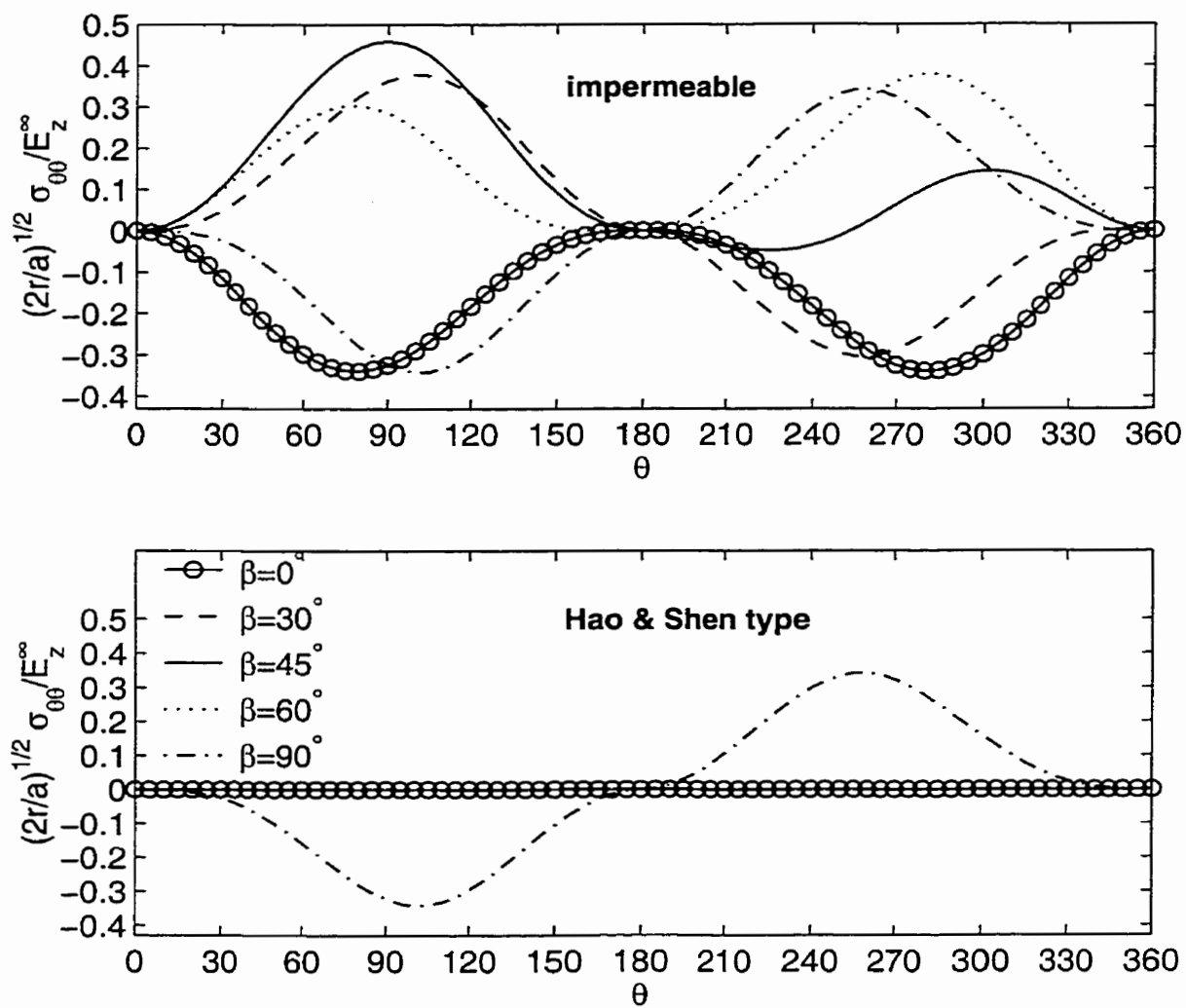


Figure 2.13: Variation of crack tip hoop stresses in PZT-4 under applied positive electric field for different crack models.

same $\sigma_{\theta\theta}$ as a permeable crack for $\beta \neq 90^\circ$, and has identical $\sigma_{\theta\theta}$ as an impermeable crack when $\beta = 90^\circ$.

Following the criterion of maximum hoop stress, fracture initiation and crack branching are generally expected for an impermeable crack, with the exception of the case $\beta = 0^\circ$. For a Hao and Shen type crack, crack extension and branching are expected only for the case that the crack is parallel to the poling direction. The observation that impermeable cracks and the Hao and Shen type cracks may deviate from a straight line is consistent with the experimental phenomenon of crack skewing (McHenry and Koepke, 1983).

2.6 Conclusions

The extended Lekhnitskii's formalism is successfully applied to study piezoelectric plane problems with an arbitrarily oriented elliptical void and a straight crack. Various types of void and crack boundary conditions are considered. A set of complete analytical solutions for electroelastic fields around the void and at the crack tip are derived in a remarkably compact form. Crack closure is taken into consideration in the analysis. Explicit solutions for fracture parameters such as hoop stress and energy release rates are also obtained. The present results can be reduced to special cases of defect orientation (*e.g.* Sosa, 1991; Pak, 1992 for defects parallel or perpendicular to the direction of polarization) reported in the literature. For arbitrarily oriented cracks containing air or vacuum, a unified formulation accounting for three existing types of electric boundary conditions, namely impermeable, permeable and the Hao and Shen type, is developed.

Numerical results reveal that the defect orientation generally has a significant effect on the critical values of hoop stress and electric displacement. Solutions based on $\beta = 0^\circ$, 90° cannot be always considered as the critical case. It is found that electric boundary conditions practically have no effect on hoop stress profile under pure mechanical loading. In the case of an impermeable crack or a conducting crack under electric loading or combined mechanical and electric loading with large values of electric mechanical load ratio, a substantial dependence of the crack tip hoop stress on crack orientations is noted. The influence of D_z^∞ on an impermeable crack is analogous to that of E_x^∞ on a conducting crack. Applied electric field has no impact on permeable cracks. The fracture behavior of Hao and Shen type cracks with $\beta \neq 90^\circ$ is practically independent of applied electric loading. However, for cracks parallel to the poling direction, the Hao & Shen type cracks behave as

impermeable cracks. Energy release rates generally decrease with increasing β . Impermeable, permeable and Hao & Shen type cracks have virtually identical energy release rates under pure mechanical loading.

A logical extension of this chapter is to examine branched cracks in piezoelectric solids, which is dealt with in the next chapter.

Chapter 3

Branched Cracks

3.1 Dislocation modeling

In this Chapter, the method of continuously distributed dislocations (Eshelby, *et al*, 1953; Gross, 1982; Zhang and Gross, 1994; Schmidt and Gross, 1997; Seeling and Gross, 1997) is extended to piezoelectrics. The extended method is then applied to derive the solution for an isolated main crack (Figure 3.1c). The result in this section is essential to the formulation of the branched crack problems considered in the ensuing sections.

Consider an infinite piezoelectric plane polarized in the z' -direction of the $x'z'$ system, as shown in Figure 3.1d. The poling direction makes angle β with the z -axis of the xz system. Assume that a single edge dislocation is located at the point $\mathbf{z}^0(x_0, z_0)$. The corresponding potentials $\varphi_n(z_n)$ can be expressed as (Nemat-Nasser and Hori, 1993),

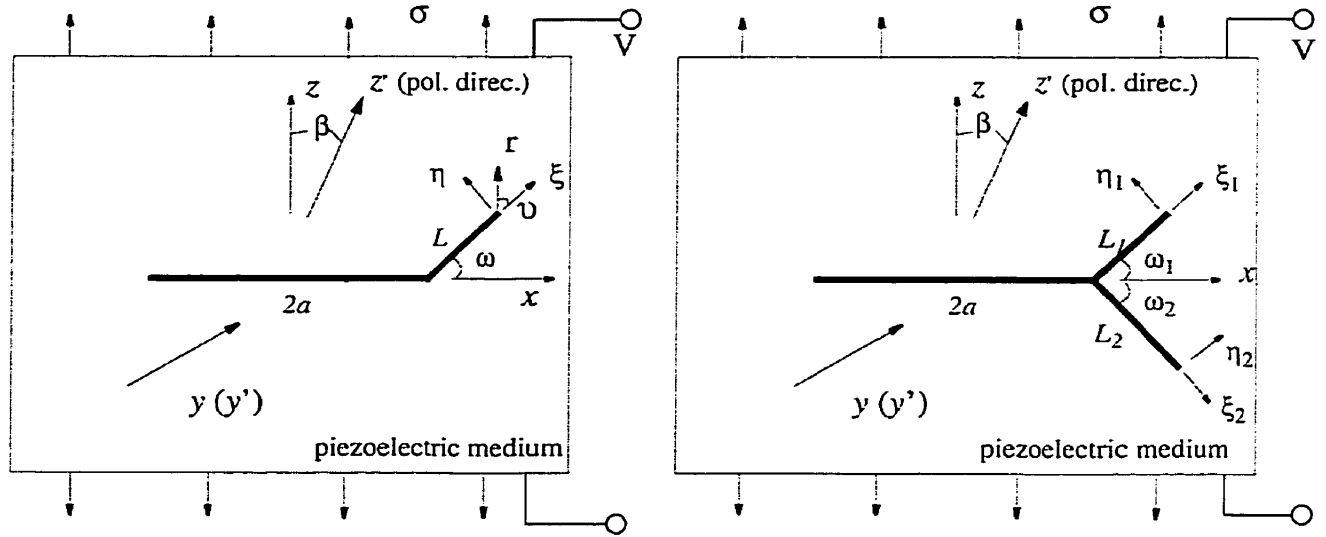
$$\varphi_n(z_n) = \frac{A_n}{2\pi i} \ln(z_n - z_n^0) \quad (n = 1, 2, 3) \quad (3.1)$$

where A_n are complex constants, $z_n^0 = x_0 + \mu_n z_0$, and μ_n are defined under eqn (2.6).

Around a loop surrounding the point \mathbf{z}^0 , the stresses and electric displacements are self-equilibrated (*i.e.* zero resultant forces F_x , F_z and electrical charge Q), and the displacements and electric potential jump are denoted by the extended Burgers vector $\mathbf{B} = (B_1, B_2, B_3)$. The complex constants A_n are determined by the following conditions.

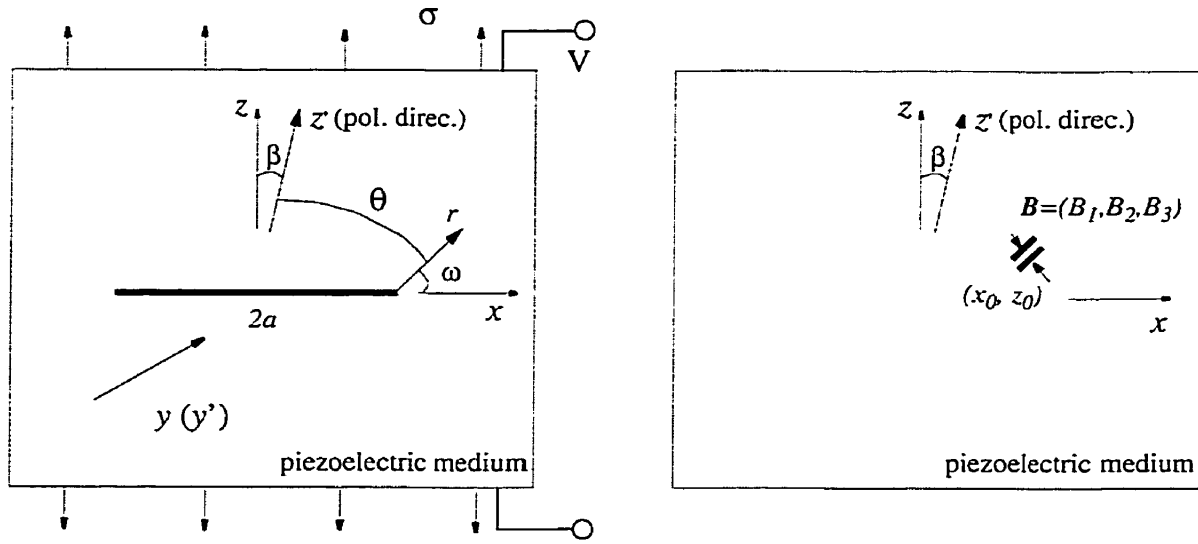
$$\begin{aligned} F_x &= 0; & F_z &= 0; & Q &= 0 \\ u_x(\mathbf{z}^0+) - u_x(\mathbf{z}^0-) &= B_1; & u_z(\mathbf{z}^0+) - u_z(\mathbf{z}^0-) &= B_2; & \phi(\mathbf{z}^0+) - \phi(\mathbf{z}^0-) &= B_3 \end{aligned} \quad (3.2)$$

Using the general solutions for plane piezoelectrics given by eqn (2.9), and eqns (3.1)



(a) A branched crack.

(b) A bifurcated crack.



(c) A straight crack.

(d) An edge dislocation.

Figure 3.1: Crack configuration.

and (3.2), it can be shown that,

$$\begin{aligned}\varphi_n(z_n) &= \frac{k_{ni}B_i}{2\pi i} \ln(z_n - z_n^0) \\ \varphi'_n(z_n) &= \frac{k_{ni}B_i}{2\pi i} \frac{1}{z_n - z_n^0}\end{aligned}\quad (3.3)$$

where complex constants k_{ni} ($n, i = 1, 2, 3$) defined in Appendix B are functions of material properties and crack orientation angle.

The normal and shear stresses, and normal electric displacement at (x, z) due to an edge dislocation at (x_0, z_0) can be expressed as,

$$\begin{aligned}\sigma_{zz}(x, z; x_0, z_0) &= \frac{1}{\pi} Im \sum_{n=1}^3 \frac{k_{ni}B_i}{z_n - z_n^0}; \quad \sigma_{xz}(x, z; x_0, z_0) = -\frac{1}{\pi} Im \sum_{n=1}^3 \mu_n \frac{k_{ni}B_i}{z_n - z_n^0} \\ D_z(x, z; x_0, z_0) &= -\frac{1}{\pi} Im \sum_{n=1}^3 \delta_n \frac{k_{ni}B_i}{z_n - z_n^0}\end{aligned}\quad (3.4)$$

The isolated main crack in Figure 3.1c is now considered. Far field mechanical and electrical loading are denoted by σ_{xx}^∞ , σ_{zz}^∞ , σ_{xz}^∞ and D_x^∞ , D_z^∞ (or E_x^∞ , E_z^∞). Using an impermeable crack model, the boundary conditions on the main crack faces are:

$$\sigma_{xz} = 0; \quad \sigma_{zz} = 0; \quad D_z = 0 \quad (3.5)$$

The condition for an open crack is,

$$\Delta u_z = u_z^+ - u_z^- \geq 0 \quad (3.6)$$

Consider the simulation of the main crack by a continuous distributed dislocation field. The electroelastic field created by the distributed dislocations and the far field loading should satisfy the main crack face boundary conditions of eqn (3.5). Let $b_i(x)$ ($i = 1, 2, 3$) denote the densities of distributed dislocations along the main crack line. Integration of eqn (3.4) along the main crack line and consideration of boundary conditions given by the eqn (3.5) result in,

$$\frac{1}{\pi} Im \int_{-a}^a \sum_{n=1}^3 \{1, -\mu_n, -\delta_n\}^T \frac{k_{ni}b_i(\zeta)}{x - \zeta} d\zeta + \{\sigma_{zz}^\infty, \sigma_{xz}^\infty, D_z^\infty\}^T = 0 \quad (3.7)$$

The solution of eqn (3.7) is,

$$b_i(x) = (q_{i1}\sigma_{zz}^\infty + q_{i2}\sigma_{xz}^\infty + q_{i3}D_z^\infty) \frac{x}{\sqrt{a^2 - x^2}} \quad (3.8)$$

where coefficients q_{ij} ($i, j = 1, 2, 3$) given in Appendix B are functions of material properties and crack orientation angle.

The potential functions $F_n(z_n)$ corresponding to an isolated main crack can be determined by substituting eqn (3.8) in eqn (3.3) and integrating along the crack length ($-a \leq x \leq a$). F_n are obtained as,

$$F_n(z_n) = [t_{1n}\sigma_{zz}^\infty + t_{2n}\sigma_{xz}^\infty + t_{3n}D_z^\infty] \{z_n - \sqrt{z_n^2 - a^2}\} \quad (3.9)$$

where $t_{jn} = i/2(k_{n1}q_{1j} + k_{n2}q_{2j} + k_{n3}q_{3j})$, ($j, n = 1, 2, 3$).

With the potential functions known, the electroelastic fields associated with a main crack can be readily obtained by using the general solution of eqn (2.9) and adding the far fields.

The crack opening displacements (COD) across the main crack faces can be determined as,

$$\{\Delta u_x, \Delta u_z\}^T = 4\sqrt{a^2 - x^2} \operatorname{Im} \sum_{n=1}^3 \{p_n, q_n\}^T (t_{1n}\sigma_{zz}^\infty + t_{2n}\sigma_{xz}^\infty + t_{3n}D_z^\infty) \quad (3.10)$$

For an open crack,

$$\operatorname{Im} \sum_{n=1}^3 q_n (t_{1n}\sigma_{zz}^\infty + t_{2n}\sigma_{xz}^\infty + t_{3n}D_z^\infty) \geq 0 \quad (3.11)$$

Using the polar coordinate system (r, ω) defined at the right crack tip (Figure 3.1c), the electroelastic asymptotic fields near the crack tip can be obtained. Crack tip hoop stress, shear stress and hoop electric displacement can be expressed as,

$$\begin{aligned} \sigma_{\omega\omega}(r, \omega) &= \frac{1}{\sqrt{2r}} \operatorname{Re} \sum_{n=1}^3 H_n (\cos \omega + \mu_n \sin \omega)^{3/2} \\ \sigma_{r\omega}(r, \omega) &= \frac{-1}{\sqrt{2r}} \operatorname{Re} \sum_{n=1}^3 H_n (\mu_n \cos \omega - \sin \omega) (\cos \omega + \mu_n \sin \omega)^{1/2} \\ D_\omega(r, \omega) &= \frac{-1}{\sqrt{2r}} \operatorname{Re} \sum_{n=1}^3 H_n \delta_n (\cos \omega + \mu_n \sin \omega)^{1/2} \end{aligned} \quad (3.12)$$

where $H_n = -\frac{2}{\sqrt{\pi}}(t_{1n}K_I + t_{2n}K_{II} + t_{3n}K_D)$, and K_I , K_{II} and K_D are conventional field intensity factors given by eqn (2.41).

It is noted that the solution for an impermeable crack has been obtained in Chapter 2 by the approach of collapsing an arbitrarily oriented ellipsoidal void to a crack. It is worth mentioning that the solution obtained in this section and the solution in Chapter 2

generate identical results according to numerical experiments, although it seems tedious to show analytically that the two solutions agree due to the complexity of expressions.

The conventional \mathbf{K} (K_I, K_{II}, K_D) of eqn (2.41) based on crack tip self-similar extension shows no electromechanical coupling. On the other hand, Azhdari and Nemat-Nasser (1996) used a set of generalized intensity factors based on crack tip hoop and shear stresses for anisotropic elastic solids. For piezoelectric crack problems, similar generalized intensity factors (hoop stress intensity factor $K_{\omega\omega}$, shear stress intensity factor $K_{\tau\omega}$ and hoop electric displacement intensity factor $K_{D\omega}$) can be defined as

$$K_{\omega\omega} = \lim_{r \rightarrow 0} \sqrt{2\pi r} \sigma_{\omega\omega}; \quad K_{\tau\omega} = \lim_{r \rightarrow 0} \sqrt{2\pi r} \sigma_{\tau\omega}; \quad K_{D\omega} = \lim_{r \rightarrow 0} \sqrt{2\pi r} D_{\omega}; \quad (3.13)$$

where $\sigma_{\omega\omega}$, $\sigma_{\tau\omega}$ and D_{ω} are given in eqn (3.12).

3.2 Branched crack

Assuming that the main crack remains open under far-field loading, *i.e.* eqn (3.6) is satisfied, the problem of a branched crack shown in Figure 3.1a is formulated in this section. The condition for an open branch is verified numerically.

Referring to Figure 3.1a, the branched crack model consists of an arbitrarily oriented main crack and a branch initiating from the main crack tip at an angle ω . A Cartesian coordinate system (ξ, η) and a polar coordinate system (r, ν) are defined at the tip of the crack branch.

Certain relationship between field quantities corresponding to two different coordinate systems can be derived. Such relations are convenient when dealing with coordinate transformations. For example, referring to Figure 3.1a, μ_n , δ_n and φ'_n in the xz system are related to $\bar{\mu}_n$, $\bar{\delta}_n$ and $\bar{\varphi}'_n$ in the $\xi\eta$ system in the following manner.

$$\bar{\mu}_n = \frac{\mu_n \cos \omega - \sin \omega}{\cos \omega + \mu_n \sin \omega}; \quad \bar{\delta}_n = \frac{1}{\cos \omega + \mu_n \sin \omega} \delta_n; \quad \bar{\varphi}'_n = (\cos \omega + \mu_n \sin \omega)^2 \varphi'_n \quad (3.14)$$

Assuming traction free and electrically impermeable, the boundary conditions of the branched crack are:

$$\sigma_{xz} = 0; \quad \sigma_{zz} = 0; \quad D_z = 0; \quad \text{on the main crack} \quad (3.15)$$

$$\sigma_{\xi\eta} = 0; \quad \sigma_{\eta\eta} = 0; \quad D_{\eta} = 0; \quad \text{on the branch} \quad (3.16)$$

The conditions for an open branched crack are given by

$$\Delta u_z = u_z^+ - u_z^- \geq 0 \quad (\text{main crack}) \quad (3.17)$$

$$\Delta u_{\eta} = u_{\eta}^+ - u_{\eta}^- \geq 0 \quad (\text{branch}) \quad (3.18)$$

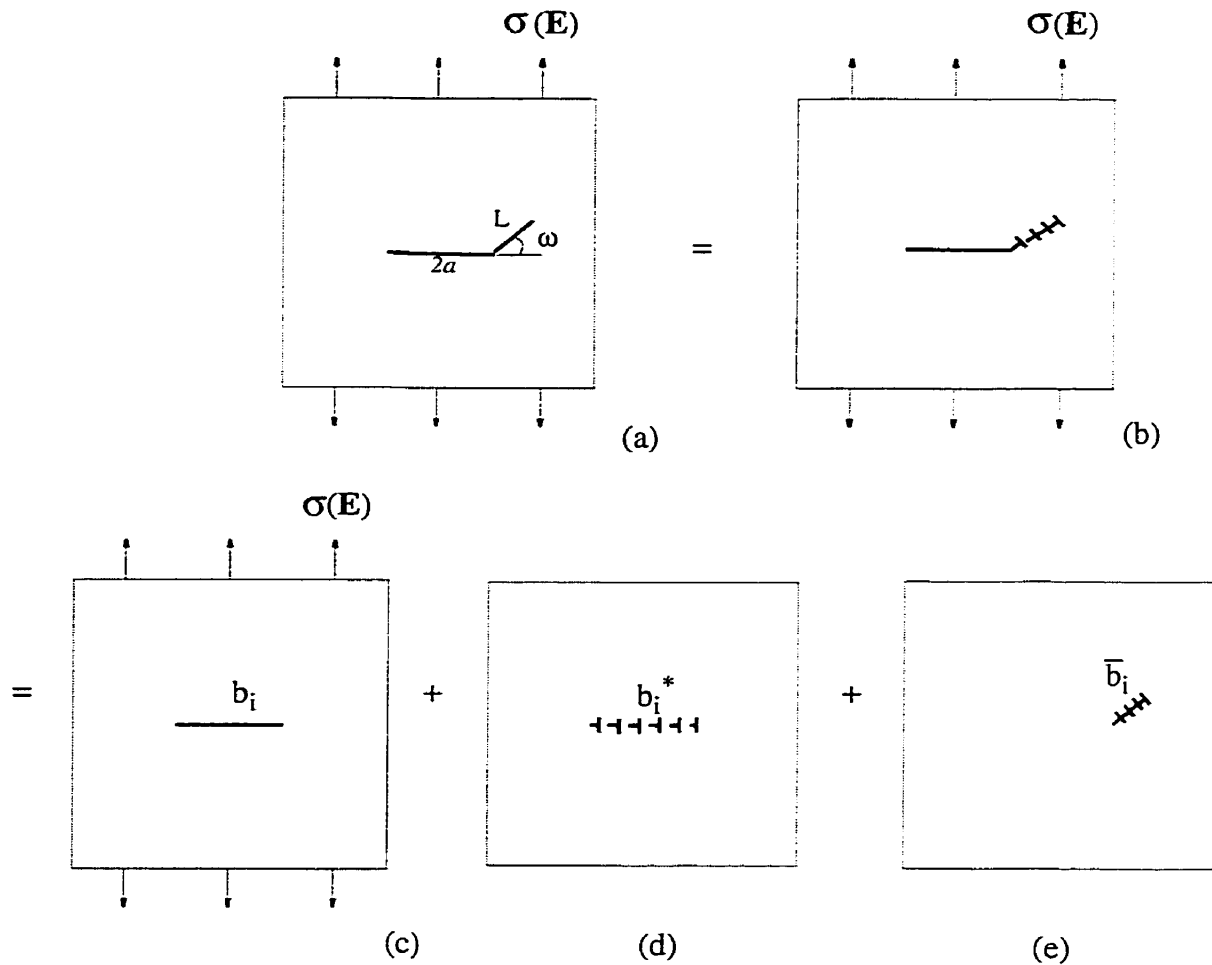


Figure 3.2: Superposition scheme for a branched crack.

Employing the dislocation approach described previously for a main crack, the branch in Figure 3.2a is also simulated by an unknown distributed dislocation field as shown in Figure 3.2b. The main crack face boundary conditions (*i.e.* eqn (3.15)) are violated due to the introduction of the dislocation field along the branch line. To satisfy the main crack boundary conditions, an additional distributed dislocation wall is built along the main crack line (Fig. 3.2d). Accordingly, the problem shown in Figure 3.2b is decomposed into three problems as shown in Figures 3.2c, 3.2d and 3.2e. The problem shown in Figure 3.2c (unbranched crack) was solved in the preceding section. Problems shown in Figures 3.2d and 3.2e are solved in this section.

The superposition of problems shown in Figures 3.2d and 3.2e should satisfy the main

crack boundary conditions. By enforcing this requirement, the densities of distributed dislocation field along the main crack line (Figure 3.2d) can be expressed in terms of those on the branch line (Figure 3.2e). Consequently, the electroelastic fields for problems shown in Figures 3.2d and 3.2e can be expressed in terms of dislocation densities on the branch. The requirement that the resultant electroelastic fields of Figures 3.2c, 3.2d and 3.2e should satisfy eqn (3.16) yields a system of equations for unknown dislocation densities on the branch line.

First, consider a plane problem identical to Figure 3.2d, with an edge dislocation $\mathbf{B} = (B_1, B_2, B_3)$ located at an arbitrary point $\mathbf{z}^0(x_0, z_0)$. Let the sum of electroelastic fields due to the edge dislocation \mathbf{B} and distributed dislocations $b_i^*(i = 1, 2, 3)$ along main crack line satisfy the boundary conditions given by eqn (3.15). Then, using the notation of eqn (3.4),

$$\begin{aligned} \int_{-a}^a \sigma_{zz}(x, 0; \zeta, 0) d\zeta + \sigma_{zz}(x, 0; x_0, z_0) &= 0; & \int_{-a}^a \sigma_{xz}(x, 0; \zeta, 0) d\zeta + \sigma_{xz}(x, 0; x_0, z_0) &= 0 \\ \int_{-a}^a D_z(x, 0; \zeta, 0) d\zeta + D_z(x, 0; x_0, z_0) &= 0 \end{aligned} \quad (3.19)$$

Subsequent manipulation of eqn (3.19) using eqn (3.4) leads to,

$$Im \sum_{n=1}^3 \{1, \mu_n, \delta_n\}^T k_{ni} b_i^*(x) = -\frac{1}{\pi^2} \frac{1}{\sqrt{a^2 - x^2}} \int_{-a}^a Im \sum_{n=1}^3 \{1, \mu_n, \delta_n\}^T k_{ni} B_i \frac{\sqrt{a^2 - \zeta^2}}{x - \zeta} \frac{1}{\zeta - z_n^0} d\zeta \quad (3.20)$$

The solution of eqn (3.20) can be expressed as,

$$\begin{aligned} b_i^*(x) &= \frac{-1}{\pi \sqrt{a^2 - x^2}} \left(J_{i1} Im \sum_{n=1}^3 k_{nk} \frac{\sqrt{z_n^{02} - a^2}}{x - z_n^0} + J_{i2} Im \sum_{n=1}^3 \mu_n k_{nk} \frac{\sqrt{z_n^{02} - a^2}}{x - z_n^0} \right. \\ &\quad \left. + J_{i3} Im \sum_{n=1}^3 \delta_n k_{nk} \frac{\sqrt{z_n^{02} - a^2}}{x - z_n^0} \right) B_k; \quad (-a < x < a) \end{aligned} \quad (3.21)$$

where complex-valued constants J_{ij} ($i, j = 1, 2, 3$) are defined in Appendix B.

Therefore, when an edge dislocation \mathbf{B} exists at an arbitrary point (x_0, z_0) in an infinite plane, the boundary conditions of eqn (3.15) along the main crack line can be satisfied by introducing a dislocation field $b_i^*(x)$ along the main crack line.

Replacing B_i in eqn (3.3) by b_i^* in eqn (3.21), and integrating along the main crack line yield the following potential functions corresponding to distributed dislocation field $b_i^*(x)$.

$$\varphi'_n(z_n) = -\frac{1}{4\pi} k_{ni} N_{kin}(z_i, z_i^0) B_k \quad (3.22)$$

where N_{kin} ($k, \bar{z}, n = 1, 2, 3$) defined below are functions of material properties, main crack orientation, branch angle, z_i and z_i^0 .

$$\begin{aligned} N_{kin}(z_i, z_i^0) &= J_{i1}(k_1 k_{l_{n1}} + k_2 k_{l_{n2}} + k_3 k_{l_{n3}} - \bar{k}_1 k_{l_{n1}}^* - \bar{k}_2 k_{l_{n2}}^* - \bar{k}_3 k_{l_{n3}}^*) \\ &+ J_{i2}(\mu_1 k_1 k_{l_{n1}} + \mu_2 k_2 k_{l_{n2}} + \mu_3 k_3 k_{l_{n3}} - \bar{\mu}_1 \bar{k}_1 k_{l_{n1}}^* - \bar{\mu}_2 \bar{k}_2 k_{l_{n2}}^* - \bar{\mu}_3 \bar{k}_3 k_{l_{n3}}^*) \\ &+ J_{i3}(\delta_1 k_1 k_{l_{n1}} + \delta_2 k_2 k_{l_{n2}} + \delta_3 k_3 k_{l_{n3}} - \bar{\delta}_1 \bar{k}_1 k_{l_{n1}}^* - \bar{\delta}_2 \bar{k}_2 k_{l_{n2}}^* - \bar{\delta}_3 \bar{k}_3 k_{l_{n3}}^*) \end{aligned} \quad (3.23)$$

and

$$l_{ij} = \frac{1}{z_i - z_j^0} \left(\frac{\sqrt{(z_j^0)^2 - a^2}}{\sqrt{z_i^2 - a^2}} - 1 \right); \quad l_{ij}^* = \frac{1}{z_i - \bar{z}_j^0} \left(\frac{\sqrt{(\bar{z}_j^0)^2 - a^2}}{\sqrt{z_i^2 - a^2}} - 1 \right) \quad (3.24)$$

Now consider the problems in Figures 3.2d and 3.2e. Treat the dislocation field along the branch line in Figure 3.2e as a continuous distribution of infinitesimal edge dislocations, *i.e.* $\bar{b}_k ds = B_k$. The corresponding potential functions in Figure 3.2d is obtained by integrating eqn (3.22) as,

$$\varphi'_n(z_n)|_{(d)} = -\frac{1}{4\pi} \int_0^L k_{ni} N_{kin}(z_i, z_i^0) \bar{b}_k(s) ds \quad (3.25)$$

Note z_i^0 in N_{kin} in eqn (3.25) are on the branch line, *i.e.* $z_i^0 = a + s(\cos \omega + \mu_i \sin \omega)$ ($0 < s < L$).

The following potential functions corresponding to the problem shown in Figure 3.2e are obtained by integrating eqn (3.3).

$$\varphi'_n(z_n)|_{(e)} = \frac{1}{2\pi i} \int_0^L \frac{k_{ni} \bar{b}_i(s)}{z_n - z_n^0} ds \quad (3.26)$$

where z_n^0 is defined under eqn (3.25).

With the aid of eqns (2.9) and (3.14), the stress $\sigma_{\xi\eta}$, $\sigma_{\eta\eta}$ and electric displacement D_η with respect to the $\xi\eta$ system can be expressed as,

$$\{\sigma_{\xi\eta}, \sigma_{\eta\eta}, D_\eta\}^T = 2Re \sum_{n=1}^3 \{-R_n T_n, T_n^2, -\delta_n T_n\}^T \varphi'_n(z_n) \quad (3.27)$$

where $R_n = \mu_n \cos \omega - \sin \omega$ and $T_n = \cos \omega + \mu_n \sin \omega$.

Applying the requirement that the superposition of electroelastic fields in Figures 3.2c, 3.2d and 3.2e should satisfy the boundary conditions given by eqn (3.16) along the branch line leads to the following system of coupled singular integral equations.

$$\int_0^L \sum_{i=1}^3 \frac{M_{mi} \bar{b}_i(s)}{\rho - s} ds + \int_0^L \sum_{k=1}^3 L_{mk} \bar{b}_k(s) ds = f_m \quad (3.28)$$

where $m = 1, 2, 3$, and M_{mi} , L_{mk} and f_m are

$$\{M_{1i}, M_{2i}, M_{3i}\}^T = \frac{1}{\pi} Im \sum_{n=1}^3 \{-R_n, T_n, -\delta_n\}^T k_{ni} \quad (3.29)$$

$$\{L_{1k}(\rho, s), L_{2k}(\rho, s), L_{3k}(\rho, s)\}^T = \frac{1}{2\pi} Re \sum_{n=1}^3 \{R_n T_n, -T_n^2, \delta_n T_n\}^T k_{ni} N_{kin}(z_i, z_i^0) \quad (3.30)$$

$$\{f_1(\rho), f_2(\rho), f_3(\rho)\}^T = 2Re \sum_{n=1}^3 \{R_n T_n, -T_n^2, \delta_n T_n\}^T F'_n(z_n) - \{\sigma_{\xi\eta}^\infty, \sigma_{\eta\eta}^\infty, D_\eta^\infty\}^T \quad (3.31)$$

and $F'_n(z_n)$ are obtained from eqn (3.9); $\sigma_{\xi\eta}^\infty$, $\sigma_{\eta\eta}^\infty$, and D_η^∞ are far field loading in the $\xi\eta$ system that can be expressed in terms of σ_{xx}^∞ , σ_{xz}^∞ , σ_{zz}^∞ and D_x^∞ , D_z^∞ , and $z_n = a + \rho(\cos \omega + \mu_n \sin \omega)$, ($0 < \rho < L$).

The dislocation density functions $\bar{b}_i(s)$ are singular at the branch knee and the branch tip. Extract the singularity from the dislocation densities $\bar{b}_i(s)$ by introducing $\bar{B}_i(s)$ as

$$\bar{b}_i(s) = \bar{B}_i(s) / \sqrt{s(L-s)} \quad (3.32)$$

After extracting the singularity from eqn (3.28), the three unknown dislocation densities \bar{B}_i ($i = 1, 2, 3$) can be determined by solving the equation system numerically. A quadrature method proposed by Gerasoulis (Gerasoulis, 1982) is used in the present study to solve the equation system. It will be shown in Chapter 5 that the electroelastic singularity at the knee of the branch is less than 1/2. Therefore the solution of eqn (3.28) is rendered unique (Miller and Stock, 1989).

Once the dislocation densities are known, the electroelastic fields and fracture parameters such as the branch tip intensity factors K_I^b , K_{II}^b and K_D^b can be computed as

$$\{K_I^b, K_{II}^b, K_D^b\}^T = \pi \sqrt{2\pi/L} \sum_{i=1}^3 \{M_{1i}, M_{2i}, M_{3i}\}^T \bar{B}_i(L) \quad (3.33)$$

Making use of eqn (3.14), the generalized intensity factors (hoop stress intensity factor $K_{\nu\nu}^b$, shear stress intensity factor $K_{\tau\nu}^b$ and electric displacement intensity factor $K_{D\nu}^b$), which are counterparts of eqn (3.13) for a straight crack, can also be obtained.

The branch opening displacements and jump in the electric potential can be expressed in terms of the dislocation densities \bar{b}_i as (Nemat-Nasser and Hori, 1993)

$$\{\Delta u_x(s), \Delta u_z(s), \Delta \phi(s)\}^T = - \int_L^s \{\bar{b}_1(\xi), \bar{b}_2(\xi), \bar{b}_3(\xi)\}^T d\xi \quad (3.34)$$

For an open branch, it is required that

$$\Delta u_\eta(s) = \Delta u_z(s) \cos \omega - \Delta u_x(s) \sin \omega \geq 0 \quad (0 \leq s \leq L) \quad (3.35)$$

3.3 Bifurcated crack

The problem of a bifurcated crack is considered in this section. The analytical model consists of a main crack with length $2a$ along the x -axis and two branches initiating from the main crack right tip, as shown in Figure 3.1b. Branches 1 and 2 are located along the ω_1 -direction with length L_1 and ω_2 -direction with length L_2 , respectively, and ω_1, ω_2 are measured counter-clockwise with respect to the x -axis. Cartesian coordinate systems (ξ_1, η_1) is defined at the branch 1 tip, and system (ξ_2, η_2) at the branch 2 tip.

Assume traction free and electrically impermeable on crack faces. The boundary conditions of the bifurcated crack are:

$$\sigma_{xz} = 0; \quad \sigma_{zz} = 0; \quad D_z = 0; \quad \text{on the main crack} \quad (3.36)$$

$$\sigma_{\xi_1\eta_1} = 0; \quad \sigma_{\eta_1\eta_1} = 0; \quad D_{\eta_1} = 0; \quad \text{on the branch 1} \quad (3.37)$$

$$\sigma_{\xi_2\eta_2} = 0; \quad \sigma_{\eta_2\eta_2} = 0; \quad D_{\eta_2} = 0; \quad \text{on the branch 2} \quad (3.38)$$

The conditions for an open crack are given by

$$\begin{aligned} \Delta u_z &= u_z^+ - u_z^- \geq 0 \text{ (main crack)} \\ \Delta u_{\eta_1} &= u_{\eta_1}^+ - u_{\eta_1}^- \geq 0 \text{ (branch 1); } \quad \Delta u_{\eta_2} = u_{\eta_2}^+ - u_{\eta_2}^- \geq 0 \text{ (branch 2)} \end{aligned} \quad (3.39)$$

Applying the technique of dislocation modeling, the two branches in Figure 3.3a is simulated by two unknown distributed dislocation fields in Figure 3.3b. Similar to the case of a branched crack (Figure 3.2), the bifurcated crack is decomposed into four problems shown in Figure 3.3c, 3.3d, 3.3e and 3.3f. The solution for the main crack problem in Figure 3.3c is known.

The problem in Figure 3.3d is now considered. The dislocation field $b_i^*(x)$ along the main crack line is constructed such that the resultant electroelastic fields of Figures 3.3d, 3.3e and 3.3f should satisfy the boundary condition of eqn (3.36) on the main crack faces. The results given by eqns (3.21) and (3.22) are recalled here. Treat the dislocation field along each branch line in Figures 3.3e and 3.3f as a continuous distribution of infinitesimal edge dislocations. Integrating eqn (3.22) along the branch 1 and branch 2 lines, the potential functions in Figure 3.3d are obtained as,

$$\varphi'_n(z_n)|_{(d)} = -\frac{1}{4\pi} \int_0^{L_1} k_{ni} N_{kin}(z_i, z_{1i}^0) \bar{b}_k(s) ds - \frac{1}{4\pi} \int_0^{L_2} k_{ni} N_{kin}(z_i, z_{2i}^0) \hat{b}_k(s) ds \quad (3.40)$$

where the first part corresponds to branch 1, and the second part corresponds to branch 2; z_{1i}^0 ($i = 1, 2, 3$) are on the branch 1 line, and $z_{1i}^0 = a + s(\cos \omega_1 + \mu_i \sin \omega_1)$ ($0 < s < L_1$); z_{2i}^0 ($i = 1, 2, 3$) are on the branch 2 line, and $z_{2i}^0 = a + s(\cos \omega_2 + \mu_i \sin \omega_2)$ ($0 < s < L_2$).

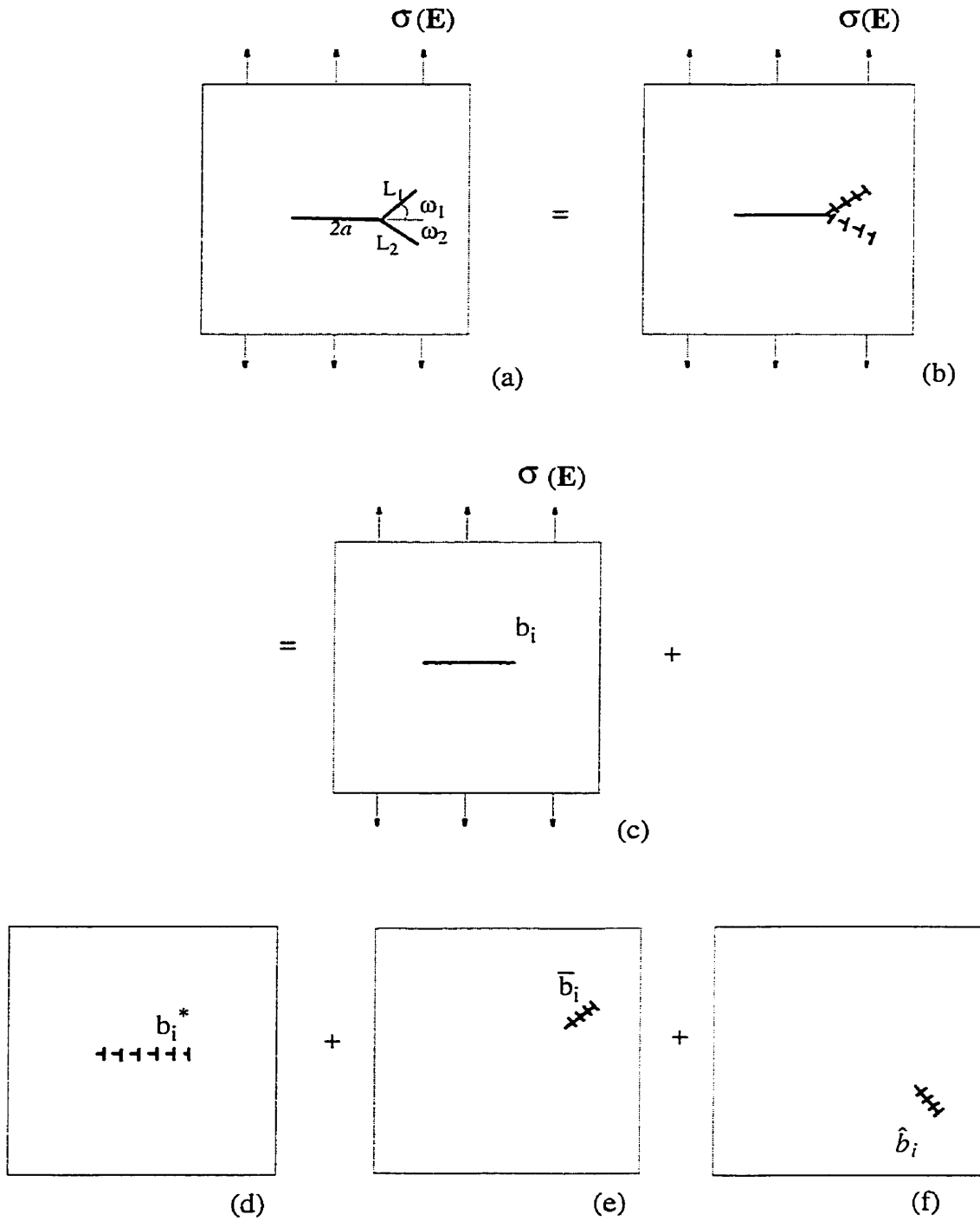


Figure 3.3: Superposition scheme for a bifurcated crack.

By integrating eqn (3.3), the potential functions corresponding to the problems shown in Figures 3.3e and 3.3f are obtained as

$$\varphi'_n(z_n)|_{(e)} = \frac{1}{2\pi i} \int_0^{L_1} \frac{k_{ni} \bar{b}_i(s)}{z_n - z_{1n}^0} ds \quad (3.41)$$

$$\varphi'_n(z_n)|_{(f)} = \frac{1}{2\pi i} \int_0^{L_2} \frac{k_{ni} \hat{b}_i(s)}{z_n - z_{2n}^0} ds \quad (3.42)$$

where z_{1n}^0 and z_{2n}^0 ($n = 1, 2, 3$) are defined under eqn (3.40).

Define $R_{1n} = \mu_n \cos \omega_1 - \sin \omega_1$, $T_{1n} = \cos \omega_1 + \mu_n \sin \omega_1$, and $R_{2n} = \mu_n \cos \omega_2 - \sin \omega_2$, $T_{2n} = \cos \omega_2 + \mu_n \sin \omega_2$, it can be shown that,

$$\begin{aligned} \{\sigma_{\xi_1 \eta_1}, \sigma_{\eta_1 \eta_1}, D_{\eta_1}\}^T &= 2Re \sum_{n=1}^3 \{-R_{1n} T_{1n}, T_{1n}^2, -\delta_n T_{1n}\}^T \varphi'_n(z_n) \\ \{\sigma_{\xi_2 \eta_2}, \sigma_{\eta_2 \eta_2}, D_{\eta_2}\}^T &= 2Re \sum_{n=1}^3 \{-R_{2n} T_{2n}, T_{2n}^2, -\delta_n T_{2n}\}^T \varphi'_n(z_n) \end{aligned} \quad (3.43)$$

Applying the requirement that the superposition of electroelastic fields in Figures 3.3c, 3.3d, 3.3e and 3.3f should satisfy the boundary conditions given by eqns (3.37) and (3.38) along the two branches leads to the following system of coupled singular integral equations.

$$\begin{aligned} \int_0^{L_1} \sum_{i=1}^3 \frac{D_{mi} \bar{b}_i(s)}{\rho_1 - s} ds + \int_0^{L_1} \sum_{k=1}^3 E_{mk} \bar{b}_k(s) ds + \int_0^{L_2} \sum_{k=1}^3 \hat{E}_{mk} \hat{b}_k(s) ds \\ + \int_0^{L_2} \sum_{k=1}^3 \frac{\hat{G}_{mk} \hat{b}_k(s)}{\rho_1 T_{1n} - s T_{2n}} ds = F_m \quad (m = 1, 2, 3) \end{aligned} \quad (3.44)$$

$$\begin{aligned} \int_0^{L_2} \sum_{i=1}^3 \frac{P_{mi} \hat{b}_i(s)}{\rho_2 - s} ds + \int_0^{L_1} \sum_{k=1}^3 Q_{mk} \bar{b}_k(s) ds + \int_0^{L_2} \sum_{k=1}^3 \hat{Q}_{mk} \hat{b}_k(s) ds \\ + \int_0^{L_1} \sum_{k=1}^3 \frac{\hat{V}_{mk} \bar{b}_k(s)}{\rho_2 T_{2n} - s T_{1n}} ds = S_m \quad (m = 1, 2, 3) \end{aligned} \quad (3.45)$$

where D_{mi} , E_{mk} , \hat{E}_{mk} , \hat{G}_{mk} , F_m and P_{mi} , Q_{mk} , \hat{Q}_{mk} , \hat{V}_{mk} , S_m ($i, k = 1, 2, 3$) are

$$\begin{aligned} \{D_{1i}, D_{2i}, D_{3i}\}^T &= \frac{1}{\pi} Im \sum_{n=1}^3 \{-R_{1n}, T_{1n}, -\delta_n\}^T k_{ni} \\ \{E_{1k}, E_{2k}, E_{3k}\}^T &= \frac{1}{2\pi} Re \sum_{n=1}^3 \{R_{1n} T_{1n}, -T_{1n}^2, \delta_n T_{1n}\}^T k_{ni} N_{kin}(z_{1i}, z_{1i}^0) \\ \{\hat{E}_{1k}, \hat{E}_{2k}, \hat{E}_{3k}\}^T &= \frac{1}{2\pi} Re \sum_{n=1}^3 \{R_{1n} T_{1n}, -T_{1n}^2, \delta_n T_{1n}\}^T k_{ni} N_{kin}(z_{1i}, z_{2i}^0) \end{aligned}$$

$$\begin{aligned}
\{\widehat{G}_{1k}, \widehat{G}_{2k}, \widehat{G}_{3k}\}^T &= \frac{1}{\pi} \operatorname{Re} \sum_{n=1}^3 \{-R_{1n}T_{1n}, T_{1n}^2, -\delta_n T_{1n}\}^T k_{ni} \\
\{F_1, F_2, F_3\}^T &= 2 \operatorname{Re} \sum_{n=1}^3 \{R_{1n}T_{1n}, -T_{1n}^2, \delta_n T_{1n}\}^T F'_n(z_{1n}) - \{\sigma_{\xi_1 \eta_1}^\infty, \sigma_{\eta_1 \eta_1}^\infty, D_{\eta_1}^\infty\}^T \\
\{P_{1i}, P_{2i}, P_{3i}\}^T &= \frac{1}{\pi} \operatorname{Im} \sum_{n=1}^3 \{-R_{2n}, T_{2n}, -\delta_n\}^T k_{ni} \\
\{Q_{1k}, Q_{2k}, Q_{3k}\}^T &= \frac{1}{2\pi} \operatorname{Re} \sum_{n=1}^3 \{R_{2n}T_{2n}, -T_{2n}^2, \delta_n T_{2n}\}^T k_{ni} N_{kin}(z_{2i}, z_{1i}^0) \\
\{\widehat{Q}_{1k}, \widehat{Q}_{2k}, \widehat{Q}_{3k}\}^T &= \frac{1}{2\pi} \operatorname{Re} \sum_{n=1}^3 \{R_{2n}T_{2n}, -T_{2n}^2, \delta_n T_{2n}\}^T k_{ni} N_{kin}(z_{2i}, z_{2i}^0) \\
\{\widehat{V}_{1k}, \widehat{V}_{2k}, \widehat{V}_{3k}\}^T &= \frac{1}{\pi} \operatorname{Re} \sum_{n=1}^3 \{-R_{2n}T_{2n}, T_{2n}^2, -\delta_n T_{2n}\}^T k_{ni} \\
\{S_1, S_2, S_3\}^T &= 2 \operatorname{Re} \sum_{n=1}^3 \{R_{2n}T_{2n}, -T_{2n}^2, \delta_n T_{2n}\}^T F'_n(z_{2n}) - \{\sigma_{\xi_2 \eta_2}^\infty, \sigma_{\eta_2 \eta_2}^\infty, D_{\eta_2}^\infty\}^T \quad (3.46)
\end{aligned}$$

In eqns (3.44) and (3.45), F'_n are obtained from eqn (3.9); $\sigma_{\xi_1 \eta_1}^\infty$, $\sigma_{\eta_1 \eta_1}^\infty$ and $D_{\eta_1}^\infty$ are far field loading in the $\xi_1 \eta_1$ system, $\sigma_{\xi_2 \eta_2}^\infty$, $\sigma_{\eta_2 \eta_2}^\infty$ and $D_{\eta_2}^\infty$ are far field loading in the $\xi_2 \eta_2$ system; and $z_{1n} = a + \rho_1(\cos \omega_1 + \mu_n \sin \omega_1)$, ($0 < \rho_1 < L$), $z_{2n} = a + \rho_2(\cos \omega_2 + \mu_n \sin \omega_2)$, ($0 < \rho_2 < L$).

Extracting the singularity from the dislocation densities by using

$$\bar{b}_i(s) = \bar{B}_i(s)/\sqrt{s(L_1 - s)}; \quad \hat{b}_i(s) = \hat{B}_i(s)/\sqrt{s(L_2 - s)} \quad (3.47)$$

The six non-singular unknown functions \bar{B}_i and \hat{B}_i ($i = 1, 2, 3$) can then be determined by solving the equation system of eqns (3.44) and (3.45) numerically. The solving scheme is similar to the case of the branched crack discussed in the previous section.

The intensity factors $K_I^{b_1}$, $K_{II}^{b_1}$ and $K_D^{b_1}$ at the branch 1 tip, and $K_I^{b_2}$, $K_{II}^{b_2}$ and $K_D^{b_2}$ at the branch 2 tip are

$$\begin{aligned}
\{K_I^{b_1}, K_{II}^{b_1}, K_D^{b_1}\}^T &= \pi \sqrt{2\pi/L_1} \sum_{i=1}^3 \{D_{1i}, D_{2i}, D_{3i}\}^T \bar{B}_i(L_1) \\
\{K_I^{b_2}, K_{II}^{b_2}, K_D^{b_2}\}^T &= \pi \sqrt{2\pi/L_2} \sum_{i=1}^3 \{P_{1i}, P_{2i}, P_{3i}\}^T \hat{B}_i(L_2) \quad (3.48)
\end{aligned}$$

The branch opening displacements are

$$\begin{aligned} \Delta u_{1x}(s) &= - \int_{L_1}^s \bar{b}_1(\xi_1) d\xi_1; & \Delta u_{1z}(s) &= - \int_{L_1}^s \bar{b}_2(\xi_1) d\xi_1 & \text{for branch 1} \\ \Delta u_{2x}(s) &= - \int_{L_2}^s \hat{b}_1(\xi_2) d\xi_2; & \Delta u_{2z}(s) &= - \int_{L_2}^s \hat{b}_2(\xi_2) d\xi_2 & \text{for branch 2} \end{aligned} \quad (3.49)$$

For open branch 1,

$$\Delta u_{\eta_1}(s) = \Delta u_{1z}(s) \cos \omega_1 - \Delta u_{1x}(s) \sin \omega_1 \geq 0 \quad (0 \leq s \leq L_1) \quad (3.50)$$

and for open branch 2,

$$\Delta u_{\eta_2}(s) = \Delta u_{2z}(s) \cos \omega_2 - \Delta u_{2x}(s) \sin \omega_2 \geq 0 \quad (0 \leq s \leq L_2) \quad (3.51)$$

3.4 Numerical results and discussion

In this section, a selected set of problems are studied to understand the basic fracture characteristics of branched cracks in piezoelectrics. Plane strain conditions are assumed. The condition for an open main crack is satisfied in all examples, and the condition for an open branch is checked during computations. PZT-4 (material properties are given in Appendix A) is used in the numerical study.

3.4.1 A branched crack

The accuracy of present results for a branched crack in piezoelectrics is first verified by comparing with the solutions for a branched crack in an ideal elastic material. Obata *et al* (1989) examined infinitesimally small branched cracks in plane anisotropic elastic solids with following elastic constants: $a_{13} = a_{23} = 0$, $a_{12} = -0.25a_{11}$, $a_{33} = 2.5a_{11}$, and $a_{22} = a_{11}/c^*$ (c^* is constant). Consider a fictitious piezoelectric material with same a_{ij} as above, identical dielectric constants as PZT-4, and negligible piezoelectric coefficients ($b_{ij} \approx 10^{-12}$). Taking $L/a = 10^{-6}$ and $\beta = 0^\circ$, the normalized stress intensity factors K_I^b/K_I and K_{II}^b/K_I are shown in Figures 3.4a and 3.4b for various c^* values under remote uniform tension, where K_I denotes the mode I stress intensity factor for a straight crack. Close agreement is noted confirming the accuracy of the present solution scheme.

The accuracy of present scheme is also confirmed by comparing with the numerical results for piezoelectrics with $\beta = 0$ reported by Zhu and Yang (1999). Consider a crack with an infinitesimal branch length ($L/a = 10^{-6}$) in PZT-4. Table 3.1 compares the mode I intensity factor K_I^b/K_I and the electric displacement intensity factor K_D^b/K_I at branch

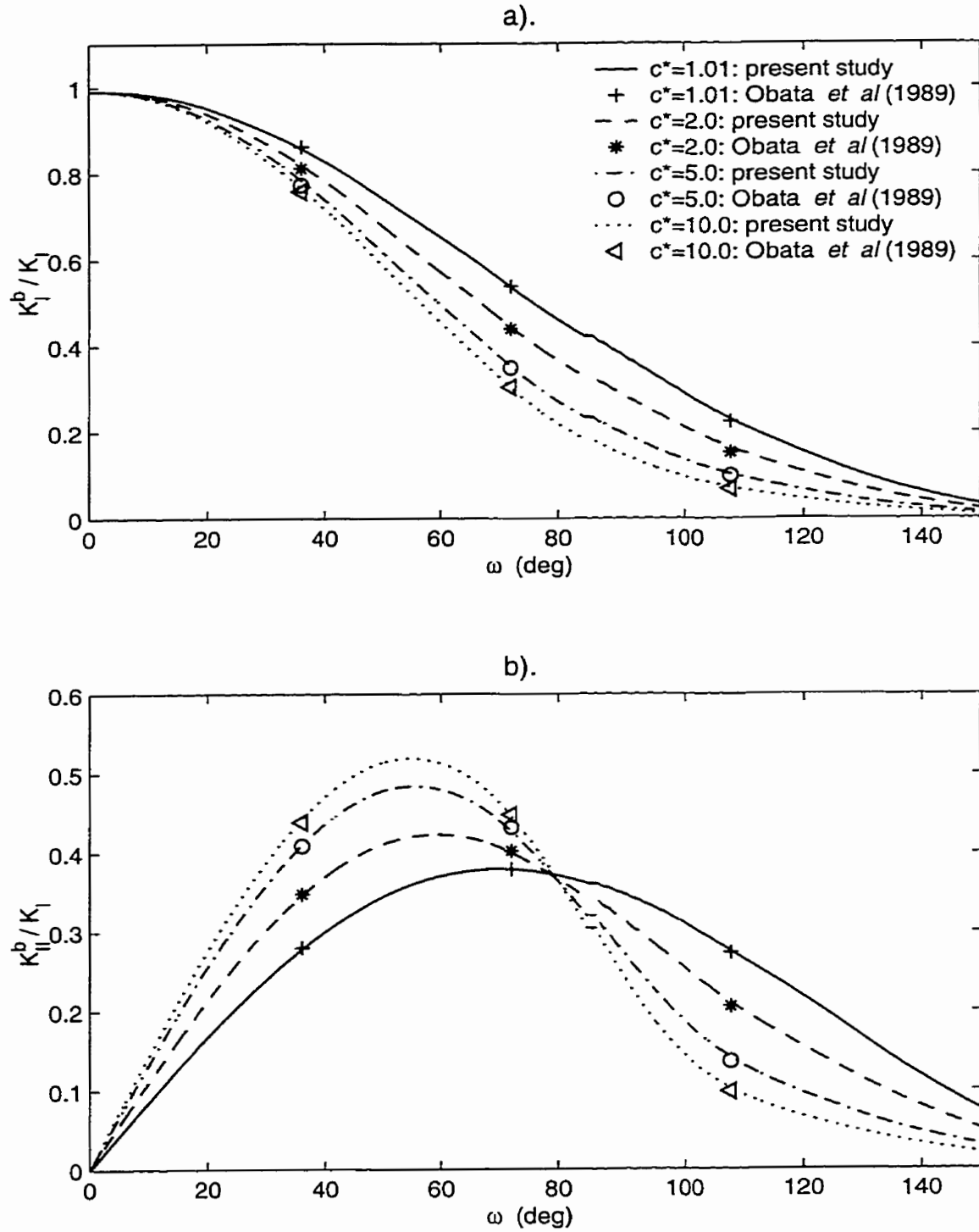


Figure 3.4: Comparison of stress intensity factors at the tip of a branched crack in an orthotropic elastic solid under remote tension.

Table 3.1: Comparison of field intensity factors at branch tip in PZT-4 for the special case of a branched crack ($\beta = 0$, $L/a = 10^{-6}$).

loading ($\sigma_{zz}^\infty = 1$, D_z^∞)	ω/π	K_I^b/K_I		K_D^b/K_I ($10^{-9} C/N$)	
		Zhu & Yang (1999)	Present Study	Zhu & Yang (1999)	Present Study
$D_z^\infty = 0$	0.1	0.97	0.9720	-0.01	-0.0095
	0.2	0.90	0.9017	-0.03	-0.0328
	0.3	0.79	0.7884	-0.06	-0.0606
	0.4	0.64	0.6407	-0.09	-0.0872
	0.5	0.46	0.4640	-0.11	-0.1060
	0.6	0.30	0.3012	-0.12	-0.1190
$D_z^\infty = 0.5 \times 10^{-8}$	0.1	0.95	0.9529	-	4.950
	0.2	0.83	0.8317	-	4.839
	0.3	0.66	0.6610	-	4.634
	0.4	0.48	0.4978	-	4.327
	0.5	0.33	0.3267	-	3.928
	0.6	0.19	0.1919	-	3.421

tip computed from the present scheme with corresponding results given by Zhu and Yang (1999), where K_I is the stress intensity factor for a straight crack. A pure tensile loading and a combined tensile and positive electric displacement loading are considered. Very good agreement is observed in Table 3.1.

Azhdari and Nemat-Nasser (1996) analyzed crack-branching in an anisotropic elastic solid by using a straight crack model. They compared the hoop stress intensity factor $K_{\omega\omega}$ and the shear stress intensity factor $K_{r\omega}$ at the straight crack tip with K_I^b and K_{II}^b based on the branched crack model. It was found that, in the limiting case of a branched crack with an infinitesimal branch length, the differences between \mathbf{K}^s ($K_{\omega\omega}$, $K_{r\omega}$) and \mathbf{K}^b (K_I^b , K_{II}^b) are less than 1.0% provided branch angles are between -8° and $+8^\circ$. For piezoelectric solids, \mathbf{K}^s ($K_{\omega\omega}$, $K_{r\omega}$, $K_{D\omega}$) and \mathbf{K}^b (K_I^b , K_{II}^b , K_D^b) contain three intensity factors in each. Setting $L/a = 10^{-6}$, \mathbf{K}^s and \mathbf{K}^b were compared for different β and loading. It is found that under pure mechanical or electric loading, the corresponding intensity factors satisfy the 1.0%

Table 3.2: Range of branch angles (deg) for an open branch in PZT-4.

β	loading	L/a			
		0.001	0.01	0.1	0.5
0 (deg)	$\sigma_{zz}^\infty = 1$	[-120, 120]	[-120, 120]	[-102, 102]	[-78, 78]
	$D_z^\infty(E_z^\infty) = 1$	[-88, 88]	[-89, 89]	[-90, 90]	[-91, 91]
30 (deg)	$\sigma_{zz}^\infty = 1$	[-120, 120]	[-120, 120]	[-107, 98]	[-79, 80]
	$D_z^\infty(E_z^\infty) = 1$	[-117, 61]	[-117, 61]	[-117, 60]	[-119, 60]
-30 (deg)	$\sigma_{zz}^\infty = 1$	[-120, 120]	[-120, 120]	[-98, 107]	[-80, 79]
	$D_z^\infty(E_z^\infty) = 1$	[-61, 117]	[-61, 117]	[-60, 117]	[-60, 119]

requirement between the two models for a remarkably wide range of ω . For example, when $\beta = 0^\circ$, \mathbf{K}^s and \mathbf{K}^b show less than 1.0% difference for $-58^\circ \leq \omega \leq 58^\circ$ and $-36^\circ \leq \omega \leq 36^\circ$ for pure tensile and normal electric displacement loading, respectively.

The electroelastic fields at a branch tip (Figure 3.1a) are illustrated in Figures 3.5-3.8 through intensity factors (K_I^b, K_{II}^b, K_D^b) and hoop stress intensity factor $K_{\theta\theta}^b$. These parameters reflect the disturbed electroelastic fields due to the presence of a branch. In view of practical applications, branch angles in the range $[-120^\circ, 120^\circ]$ are considered.

It is important to check the condition for an open branch given by eqn (3.35). The ranges of branch angles within which a branch is open are given in Table 3.2 for three different crack orientations ($\beta = 0^\circ, 30^\circ, -30^\circ$) under remote mechanical and electric loading. Generally, the ranges are larger for mechanical loading than for electric loading. Under mechanical loading, a branch is in open mode for all small branch lengths ($L/a \leq 0.01$) and $|\omega| \leq 120^\circ$. However, the branch angle range for an open branch becomes smaller with increasing L/a . The length of a branch has negligible influence on branch closure under electric loading. The branch remains always open for $L/a \leq 0.5$ and $|\omega| \leq 60^\circ$.

Figures 3.5 and 3.6 show the field intensity factors K_I^b, K_{II}^b and K_D^b for $\beta = 0^\circ$ under remote tension σ_{zz}^∞ and positive electric displacement D_z^∞ , respectively. Four cases of branch lengths ($L/a = 0.001, 0.01, 0.1$ and 0.5) are considered. The intensity factors in Figures 3.5 and 3.6 are normalized by K_I and K_D given in eqn (2.41), respectively. For

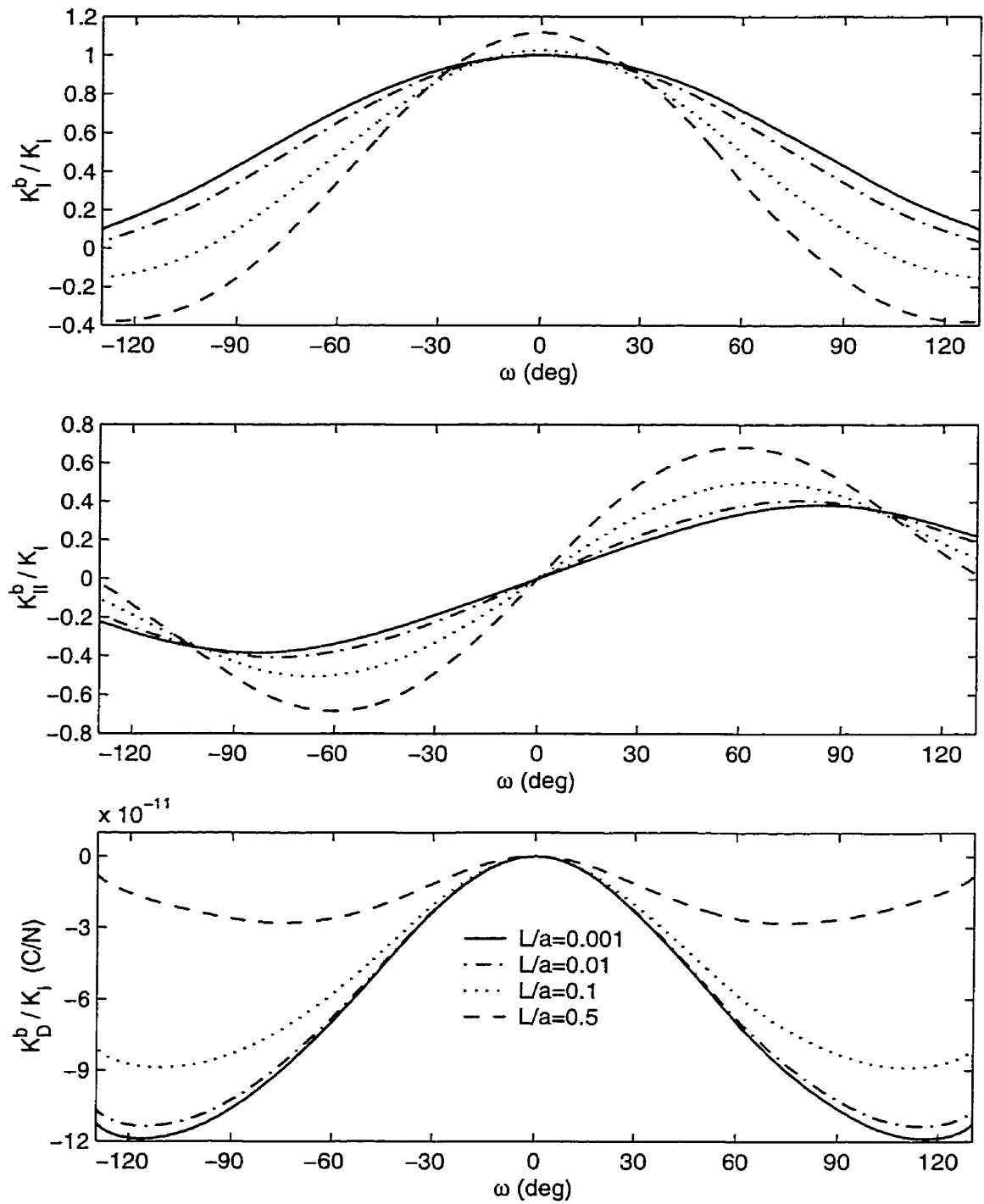


Figure 3.5: Normalized stress/electric intensity factors at the tip of a branched crack in PZT-4 due to remote tension for crack orientation $\beta = 0$ and different branch length L/a .

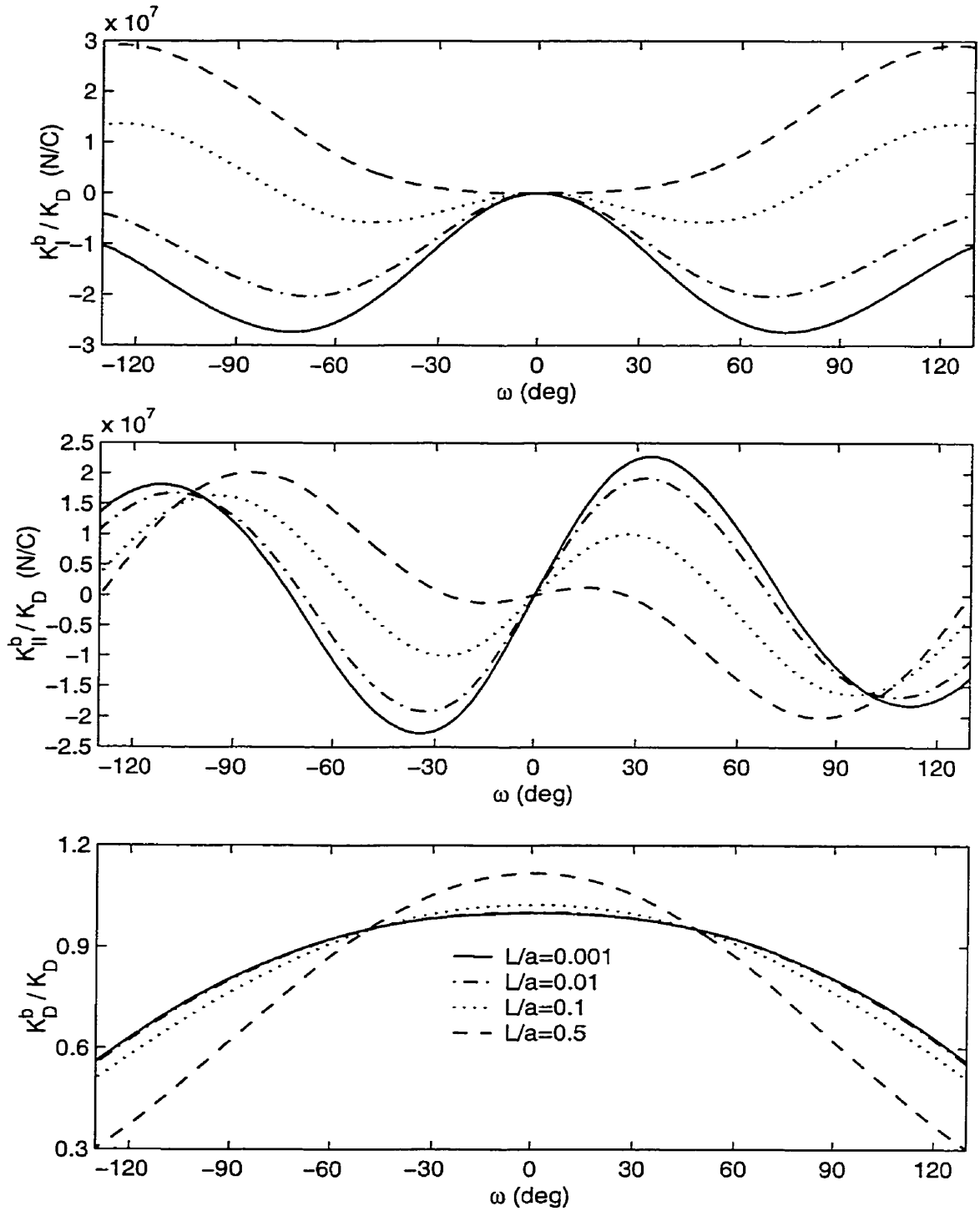


Figure 3.6: Normalized stress/electric intensity factors at the tip of a branched crack in PZT-4 due to positive electric displacement for crack orientation $\beta = 0$ and different branch length L/a .

both mechanical and electric loading, K_I^b and K_D^b are symmetric with respect to the main crack line, whereas K_{II}^b is antisymmetric. Unlike the case of a straight crack, generally K_I^b , K_{II}^b and K_D^b all have non-zero values. When $\omega = 0^\circ$ (*i.e.* a branch along the main crack line), K_{II}^b and K_D^b (Figure 3.5) and K_I^b and K_{II}^b (Figure 3.6) vanish confirming the decoupling of stress and electric fields at a straight crack tip (Suo *et al*, 1992). A weak influence of branch length on intensity factors is observed for $L/a \leq 0.01$. Additional results show that intensity factors are virtually independent of L/a for $L/a \leq 0.001$. A similar conclusion was drawn by Zhu and Yang (1999) while examining K_I^b for varying L/a .

In the case of mechanical loading, $K_I^b(\omega \neq 0^\circ) < K_I^b(\omega = 0^\circ)$ and $K_D^b(\omega \neq 0^\circ) < K_D^b(\omega = 0^\circ)$, which mean a deviated branch plays a shielding effect on Mode I stress and electric displacement intensity factors for the branch lengths considered in Figure 3.5 (compared to self-similar crack extension). For positive values of ω , a branch has an amplifying effect on the Mode II stress intensity factor, while a shielding effect is noted for negative ω . In the case of positive electric loading (Figure 3.6), a shielding effect is also observed for the electric displacement intensity factor. However the effect on K_I^b and K_{II}^b depends on both the branch length and branch angle. For example, shielding effects on K_I^b are observed when $L/a \leq 0.01$ for all ω and for $L/a = 0.1$ when $|\omega| < 80^\circ$, whereas amplifying effects for $L/a = 0.1$ with $|\omega| > 80^\circ$ and $L/a = 0.5$. However, branch closure generally happens when $|\omega| > 90^\circ$. Compared to the case of mechanical loading, the dependence of intensity factors on L/a and ω is more complex under electric loading.

The case of a main crack not perpendicular to the poling direction ($\beta \neq 0^\circ$) is also considered. As expected, the field intensity factors are no longer symmetric or anti-symmetric with respect to the main crack line. In the case of tensile loading, crack orientation has a weak influence on K_I^b and K_{II}^b , but quite strong influence on K_D^b . In contrast, crack orientation has a strong influence on K_I^b and K_{II}^b , but a relatively weak influence on K_D^b under remote electric displacement loading. Numerical results are not presented here for brevity.

Setting $L/a = 0.01$, Figures 3.7 and 3.8 present the normalized hoop stress intensity factors $K_{\nu\nu}^b/(\sqrt{\pi a}\sigma_{zz}^\infty)$ and $K_{\nu\nu}^b/(\sqrt{\pi a}E_z^\infty)$ under remote tension and positive electric field, respectively. Five cases of branch angles ($\omega = 0^\circ, 30^\circ, 45^\circ, 60^\circ$ and 90°) and three values of main crack orientation angles ($\beta = 0^\circ, 30^\circ$ and -30°) are considered. Based on Table 3.2, branch closure occurs for $\omega = 90^\circ$ and $\beta = 0^\circ$ or 30° under electric loading. The corresponding results are not shown in Figure 3.8. In the case of mechanical loading (Figure 3.7), crack orientation shows weak effect on hoop stress intensity factor. Critical hoop stress intensity factors are found at $\nu = 0^\circ$ when $\omega = 0^\circ$ for all values of β , implying the shielding

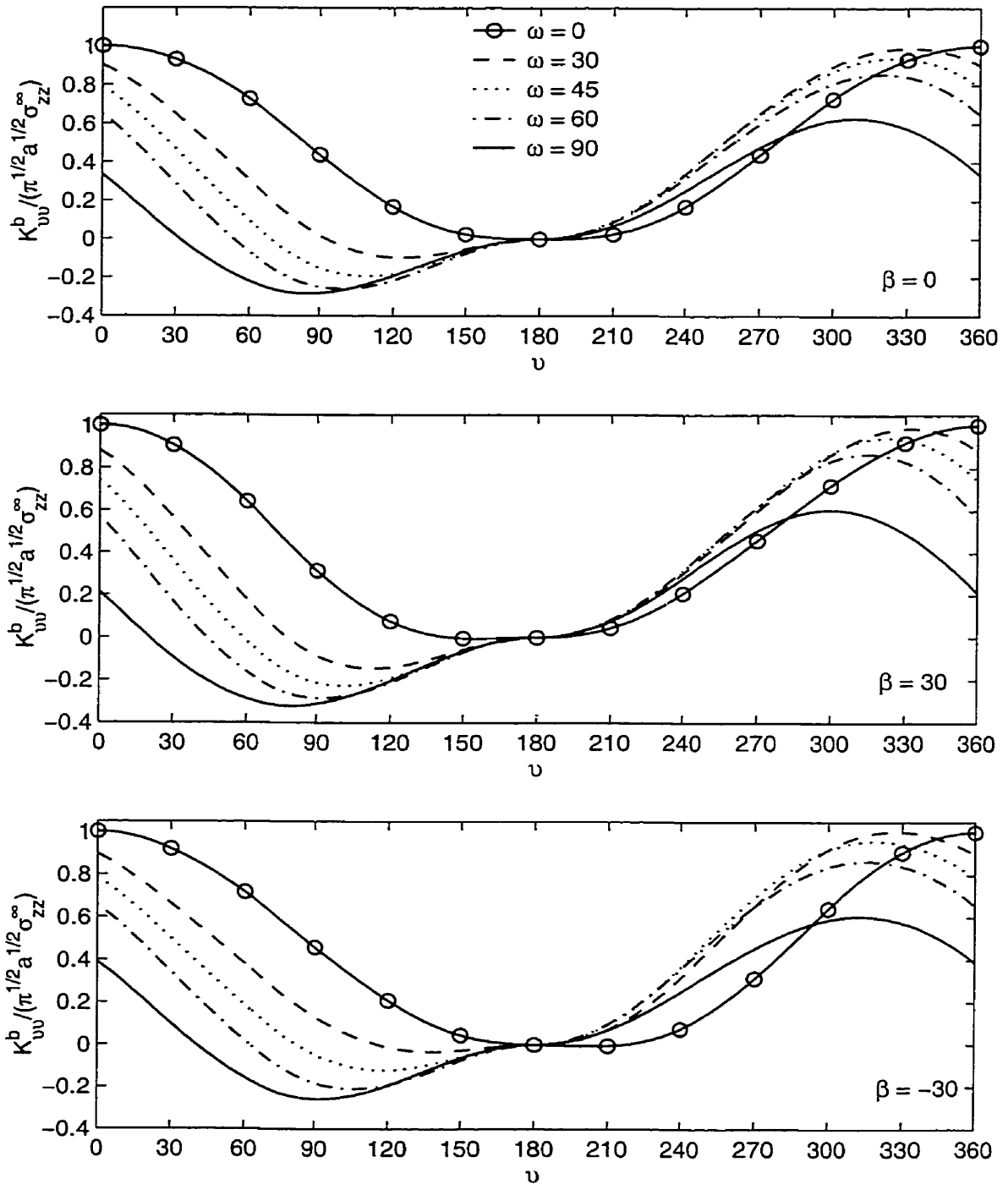


Figure 3.7: Variation of branch tip hoop stress intensity factors under remote tension for different branch angles and crack orientations (branch length $L/a = 0.01$).

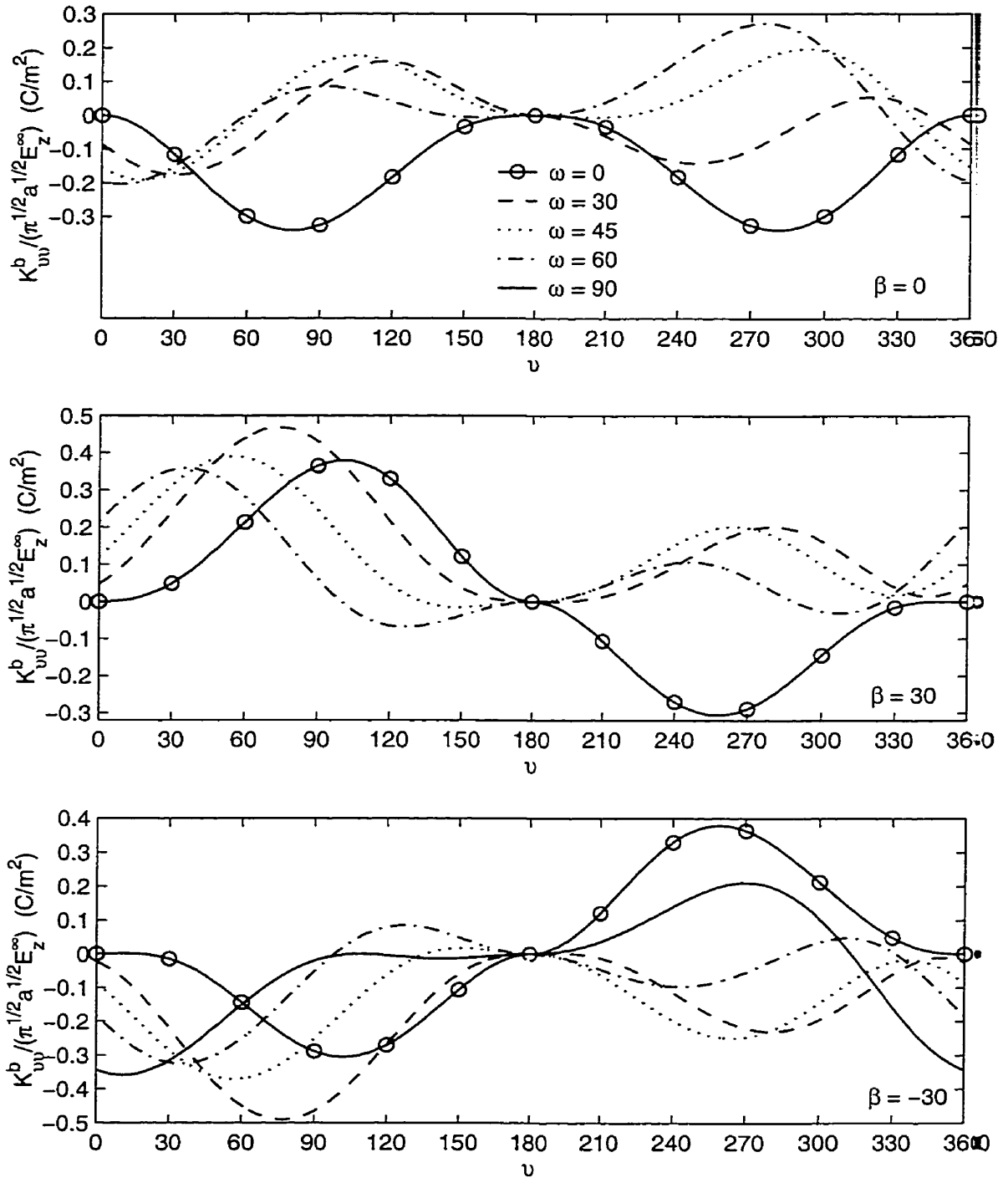


Figure 3.8: Variation of branch tip hoop stress intensity factors under positive electric field for different branch angles and crack orientations (branch length $L/a = 0.01$).

Table 3.3: Comparison of stress intensity factors at the tip of a symmetrically branched crack in an isotropic elastic solid under remote tension ($L_1 = L_2 = 2a$, $\omega_1 = -\omega_2 = \omega$).

ω (deg)	$K_I^{b_1}/K_I$		$K_{II}^{b_1}/K_I$	
	Theocaris & Ioakimidis (1976)	Present Study	Theocaris & Ioakimidis (1976)	Present Study
30	0.90	0.90	0.46	0.47
45	0.65	0.65	0.66	0.66
60	0.34	0.34	0.70	0.71
90	-0.11	-0.11	0.39	0.39

effect of a branch. In the case of electric field loading (Figure 3.8), the hoop stress intensity factors are significantly influenced by the crack orientation and branch angle. A branch may play either an amplifying or a shielding effect on the hoop stress intensity factor depending on the crack orientation and branch angle.

3.4.2 A bifurcated crack

In the absence of any known solutions for a bifurcated crack in piezoelectrics, the present results are compared with two solutions for isotropic elastic solids reported in the literature. Theocaris and Ioakimidis (1976) analyzed a symmetrically branched crack in an isotropic elastic solid and presented the results for the stress intensity factors. Let $\omega_1 = -\omega_2 = \omega$, $L_1 = L_2 = 2a$ and $\beta = 0^\circ$ in Figure 3.1b. Consider a fictitious piezoelectric material with $a_{13} = a_{23} = 0$, $a_{12} = -0.25a_{11}$, $a_{33} = 2.5a_{11}$, $a_{22} = a_{11}/1.001$ ($a_{22} = a_{11}$ corresponds to ideal isotropic case), negligible piezoelectric coefficients ($b_{ij} \approx 10^{-12}$), and identical dielectric constants as PZT-4. The normalized stress intensity factors $K_I^{b_1}/K_I$ and $K_{II}^{b_1}/K_I$ at the branch 1 tip are shown in Table 3.3 for various branch angle ω under remote uniform tension, where K_I denotes the mode I stress intensity factor for a straight crack. Close agreement is observed confirming the accuracy of the present solution scheme. The problem of an asymmetrically branched crack with $L_1/a = 0.8$ and $L_2/a = 0.4$ (Figure 3.1b) in an isotropic elastic solid is considered in Table 3.4. The fictitious piezoelectric material described above is used again in the computation. The results for the stress intensity factor ratio $K_{II}^{b_1}/K_I^{b_1}$ at the branch 1 tip are presented in Table 3.4 for two cases of branch angles, along with the results given by Theocaris (1972) for isotropic elastic solids. Again good

Table 3.4: Comparison of stress intensity factor ratios at the tip of an asymmetrically branched crack in an isotropic elastic solid under remote tension ($L_1/a = 0.8$, $L_2/a = 0.4$).

ω_1 (deg)	ω_2 (deg)	$K_{II}^{b_1}/K_I^{b_1}$	
		Theocaris (1972)	Present Study
30	0	0.56	0.53
15	0	0.24	0.24

agreement is observed.

The electroelastic fields at branch tips of a bifurcated crack in PZT-4 (Figure 3.1b) are computed in terms of intensity factors (K_I^b , K_{II}^b , K_D^b). Branch angles ($|\omega_1|$ and $|\omega_2|$) in the range $[0^\circ, 120^\circ]$ are considered in view of practical applications. The conditions given by eqn (3.39) for an open bifurcated crack are checked during the computation, and only results satisfy these conditions are presented.

A special case of crack bifurcation in PZT-4, namely the problem of a symmetrically branched crack ($\omega_1 = -\omega_2 = \omega$ and $L_1 = L_2 = L$ in Figure 3.1b), is examined first. Four cases of branch lengths ($L/a = 0.001, 0.01, 0.1$ and 0.5) are considered. It is found that the trends of branch tip field intensity factors are similar to those of a branched crack. The field intensity factors at the branch tip of a bifurcated crack are generally smaller than those of a branched crack. The field intensity factors for large values of ω are close to the corresponding values of a branched crack, which confirms the fact that the interaction between the two branches becomes weak. The branch length has a weak effect on intensity factors when $L/a \leq 0.01$. It is noted that, compared to the case of a branched crack, the range of branch angle ω within which a crack remains open is narrower for a bifurcated crack, especially under electrical loading and with a large value of L/a . For example, a symmetrically branched crack with $L_1 = L_2 = 0.01a$ remains open only for $|\omega| < 30^\circ$ when $\beta = 60^\circ$ under positive electric loading. The details of numerical results are not shown for brevity.

The general case of a bifurcated crack (*i.e.*, the problem of an asymmetrically branched crack) is now considered. Let $L_2/a = 0.1$, $\omega_1 = 30^\circ$, $\omega_2 = 0^\circ$ in Figure 3.1b. Figures 3.9 and 3.10 present the stress intensity factor K_I^b under remote tension σ_{zz}^∞ and positive electric displacement D_z^∞ , respectively. Three values of crack orientation angles, namely $\beta = 0^\circ$, 30° and 90° , are considered. The value of branch length ratio L_1/L_2 varies from 0.5 to 2.0.

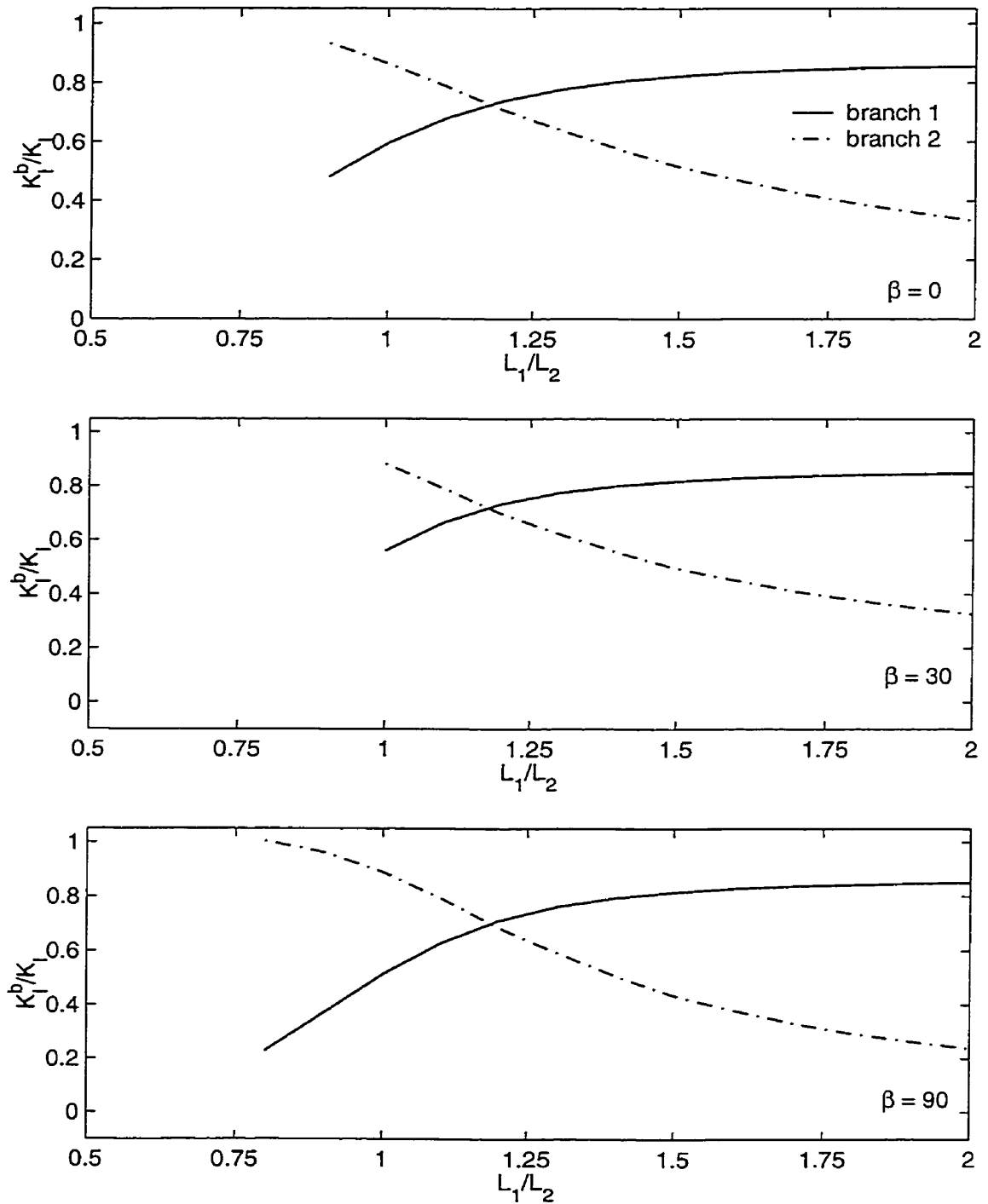


Figure 3.9: Stress intensity factors at the tips of an asymmetrically branched crack in PZT-4 under remote tension for different branch length ratios ($L_2/a = 0.1$, $\omega_1 = 30$, $\omega_2 = 0$ in Figure 3.1b).

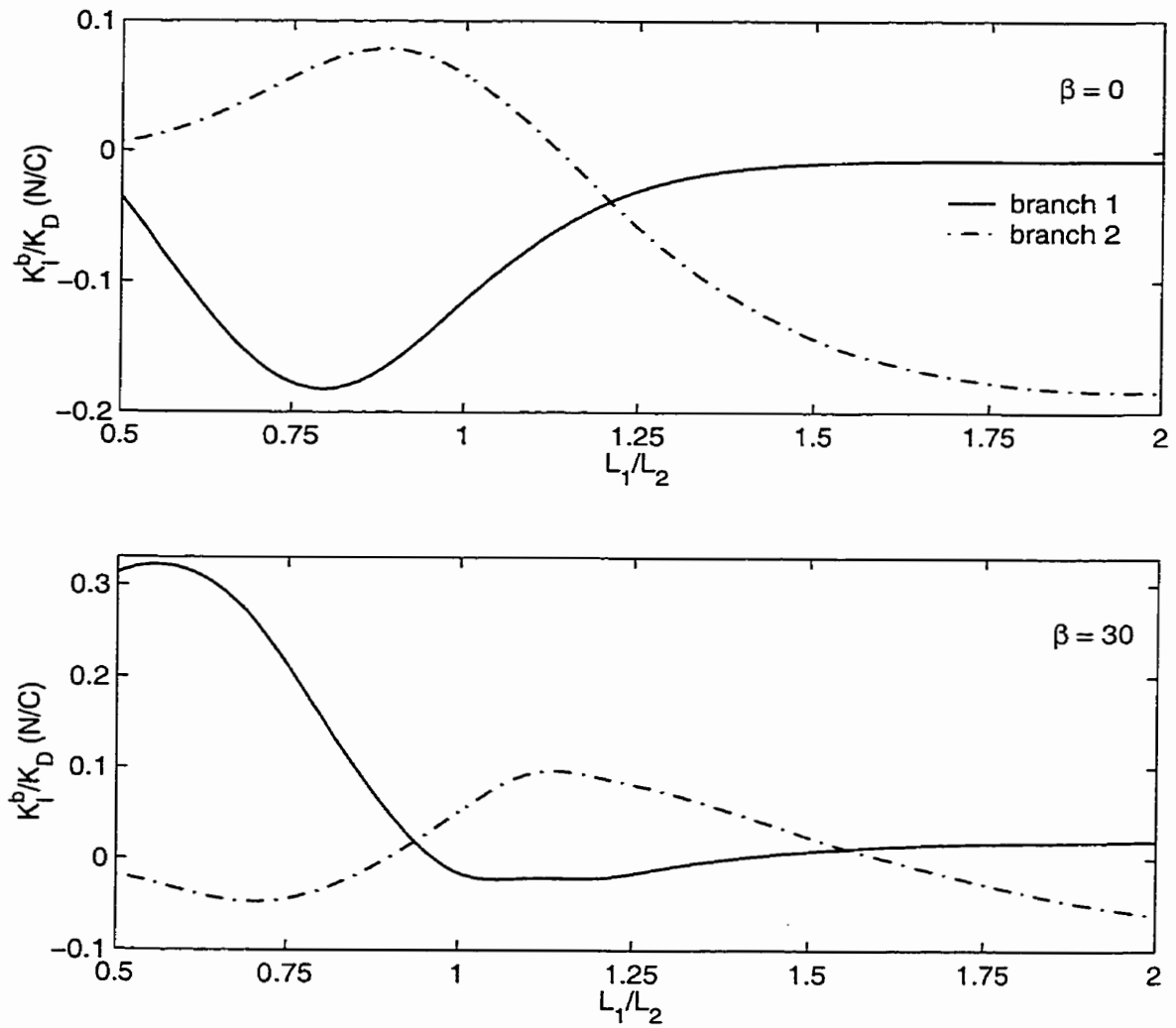


Figure 3.10: Stress intensity factors at the tips of an asymmetrically branched crack in PZT-4 under positive electric field for different branch length ratios ($L_2/a = 0.1$, $\omega_1 = 30$, $\omega_2 = 0$ in Figure 3.1b).

In the case of mechanical loading (Figure 3.9), crack orientation has a negligible influence on the stress intensity factor, but a different crack orientation angle corresponds to a different range of L_1/L_2 which renders an open crack. The case of $\beta = 90^\circ$ has the widest range of L_1/L_2 while $\beta = 30^\circ$ corresponds to the narrowest range. An open crack is expected for all three values of β when branch 1 is longer than branch 2. It is found that, when the branch length ratio L_1/L_2 is larger than 1.2, the stress intensity factor of branch 1 increases steadily and that of branch 2 decreases quite fast. The opposite trend is true when the length ratio L_1/L_2 is smaller than 1.2. This observation indicates that, if the fracture process is controlled by the stress intensity factor, the occurrence of a microscopic branch would make the longer branch even longer. Therefore, there is little chance that two branches can simultaneously grow. The shorter branch cracks are frequently left behind a main crack. In the case of positive electric loading (Figure 3.10), a crack remains always open for the considered range of L_1/L_2 when $\beta = 0^\circ$ or 30° . However, crack closure happens for the whole range of L_1/L_2 when $\beta = 90^\circ$. The trend of the stress intensity factor corresponding to $\beta = 0^\circ$ is similar to that in the case of mechanical loading. The case of $\beta = 30^\circ$ is different. The trend that a longer branch accompanies a larger value of stress intensity factor is observed only in the range of $L_1/L_2 > 1.6$. Consider the same problem as in Figures 3.9 and 3.10 but with $\omega_2 = -15^\circ$. The variations of stress intensity are shown in Figures 3.11 and 3.12. A similar conclusion, as in Figures 3.9 and 3.10, is drawn with regard to the relation between the stress intensity and the branch length for both mechanical and electric loading.

3.5 Conclusion

The extended distributed dislocation modeling technique is successfully applied to study arbitrarily oriented branched cracks in piezoelectric materials. The branched crack problem is reduced to the solution of a system of singular integral equations with dislocation densities along the branch line as unknowns. The condition for an open crack has been taken into consideration.

The validation of the present scheme is confirmed by comparing with the results for special cases reported in the literature. It is noted that the asymptotic electroelastic fields at a branch tip have complex dependence on branch length, branch angle, crack orientation and the type of loading. The influence of applied electric loading is more complicated and significant than mechanical loading. The trends of field intensity factors of a branched

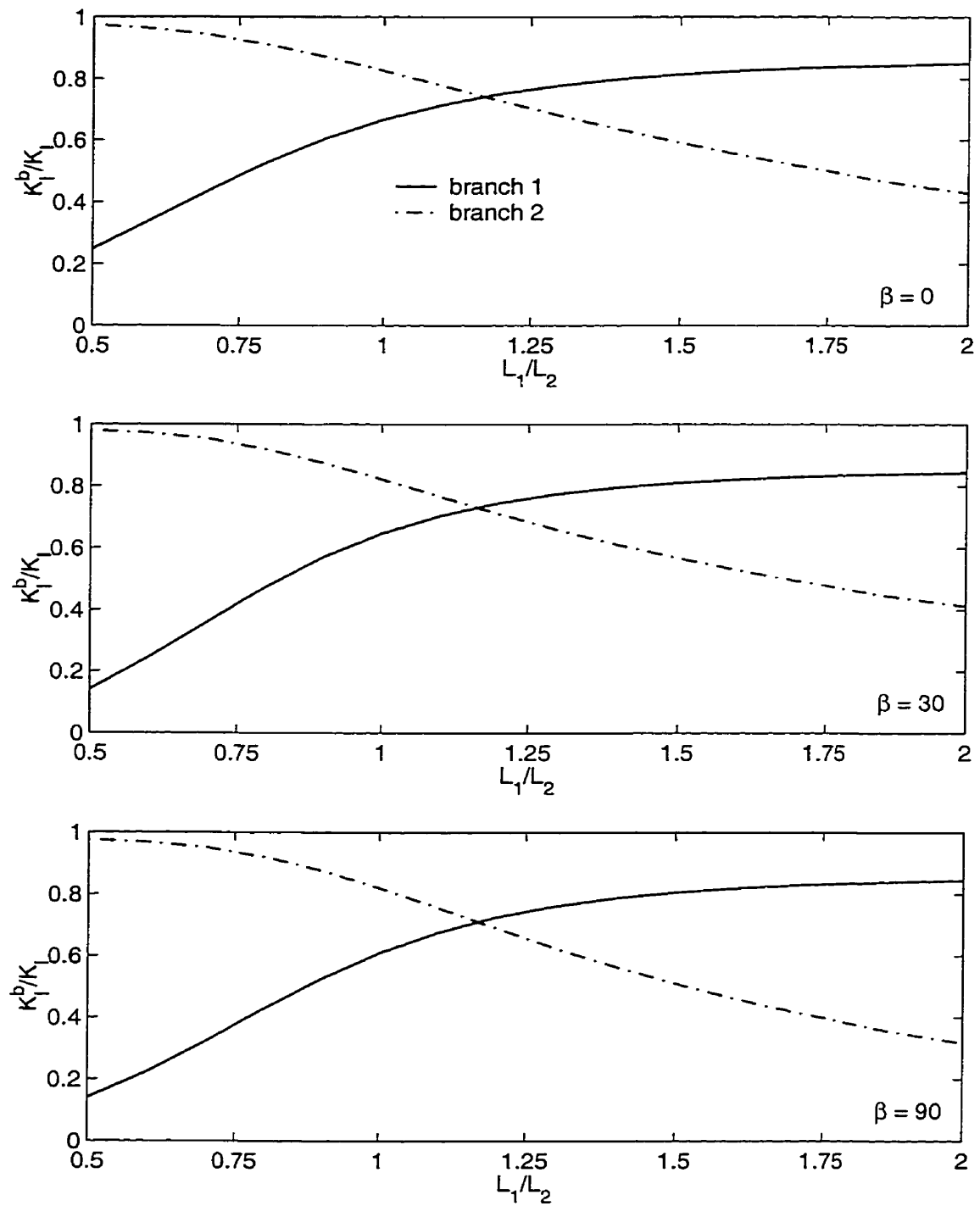


Figure 3.11: Stress intensity factors at the tips of an asymmetrically branched crack in PZT-4 under remote tension for different branch length ratios ($L_2/a = 0.1$, $\omega_1 = 30$, $\omega_2 = -15$ in Figure 3.1b).

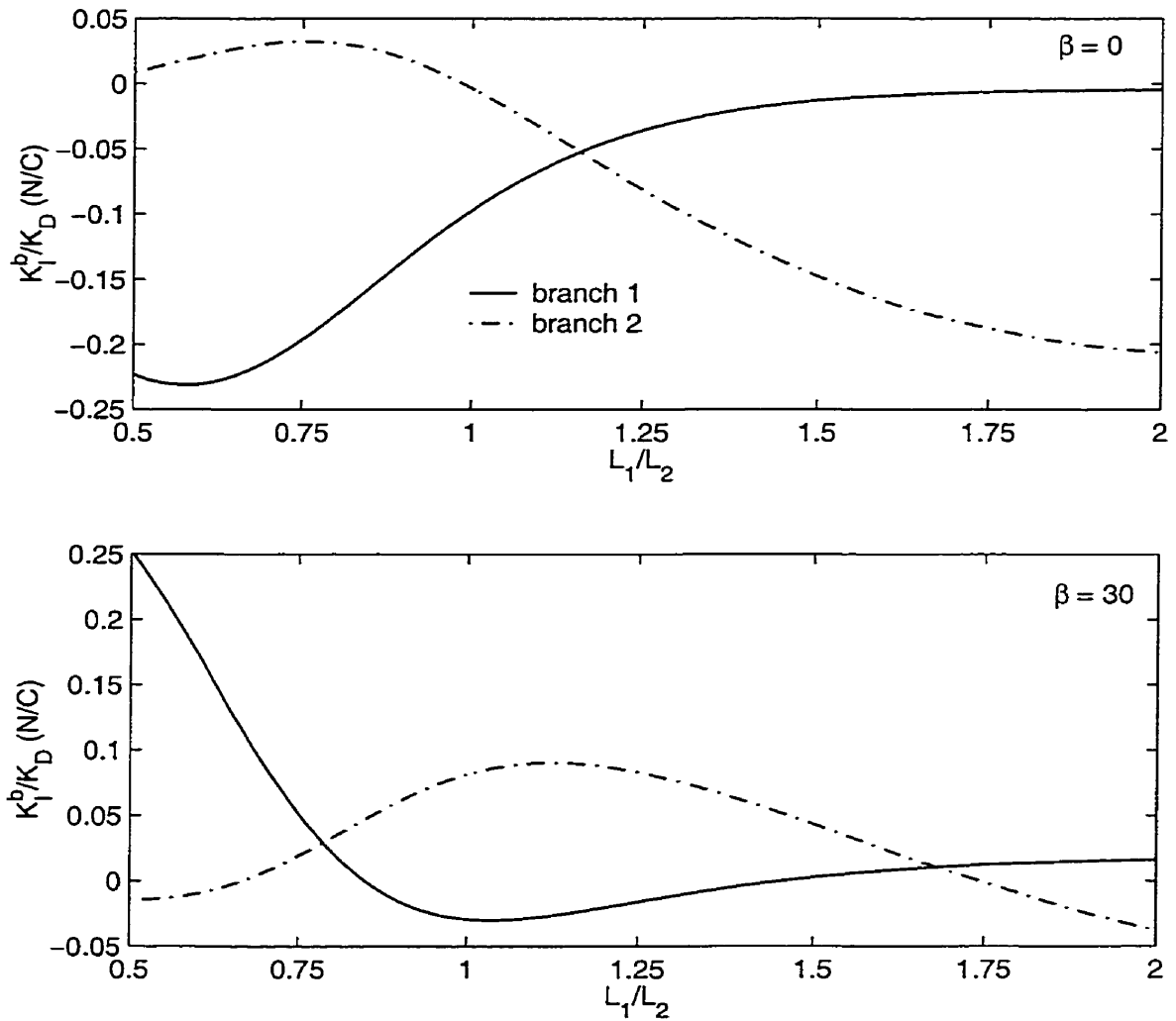


Figure 3.12: Stress intensity factors at the tips of an asymmetrically branched crack in PZT-4 under positive electric field for different branch length ratios ($L_2/a = 0.1$, $\omega_1 = 30$, $\omega_2 = -15$ in Figure 3.1b).

crack are similar to those of a symmetrically branched crack, but a symmetrically branched crack has a narrower range of branched angles which render crack open. The results for an asymmetrically branched crack indicate that, if stress intensity factor is responsible for the fracture process, it is unlikely that two branches can simultaneously grow when a bifurcated crack is under remote tension or a bifurcated crack perpendicular to the poling direction is under electric loading.

Chapter 4

Fracture Criteria

4.1 Fracture toughness anisotropy

For isotropic materials, a single parameter such as K_{IC} is adequate to describe fracture toughness. In contrast, planes of low fracture resistance exist in anisotropic materials, cracks may be trapped onto such planes even though hoop stress or energy release rate may not be maximum on these planes. Polarized ceramics generally have anisotropic material properties. Therefore, the orientation dependence of fracture toughness in piezoelectric ceramics should be considered when dealing with crack propagation. Based on the available experimental results, a simple model is developed in this section to describe the fracture toughness anisotropy in piezoelectric ceramics.

The critical stress intensity factor K_c is often used in the experimental studies to discuss fracture toughness. Fracture toughness of polarized ceramics in directions parallel to the poling direction (K_0) and perpendicular to the poling direction (K_{90}) have been experimentally measured, as well as fracture toughness of unpolled ceramics (Calderson-Moreno, *etc*, 1997; Pisarenko, *etc*, 1985; Chen, *etc*, 1999). Unpolled specimen show isotropic fracture toughness, while $K_0 > K_{90}$ is observed for polarized ceramics. The ratio K_0/K_{90} for a PZT (PC4D Type 1 from Morgan Matroc) measured by the indentation method is as large as 2.69 (Calderson-Moreno, *etc*, 1997). Pisarenko *et al* (Pisarenko, *etc*, 1985) reported that K_0/K_{90} is in the range 1.15 ~ 2.36 for four different piezoceramics.

Let $K_c(\theta)$ denote the fracture toughness along the direction θ in a piezoceramic (Figure 4.1), where θ is measured with respect to the poling direction z' . Due to material symmetry about z' ,

$$K_c(\theta + \pi) = K_c(\theta); \quad K_c(-\theta) = K_c(\theta) \quad (4.1)$$

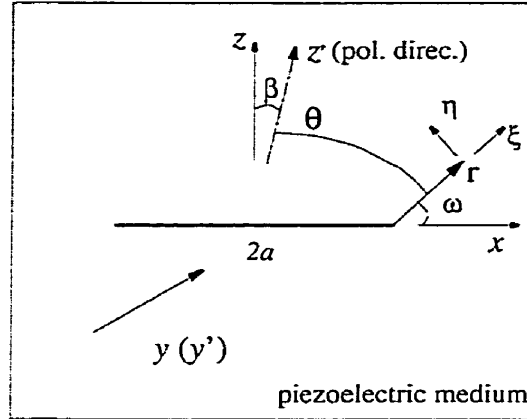


Figure 4.1: Illustration of fracture toughness anisotropy in piezoelectrics.

The general form of $K_c(\theta)$ can be expressed by (Tan, 1990),

$$K_c(\theta) = A_0 - \sum_{n=1} A_n \sin^2(n\theta) \quad (4.2)$$

where A_n are a set of constants.

When two principal toughnesses $K_c(0^\circ) = K_0$ and $K_c(90^\circ) = K_{90}$ are known, considering the two leading terms of eqn (4.2) yields,

$$K_c(\theta) = K_0 \cos^2 \theta + K_{90} \sin^2 \theta \quad (4.3)$$

If toughness along a third direction is also known, *e.g.* $K_c(45^\circ) = K_{45}$, considering the first three terms of eqn (4.2) gives,

$$K_c(\theta) = K_0 \cos^2 \theta + K_{90} \sin^2 \theta - 0.5(K_0 + K_{90} - 2K_{45}) \sin^2(2\theta) \quad (4.4)$$

Eqn (4.3) is used in this study to calculate fracture toughness at an arbitrary direction when predicting potential fracture propagation in piezoelectrics. Noting that $\theta = 90^\circ - \omega - \beta$ in Figure 4.1, eqn (4.3) can be expressed as

$$K_c^\omega = K_c(90^\circ - \omega - \beta) = K_0 \sin^2(\omega + \beta) + K_{90} \cos^2(\omega + \beta) \quad (4.5)$$

Experimental findings (Chen *et al*, 1999; *etc*) indicate that fracture toughness of piezoelectric solids is not only related to material anisotropy but also affected by applied stress σ^∞ and electric field \mathbf{E}^∞ , *i.e.* $K_c = K_c(\theta, \sigma^\infty, \mathbf{E}^\infty)$. Applied loading may cause domain reorientation near a crack tip which also contributes to toughness changes. This topic is still in its infancy requiring further experimental and theoretical studies.

Eqn (4.3) or (4.5) gives the fracture toughness in terms of the critical stress intensity factor at an arbitrary direction. The critical energy release rate need be quantitatively described in a piezoelectric solid, when applying an energy-based criterion. Currently, no experimental data of critical energy release rate G_c are available. In view of the fact that energy release rates are quadratic functions of field intensity factors (*e.g.* eqn (2.44)), it is assumed that

$$G_c^\omega = k (K_c^\omega)^2 \quad (4.6)$$

where $G_c^\omega = G_c(\theta)$ and $K_c^\omega = K_c(\theta)$ are critical values of energy release rate and stress intensity factor (Figure 4.1), respectively; k is a constant in a given material.

4.2 A stress-based criterion

Considering the anisotropic behavior of piezoceramics, the criterion of modified hoop stress intensity factor is used to predict crack propagation (Azhdari and Nemat-Nasser, 1996). Define modified hoop stress intensity factor K^* as

$$K^*(\omega) = K_{\omega\omega}/K_c^\omega \quad (4.7)$$

where $K_{\omega\omega}$ is the hoop stress intensity factor and K_c^ω is the fracture toughness.

It is assumed that at a pre-existing crack tip, crack growth takes place along the direction α which renders the modified hoop stress intensity factor $K^*(\omega)$ maximum, and a crack propagates when

$$K_{\alpha\alpha} \geq K_c^\alpha \quad (4.8)$$

Doblare *et al* (1998) and Gregory and Herakovich (1986) used criteria similar to the eqns (4.7) and (4.8) for anisotropic elastic materials. It was found that theoretical predictions generally agree with experimental results.

The criterion of modified stress intensity factor is now applied to discuss potential propagation of a pre-existing impermeable crack in PZT-4 (Appendix A) under applied mechanical or electric loading. Both the straight crack model and the branched crack model can be used to evaluate the hoop stress intensity factor $K_{\omega\omega}$ required by eqn (4.7). In the later case, a vanishingly small branch length should be used, and K_I^b should be used in place of $K_{\omega\omega}$ in eqn (4.7). It is assumed that toughness anisotropy ratio $K_0/K_{90} = 2$ in the absence of experimental data for PZT-4 material used in this study. The assumed value is within the range

of fracture toughness anisotropy for PZT materials obtained in experiments (Pisarenko, *et al.*, 1985). Figures 4.2a and 4.3a, based on the branched crack model, show the variation of normalized hoop stress intensity factor ratio $K_0K^*/(\sqrt{\pi a}\sigma_{zz}^\infty)$ and $K_0K^*/(\sqrt{\pi a}E_z^\infty)$ under remote tension and positive electric field loading, respectively. In these figures, only results corresponding to the ranges of branch angles which satisfy the condition of an open branch (eqn (3.35)) are shown. The corresponding results from the straight crack model are shown in Figures 4.2b and 4.3b. The following observations are drawn from Figures 4.2 and 4.3.

The modified hoop stress intensity factors based on the branched crack model and straight crack model have similar trends. The two models show quite identical results for mechanical loading. For electric field loading, the differences are noted in the intensity factor magnitudes and in the ranges of ω for an open branch. However, the two models show nearly equal branch angles corresponding to the maximum values of K^* for $\beta = 0^\circ$, 60° and 90° . For example, as shown in Figure 4.3, K^* has a maximum value of 0.6222 for $\omega = -69^\circ$ and $\beta = 60^\circ$ based on the branched crack model, while the straight crack model shows a maximum value 0.7156 (13% higher) at $\omega = -71^\circ$.

The requirement of an open branch can only be considered by the branched crack model. Incorrect conclusions may be drawn by neglecting this requirement, especially under electric field loading. For example in Figure 4.3, the potential propagation directions are 106° and 45° for $\beta = 45^\circ$ based on the straight crack model and the branched crack model, respectively. The branched crack model shows branch closure happens when $\omega > 45^\circ$. In addition, the effects of non-singular stress σ_{xx}^∞ and electric field E_x^∞ on crack propagation, which may significantly affect the crack path stability, can only be discussed by using a branched crack model.

In the case of remote tensile loading, a self-similar crack extension is expected for $\beta = 0^\circ$ based on the modified intensity factor criterion. For $\beta \neq 0^\circ$, the crack deviates from the straight path. The theoretical branching directions are -22° , -32° and -40° for crack orientation angles $\beta = 30^\circ$, 45° and 60° , respectively. The crack could branch into any direction between $[-31^\circ, 31^\circ]$ when the poling direction is parallel to the crack line. In the case of positive electric field loading, no crack extension is expected when the poling direction is perpendicular to the crack line. The theoretical branching angles are 61° , 45° , -69° and -95° for $\beta = 30^\circ$, 45° , 60° and 90° , respectively. Note even in a symmetric case (*e.g.* remote electric loading perpendicular to the crack and the poling direction parallel to the crack), a crack may deviate from the straight extension path.

Distinctly different branching angles would be predicted if the assumption of isotropic

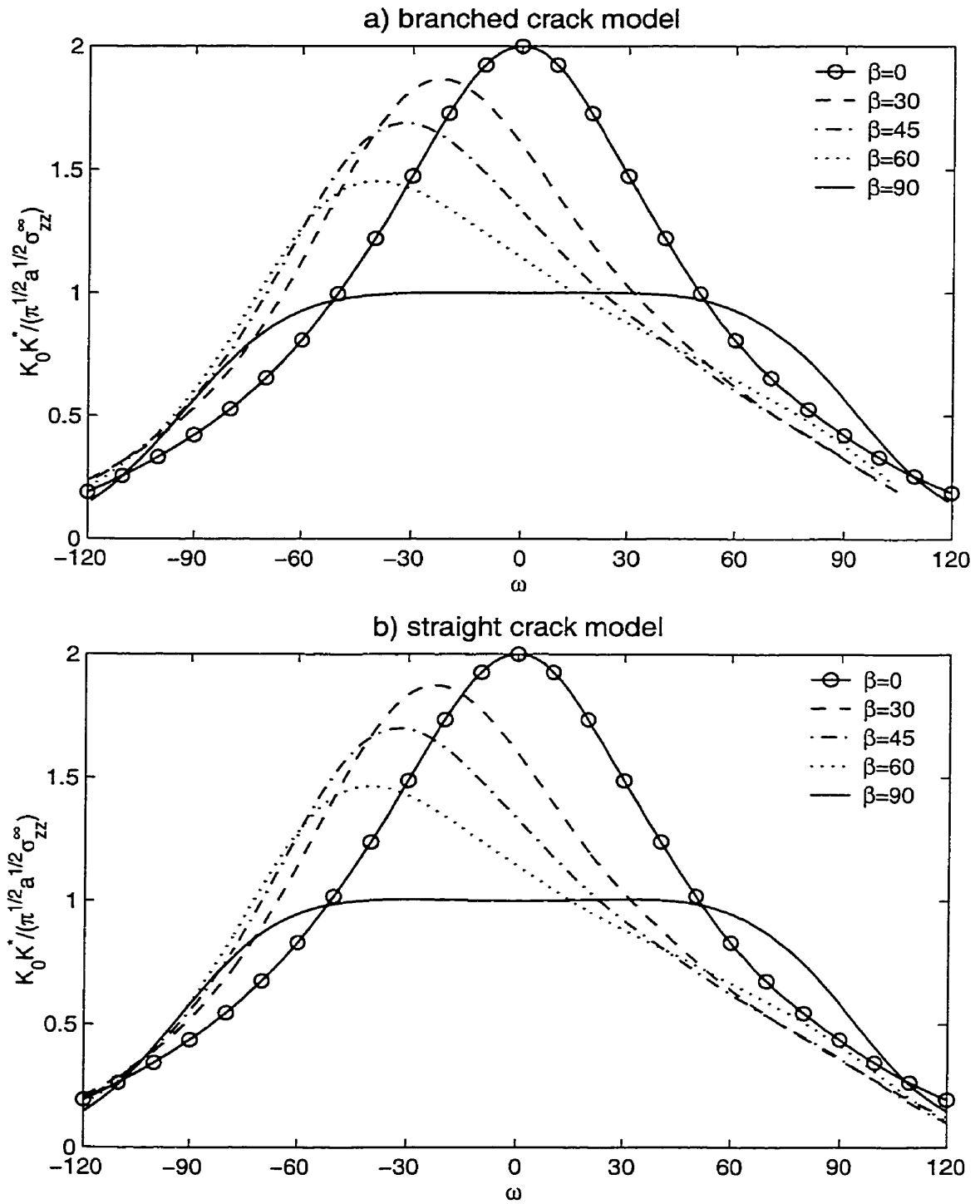


Figure 4.2: Variation of modified hoop stress intensity factor under remote tension loading for different crack orientation angles.

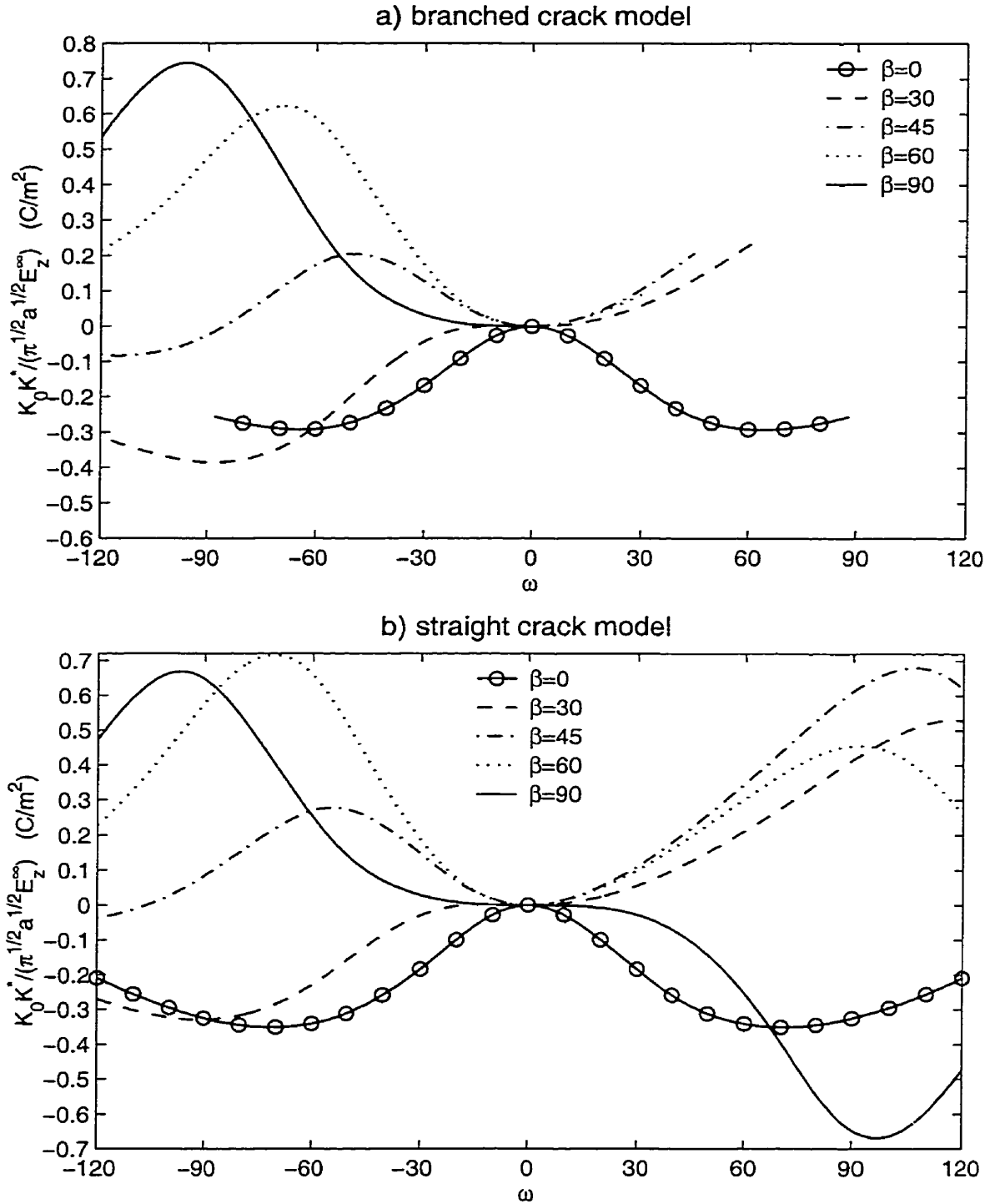


Figure 4.3: Variation of modified hoop stress intensity factor under positive electric field loading for different crack orientation angles.

fracture toughness was used in Figures 4.2 and 4.3. For example, the theoretical branching direction would be 0° rather than -22° for $\beta = 30^\circ$ under remote tensile loading.

4.3 Angular distribution of energy release rates

The energy release rate given by eqn (2.44), being based on self-similar crack extension, has limited application. In order to properly discuss crack propagation directions using energy-based criteria, energy release rates along an arbitrary direction at a crack tip should be known. Therefore, this section aims at seeking the angular distribution of energy release rates.

Consider a crack with impermeable boundary (Figure 4.1). Assuming the crack extends a small length of L along the ω -direction, the total energy release rate can be expressed by

$$G(\omega) = \lim_{L \rightarrow 0} \frac{1}{2L} \int_0^L [\sigma_{\omega\omega}(r, \omega) \Delta u_\eta + \sigma_{\tau\omega}(r, \omega) \Delta u_\xi + D_\omega(r, \omega) \Delta \phi] dr \quad (4.9)$$

where $\sigma_{\omega\omega}(r, \omega)$, $\sigma_{\tau\omega}(r, \omega)$ and $D_\omega(r, \omega)$ are the hoop stress, shear stress and hoop electric displacement at the crack tip before branching, and are given by eqns (3.12) or (3.13); Δu_η , Δu_ξ and $\Delta \phi$ are the crack branch opening displacement along the η -direction, ξ -direction, and the jump in the electric potential across the branch faces after branching.

The solution for a branched crack derived in Chapter Three is used here to evaluate Δu_η , Δu_ξ and $\Delta \phi$. L_{mk} in eqn (3.30) can be symbolically rewritten as,

$$L_{mk} = Q_{mk} l_{ij} + Q_{mk}^* l_{ij}^* \quad (4.10)$$

where l_{ij} , l_{ij}^* are defined in eqn (3.24), and Q_{mk} , Q_{mk}^* are functions of material constants, angles β and ω .

Since $z_i^0 = a + s(\cos \omega + \mu_i \sin \omega)$ and $z_i = a + \rho(\cos \omega + \mu_i \sin \omega)$, l_{ij} in eqn (3.24) can be expressed as

$$l_{ij}(\rho, s) = \frac{1}{\rho T_i - s T_j} \left(\frac{\sqrt{s T_j (s T_j + 2a)}}{\sqrt{\rho T_i (\rho T_i + 2a)}} - 1 \right) \quad (4.11)$$

Perform a variable change from $[0, L]$ to $[0, 1]$ using $\rho = \hat{\rho}L$, and $s = \hat{s}L$ on eqn (3.28) and related equations. Consider the limiting case of a vanishingly small branch ($L \rightarrow 0$). Using $L^2 = 0$, eqn (4.11) can be reduced to

$$l_{ij}(\hat{\rho}, \hat{s}) = \frac{1}{L} \frac{-1.0}{\sqrt{\hat{\rho} T_i} (\sqrt{\hat{s} T_j} + \sqrt{\hat{\rho} T_i})} \quad (4.12)$$

Similarly for l_{ij}^* ,

$$l_{ij}^*(\hat{\rho}, \hat{s}) = \frac{1}{L} \frac{-1.0}{\sqrt{\hat{\rho}T_i}(\sqrt{\hat{s}T_j} + \sqrt{\hat{\rho}T_i})} \quad (4.13)$$

$f_1(\rho)$, $f_2(\rho)$ and $f_3(\rho)$ in eqn (3.31) represent the shear stress, hoop stress and hoop electric displacement around a straight crack under uniform loading, respectively. At the crack tip ($r = L \rightarrow 0$), these electroelastic fields can be expressed in their asymptotic form. Therefore,

$$\{f_1(\hat{\rho}), f_2(\hat{\rho}), f_3(\hat{\rho})\}^T = -\frac{1}{\sqrt{2\pi L\hat{\rho}}} \{K_{r\omega}, K_{\omega\omega}, K_{D\omega}\}^T \quad (4.14)$$

Using eqns (3.32), (4.10)-(4.13), eqn (3.28) can now be rewritten as

$$\begin{aligned} & \frac{1}{L} \int_0^1 \sum_{i=1}^3 \frac{\{M_{1i}, M_{2i}, M_{3i}\}^T B_i(\hat{s})}{(\hat{\rho} - \hat{s}) \sqrt{\hat{s}(1-\hat{s})}} d\hat{s} - \frac{1}{L} \int_0^1 \sum_{k=1}^3 \left[\frac{\{Q_{1k}, Q_{2k}, Q_{3k}\}^T B_k(\hat{s})}{\sqrt{\hat{\rho}T_i}(\sqrt{\hat{s}T_j} + \sqrt{\hat{\rho}T_i})} + \right. \\ & \left. \frac{\{Q_{1k}^*, Q_{2k}^*, Q_{3k}^*\}^T B_k(\hat{s})}{\sqrt{\hat{\rho}T_i}(\sqrt{\hat{s}T_j} + \sqrt{\hat{\rho}T_i})} \right] \frac{1}{\sqrt{\hat{s}(1-\hat{s})}} d\hat{s} = -\frac{1}{\sqrt{2\pi L\hat{\rho}}} \{K_{r\omega}, K_{\omega\omega}, K_{D\omega}\}^T \end{aligned} \quad (4.15)$$

It is seen from eqn (4.15) that density functions $B_i(\hat{s})$ are proportional to \sqrt{L} . Therefore Δu_η , Δu_ξ and $\Delta\phi$ are also proportional to \sqrt{L} according to eqns (3.34) and (3.35), and intensity factors K_I^b , K_{II}^b and K_D^b are independent of the length L based on eqn (3.33). These conclusions are valid for the limiting case of a vanishingly small branch ($L \rightarrow 0$).

Performing a variable change from $[0, L]$ to $[0, 1]$ on eqn (4.9) and making use of eqn (3.13) yield

$$G(\omega) = \lim_{L \rightarrow 0} \frac{1}{2L} \int_0^1 \frac{1}{\sqrt{2\pi L\hat{s}}} [K_{\omega\omega} \Delta u_\eta(\hat{s}) + K_{r\omega} \Delta u_\xi(\hat{s}) + K_{D\omega} \Delta\phi(\hat{s})] L d\hat{s} \quad (4.16)$$

Due to the fact that Δu_η , Δu_ξ and $\Delta\phi$ are proportional to \sqrt{L} for a vanishingly small branch, eqn (4.16) can be expressed as,

$$G(\omega) = \frac{1}{2\sqrt{2\pi}} \int_0^1 \frac{1}{\sqrt{\hat{s}}} \left[K_{\omega\omega} \frac{\Delta u_\eta(\hat{s})}{\sqrt{L}} + K_{r\omega} \frac{\Delta u_\xi(\hat{s})}{\sqrt{L}} + K_{D\omega} \frac{\Delta\phi(\hat{s})}{\sqrt{L}} \right] d\hat{s} \quad (4.17)$$

Therefore, in the case of a vanishingly small branch, energy release rates (strain, electrical and total) are independent of the branch length L . Eqn (4.17) completes the solution for angular distribution of energy release rates. The numerical approach of piecewise quadratic polynomials proposed by Gerasoulis (1982) is used to evaluate integrals in eqn (4.17).

Alternatively, energy release rates along an arbitrary direction at a crack tip can be obtained by following a common practice (Azhdari and Nemat-Nasser, 1996). Transforming eqn (2.44) to $\xi\eta$ system yields,

$$\begin{aligned}
G^M(\omega) &= Im \sum_{n=1}^3 \bar{q}_n \bar{t}_{1n} (K_I^b)^2 + Im \sum_{n=1}^3 \bar{p}_n \bar{t}_{2n} (K_{II}^b)^2 + Im \sum_{n=1}^3 (\bar{q}_n \bar{t}_{2n} + \bar{p}_n \bar{t}_{1n}) K_I^b K_{II}^b \\
&\quad + Im \sum_{n=1}^3 \bar{p}_n \bar{t}_{3n} K_{II}^b K_D^b + Im \sum_{n=1}^3 \bar{q}_n \bar{t}_{3n} K_I^b K_D^b \\
G^E(\omega) &= Im \sum_{n=1}^3 \bar{s}_n \bar{t}_{1n} K_I^b K_D^b + Im \sum_{n=1}^3 \bar{s}_n \bar{t}_{2n} K_{II}^b K_D^b + Im \sum_{n=1}^3 \bar{s}_n \bar{t}_{3n} (K_D^b)^2
\end{aligned} \tag{4.18}$$

where variables \bar{p}_n , \bar{q}_n , \bar{s}_n and \bar{t}_{jn} are defined in the $\xi\eta$ system, corresponding to p_n , q_n , s_n and t_{jn} in the xz system; K_I^b , K_{II}^b and K_D^b are field intensity factors at the branch tip.

It is noted that eqn (4.18) gives the energy release rates based on an infinitesimal extension of an existing infinitesimal small branch, while eqn (4.17) gives the results due to the occurrence of branching. A comparison of results calculated by these two approaches is made in Table 4.1 through numerical examples. A general polarization angle ($\beta = 30^\circ$) is considered. Far field loading are tensile stress $\sigma_{zz}^\infty = 100N/m^2$ and electric field E_z^∞ . It is found that the total energy release rates from the two different approaches are identical for both PZT-4 and PZT-5H. However, this is not the case for the strain energy release rate, especially when the ratio of electric to mechanical load is large. For example, the difference between two approaches is 20% in PZT-5H when $E_z^\infty/\sigma_{zz}^\infty = 5$ and $\omega = 45^\circ$. Therefore, eqn (4.18) based on the common practice is generally not valid, and should not be used to calculate energy release rates. In view of this observation, eqn (4.17), corresponding to branch nucleation, is used in the ensuing part of this Chapter.

Kumar and Singh (1997a, b) used the finite element technique to calculate the angular distribution of the energy release rates in piezoelectrics. As reported by themselves, there is discrepancy between their finite element solutions and the analytical solutions by Pak (1992). Taking $\beta = 0^\circ$ and $\omega = 0^\circ$, it is found that the results of present scheme agree with Pak (1992). The accuracy of the present scheme is further confirmed by a comparison with the solutions for elastic solids reported by Azhdari and Nemat-Nasser (1996). Assume that Figure 4.1 shows an elastic medium with material coordinate system $x'z'$, a'_{ij} (corresponding to a_{ij} in eqn (2.3)) are material constants with respect to the material system, and β denotes the orientation of crack with respect to the material axis. According to Azhdari and Nemat-Nasser (1996), $a'_{13} = 0$, $a'_{23} = 0$, $a'_{11} = 1/E_{11}$, $a'_{22} = 1/E_{22}$, $a'_{33} = 1/E_{66}$, $a'_{12} = -0.25/E_{22}$ and $\beta = -\theta$, where E_{11} , E_{22} , E_{66} and angle θ are given in Table 4.2. A fictitious piezoelectric

Table 4.1: Comparison of energy release rates calculated by eqns (4.17) and (4.18) in PZT-4 and PZT-5H ($\sigma_{zz}^{\infty} = 100\text{N/m}^2$, $\beta = 30^\circ$).

	$E_z^{\infty}/\sigma_{zz}^{\infty}$ (Vm/N)	ω	G^M/a (N/m ²)		G/a (N/m ²)	
			eqn (4.18)	eqn (4.17)	eqn (4.18)	eqn (4.17)
PZT-4	0.2	30°	7.65×10^{-7}	7.69×10^{-7}	-6.25×10^{-6}	-6.25×10^{-6}
	1.0	45°	1.50×10^{-6}	1.59×10^{-6}	-1.55×10^{-4}	-1.55×10^{-4}
	5.0	30°	2.30×10^{-6}	3.48×10^{-6}	-4.03×10^{-3}	-4.03×10^{-3}
	5.0	45°	-7.71×10^{-6}	-5.81×10^{-6}	-3.87×10^{-3}	-3.87×10^{-3}
PZT-5H	0.2	30°	8.03×10^{-7}	8.08×10^{-7}	-1.24×10^{-5}	-1.24×10^{-5}
	1.0	45°	2.08×10^{-6}	2.14×10^{-6}	-2.98×10^{-4}	-2.98×10^{-4}
	5.0	30°	1.04×10^{-5}	1.10×10^{-5}	-7.88×10^{-3}	-7.88×10^{-3}
	5.0	45°	4.00×10^{-6}	4.99×10^{-6}	-7.44×10^{-3}	-7.44×10^{-3}

Table 4.2: Comparison of energy release rates $G(\omega)/G^{\infty}(0^\circ)$ in orthotropic elastic solid.

E_{11}	E_{22}	E_{66}	σ_{zz}^{∞}	σ_{xz}^{∞}	θ	ω	Azhdari <i>et al</i> (1996)	Present study
1	1	0.4	0	100	0°	-77°	1.510	1.508
1	2	0.4	100	0	-30°	-90°	0.190	0.190
1	20	0.8	50	-50	-60°	45°	1.312	1.311
2	10	0.4	100	20	-30°	-90°	0.805	0.806
8	1	0.8	32	48	-60°	-150°	0.216	0.216
9	1	1.38	-49	100	2°	-49°	0.779	0.780

material with same elastic constants used by Azhdari and Nemat-Nasser (1996), negligible piezoelectric coefficient ($b_{ij} \approx 10^{-12}$), and identical dielectric constants as PZT-4 is used. The comparison between the two results is made in Table 4.2. Good agreement is observed for a variety of material properties, loading conditions and branch angles.

4.4 Energy-based criteria

Parallel to eqn (4.7), modified strain energy release rate $H^M(\omega)$ and modified total energy release rate $H(\omega)$ are defined as

$$\begin{aligned} H^M &= G^M(\omega)/G_c^\omega \\ H &= G(\omega)/G_c^\omega \end{aligned} \quad (4.19)$$

where $G^M(\omega)$ and $G(\omega)$ are angular distributions of strain and total energy release rates, respectively.

The criterion of modified strain energy release rate assumes that, at a pre-existing crack tip, crack growth takes place along the direction α which renders the modified strain energy release rate $H^M(\omega)$ maximum, and a crack propagates when

$$G^M(\alpha) \geq G_c^\alpha \quad (4.20)$$

Similarly, the criterion of modified total energy release rate assumes that crack growth takes place along the direction α which renders $H(\omega)$ maximum, and a crack propagates when

$$G(\alpha) \geq G_c^\alpha \quad (4.21)$$

It is noted that Azhdari and Nemat-Nasser (1998) suggested an energy-based criterion similar to eqns (4.19)-(4.21) for anisotropic elastic materials based on their experimental study.

The proposed fracture criteria are now applied to discuss potential propagation of a pre-existing straight crack in PZT-4. Assuming $K_0/K_{90} = 2$, critical fracture energy release rate G_c^ω is calculated based on eqns (4.5) and (4.6). Figures 4.4 and 4.5 present the variation of modified energy-release rates with varying crack branch angles (ω) under mechanical and electric loading, respectively. The corresponding results of modified hoop stress intensity factor of eqn (4.7) based on the branched crack model are also shown for the purpose of comparison. In these figures, only results corresponding to the ranges of branch angles which satisfy the condition of an open branch are shown.

Assume tensile stress $\sigma_{zz}^{\infty} = 0.6MPa$ at far field. Normalized modified strain energy release rate $H^M G_0/a$ and modified hoop stress intensity factor $K^* K_0/(\sqrt{\pi a} \sigma_{zz}^{\infty})$ are shown in Figures 4.4a and 4.4b, respectively. G_0 and K_0 are the critical energy release rate and critical stress intensity factor along the poling direction ($\theta = 0^\circ$), respectively. The results of modified total energy release rate are virtually identical to those of strain energy release rate, and are therefore not shown. It is seen that the modified strain energy release rate and hoop stress intensity factor have very similar trends except for the case of $\beta = 90^\circ$. The theoretical branching angles based on these two criteria are also close to each other when $\beta \neq 90^\circ$. The potential branching directions, based on the energy based criterion, are -25° , -37° , -48° and $\pm 64^\circ$ for polarization angle $\beta = 30^\circ$, 45° , 60° and 90° , respectively. A self-similar extension is expected for $\beta = 0^\circ$. Therefore, in the case of mechanical loading, the criterion of modified strain energy release rate is virtually equivalent to the criterion of modified total energy release rate. The theoretical branching angles based on these two energy-based criteria are close to those predicted by the stress-based criterion except $\beta = 90^\circ$.

Now consider electric field $E_z^{\infty} = 12KV/m$ at far field. Normalized modified strain energy release rate $H^M G_0/a$, modified total energy release rate $H G_0/a$ and modified hoop stress intensity factor $K^* K_0/(\sqrt{\pi a} E_z^{\infty})$ are shown in Figures 4.5a, 4.5b and 4.5c, respectively. In contrast to the case of mechanical loading, it is found that the results of total energy release rate are now totally different from those of strain energy release rate. Negative values of total energy release rate are observed for all values of ω and β , implying no crack propagation based on the criterion of modified total energy release rate. The modified strain energy release rate and hoop stress intensity factor have somewhat similar trends, but the theoretical branching angles based on these two criteria are quite different. The potential branching directions, based on the modified strain energy release rate criterion, are $\pm 30^\circ$, -7° , -48° , -61° and -88° for polarization angles $\beta = 0^\circ$, 30° , 45° , 60° and 90° , respectively. Note that a crack tends to deviate from the straight extension path regardless of crack orientation angles. This prediction qualitatively agrees the experimental finding reported by McHenry and Koepke (1983).

Distinctly different propagation directions would be predicted if the isotropic fracture toughness were used in Figs. 4.4 and 4.5. For example, based on the criterion of strain energy release rate, a self-similar crack extension would be predicted rather than branching along $\omega = \pm 30^\circ$ for a crack under electric loading when $\beta = 0^\circ$.

The cases of combined mechanical and electric loading are considered in Figs. 4.6-4.9.

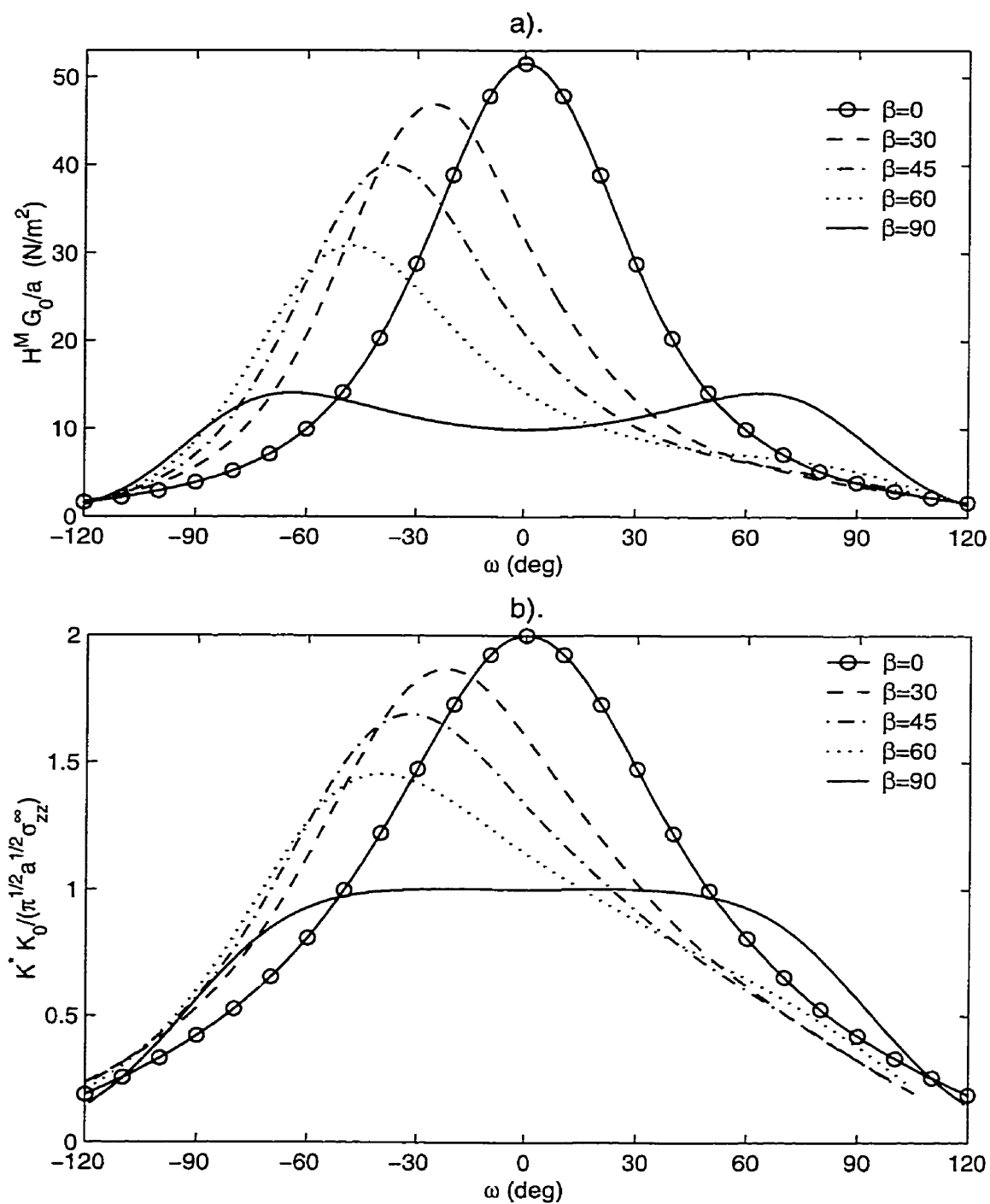


Figure 4.4: Variation of modified strain energy release rate and modified hoop stress intensity factor at crack tip in PZT-4 under remote tensile stress $\sigma_{zz}^\infty = 0.6 \text{ MPa}$.

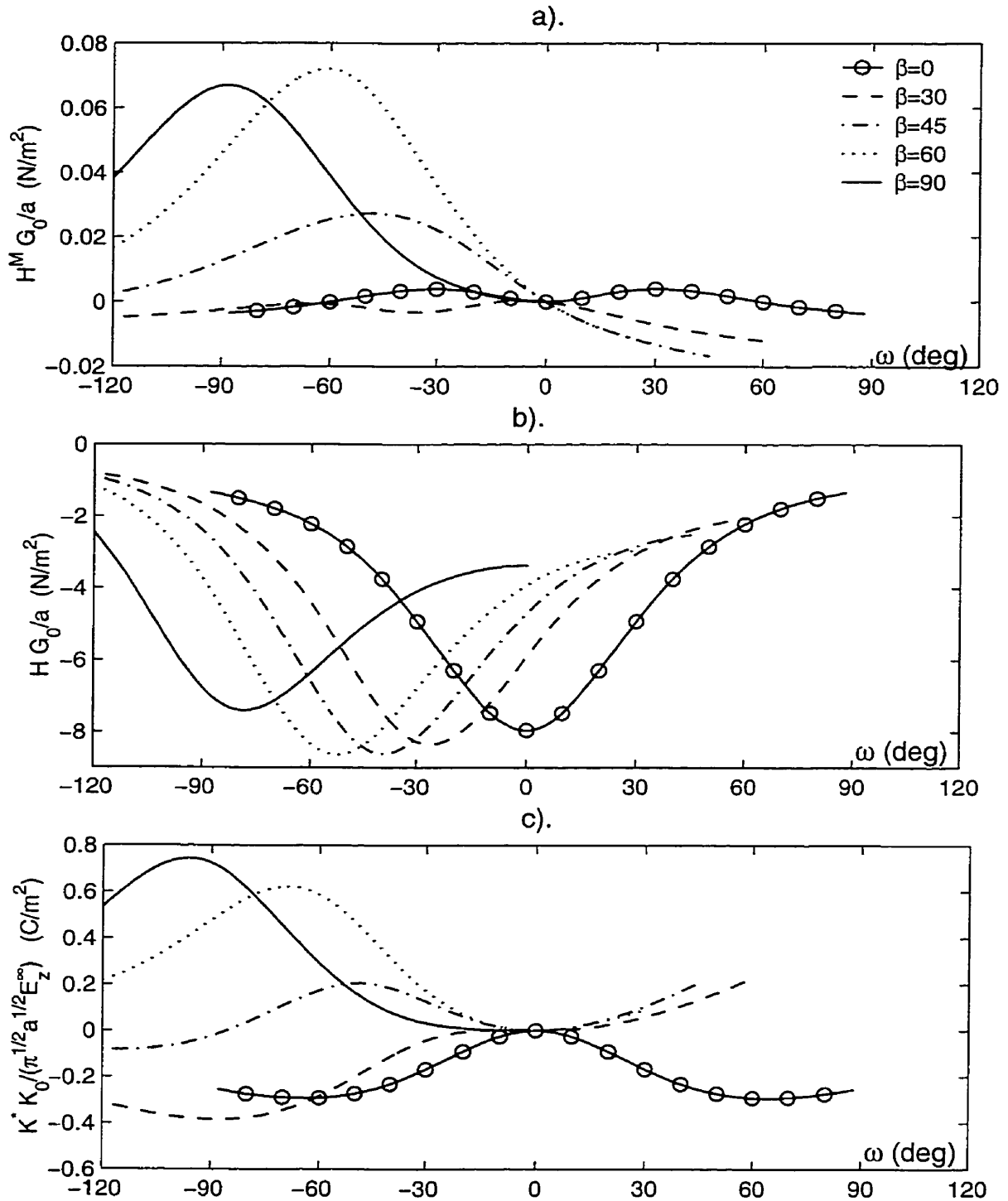


Figure 4.5: Variation of modified energy release rates and modified hoop stress intensity factor at crack tip in PZT-4 under positive electric field $E_z^\infty = 12KV/m$.

Figs. 4.6 and 4.7 are for modified strain energy release rate (H^M), and Figs. 4.8 and 4.9 are for modified total energy release rate (H). Constant tensile stress $\sigma_{zz}^\infty = 0.6MPa$ and two levels of electric field, *i.e.* $E_z^\infty = \pm 12KV/m$ (Figs. 4.6 and 4.8) and $\pm 60KV/m$ (Figs. 4.7 and 4.9), are applied at far field. Three cases of polarization angles, *i.e.* $\beta = 0^\circ, 30^\circ$ and 90° are computed. Only results corresponding to the ranges of branch angles which satisfy the condition of an open branch are shown.

Based on the criterion of modified strain energy release rate (Figs. 4.6 and 4.7), a positive electric field tends to promote crack propagation and a negative one tends to retard crack propagation for all ω values when $\beta = 0^\circ$ or 30° . When $\beta = 90^\circ$, an electric field can either promote or retard crack propagation depending on the direction of electric field and branch angle ω . A positive electric field tends to promote crack extension if branch angle $\omega < 0$, and slow down or cause crack closure if branch angle $\omega > 0$. The opposite effect is true for a negative electric field.

If the criterion of total energy release rate is applied (Figs. 4.8 and 4.9), the effect of an applied electric field on crack propagation is dramatically different. An electric field always impedes crack propagation regardless of crack orientation angles, direction of electric field and branch angles. Crack closure may happen for a wide range of branch angles when an electric field is strong (Figure 4.9).

4.5 Conclusion

Relaxing the assumption of self-similar crack extension and taking the fracture toughness anisotropy into consideration, a new stress-based fracture criterion and two energy-based criteria, namely the criteria of modified hoop stress intensity factor, modified strain energy release rate and modified total energy release rate, are proposed to predict potential propagation directions of impermeable cracks in piezoelectric ceramics.

Numerical results show that distinctly different propagation directions would be predicted if the assumption of isotropic fracture toughness were used in both stress and energy-based criteria. In the application of modified hoop stress intensity factor, the predicted results based on the branch crack model are compared with those based on the straight crack model. It is found that the straight crack model may lead to erroneous conclusions, especially in the case of electric loading. It is noted that a crack may branch off from a straight path even under symmetric loading and geometry. Under applied mechanical loading, the criteria of modified strain energy release rate and modified total energy release rate are

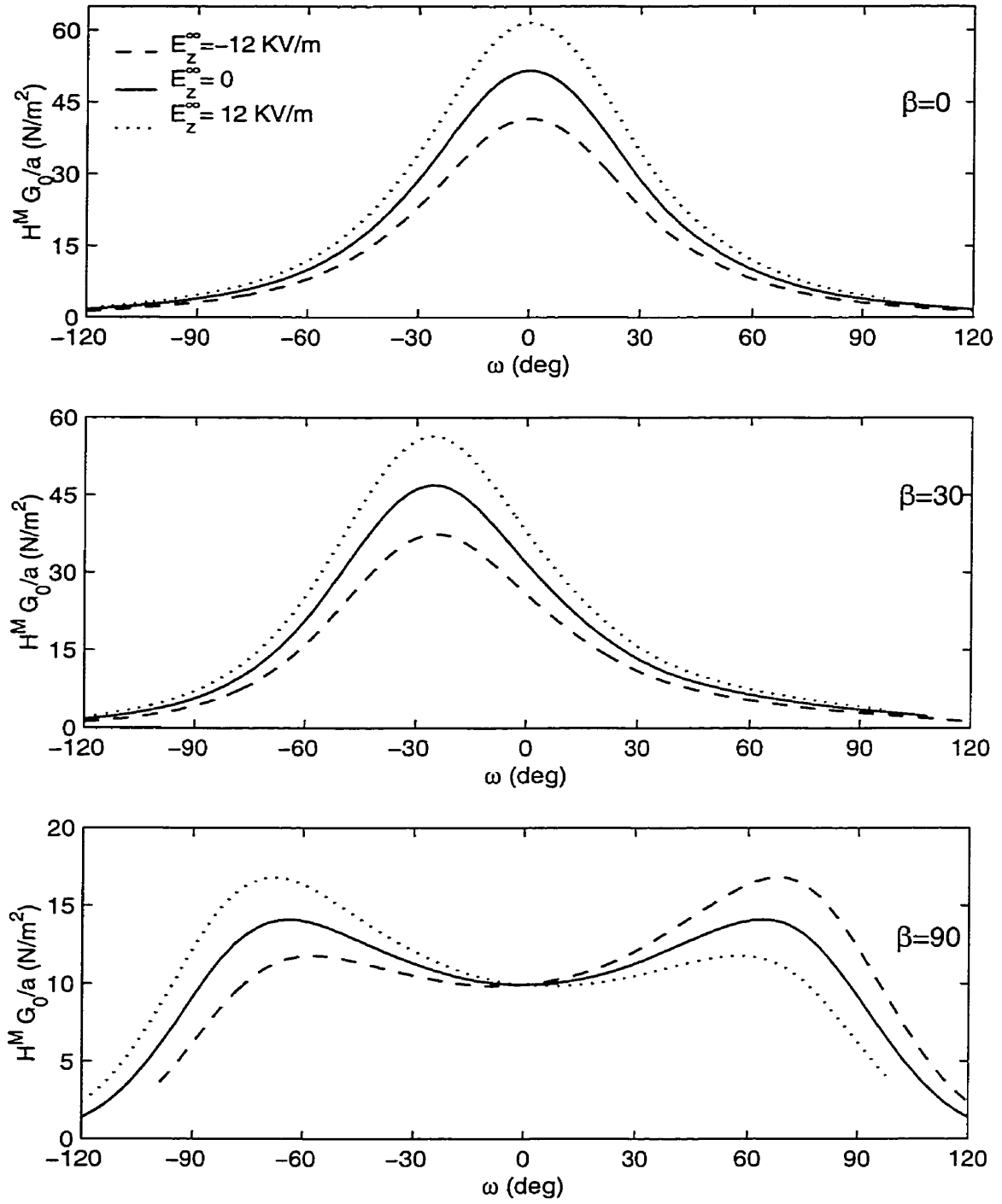


Figure 4.6: Variation of modified strain energy release rate at crack tip in PZT-4 under applied tensile stress $\sigma_{zz}^\infty = 0.6MPa$ or electric field $E_z^\infty = \pm 12KV/m$.

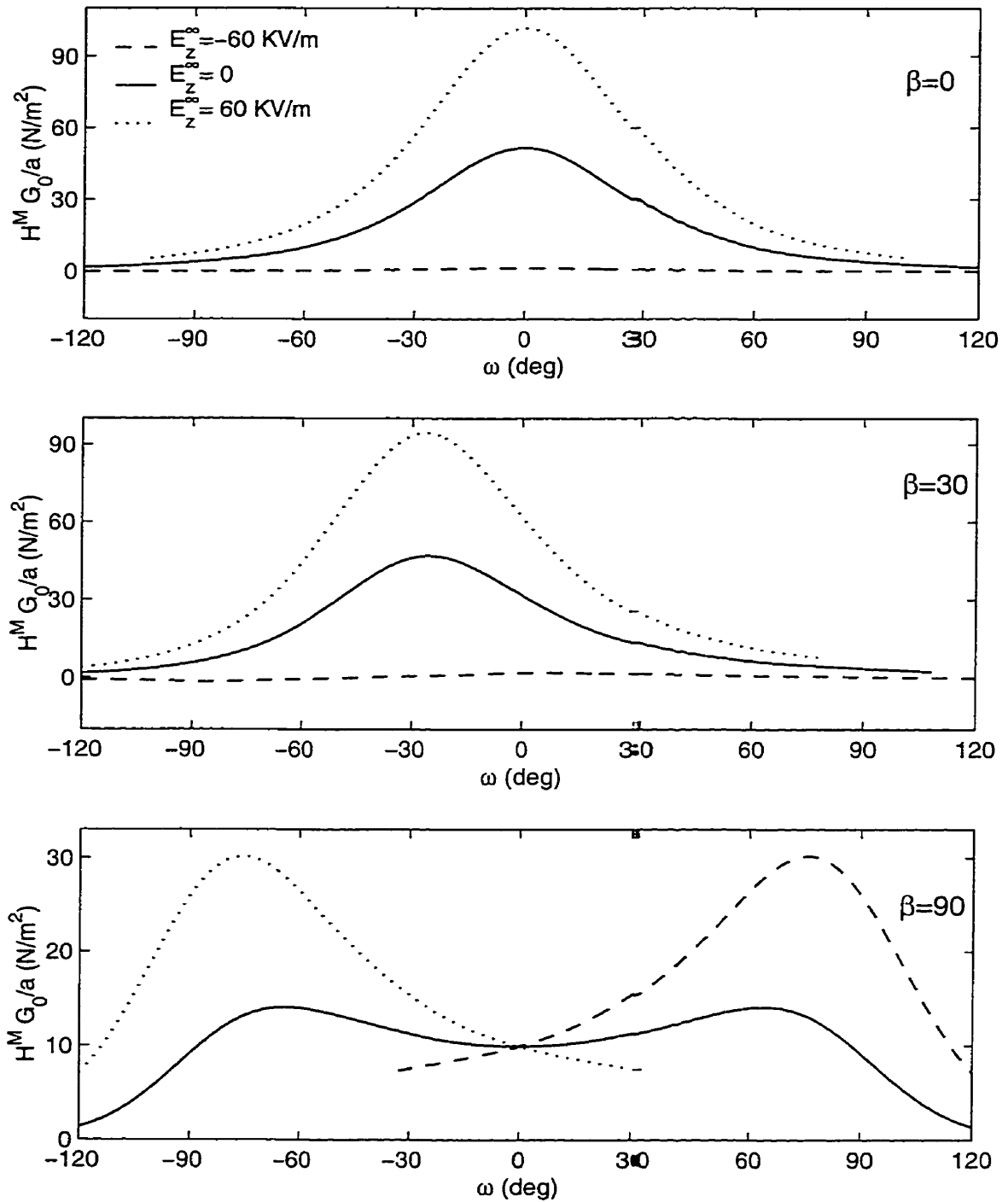


Figure 4.7: Variation of modified strain energy release rate at crack tip in PZT-4 under applied tensile stress $\sigma_{zz}^\infty = 0.6 MPa$ or electric field $E_z^\infty = \pm 60 KV/m$.

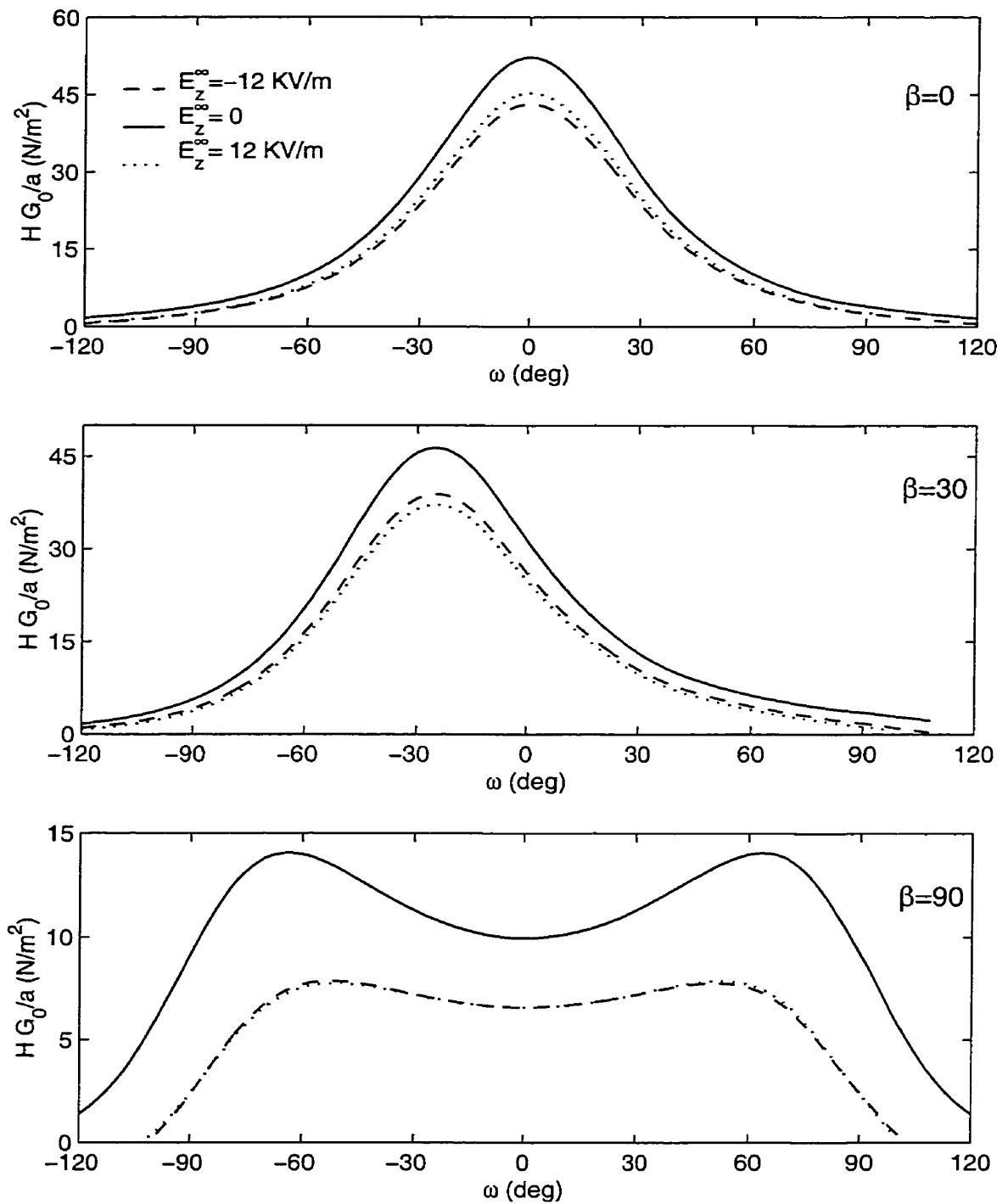


Figure 4.8: Variation of modified total energy release rate at crack tip in PZT-4 under applied tensile stress $\sigma_{zz}^\infty = 0.6$ MPa or electric field $E_z^\infty = \pm 12$ KV/m.

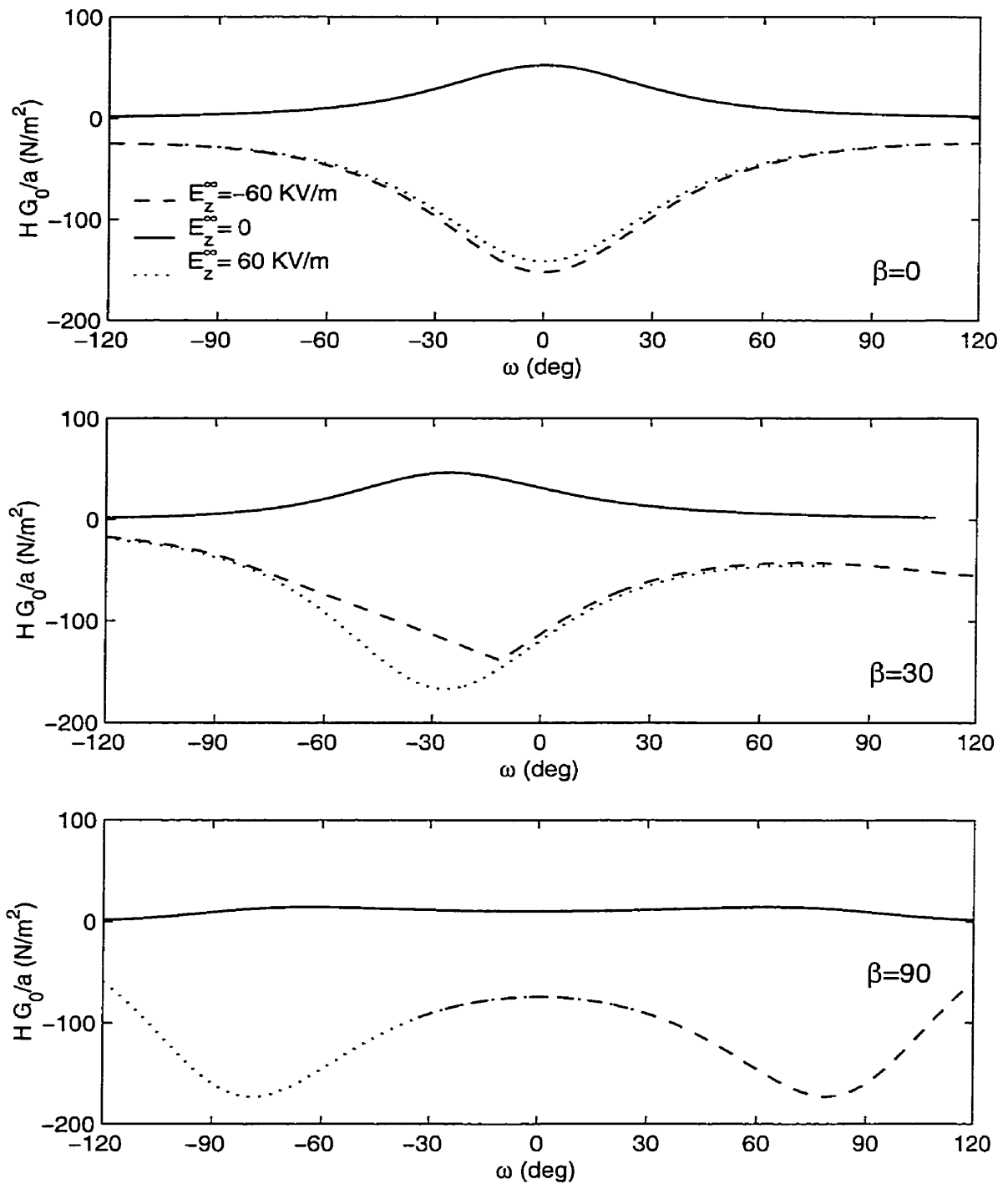


Figure 4.9: Variation of modified total energy release rate at crack tip in PZT-4 under applied tensile stress $\sigma_{zz}^\infty = 0.6 MPa$ or electric field $E_z^\infty = \pm 60 KV/m$.

virtually equivalent, and the two energy-based criteria and the stress-based criterion predict similar crack propagation paths. Under applied electrical loading, however, the predicted propagation paths by the stress-based criterion are significantly different from those by the energy-based criteria. Based on the criterion of strain energy release rate, a crack tends to branch off from a straight path regardless of the polarization angle. Under combined mechanical and electric loading, an electric field can either promote or retard crack propagation depending on the crack branching angle, the polarization angle and the direction of applied electric field.

Currently, no experimental data are available in the literature to check with the theoretical branching directions predicted in this study. Coordinated experimental studies are needed to determine the exact nature of fracture toughness anisotropy and a suitable fracture criterion for piezoelectrics. The present theoretical study complemented with such experimental work is important to advanced engineering applications of piezoelectric materials.

Chapter 5

Singularities in Piezoelectric Wedges

5.1 Governing equations

Consider a piezoelectric wedge polarized along the direction z' , as shown in Figure 5.1. The geometry of wedge is defined by the two angles α and φ with respect to the x -axis. The z -axis of the coordinate system (x, y, z) makes angle β with the direction of polarization z' of the coordinate system (x', y', z') . Assuming planar electroelastic fields independent of y (y'), the constitutive equations with respect to the (x, y, z) system can be expressed as eqn (2.3).

Using the extended Lekhnitskii's formalism of eqn (2.4) given in Chapter 1, the sixth-order differential equation of eqn (2.5) can be derived. As noted in Chapter 1, the characteristic equation of eqn (2.5) generally have distinct roots. Therefore, the solution of functions F and Ψ in eqn (2.4) can be expressed in the following form.

$$F(x, z) = \sum_{n=1}^6 F_n(z_n); \quad \Psi(x, z) = \sum_{n=1}^6 \delta_n \frac{\partial F_n(z_n)}{\partial z_n} \quad (5.1)$$

where z_n and δ_n are defined under eqn (2.8).

The functions F_n ($n = 1, \dots, 6$) in eqn (5.1) can be written as power series of z_n . Since this study is focused on singular fields, it is sufficient to consider only the leading term of the power series. Therefore,

$$F(x, z) = \sum_{n=1}^6 A_n z_n^\lambda; \quad \Psi(x, z) = \sum_{n=1}^6 \lambda \delta_n A_n z_n^{\lambda-1} \quad (5.2)$$

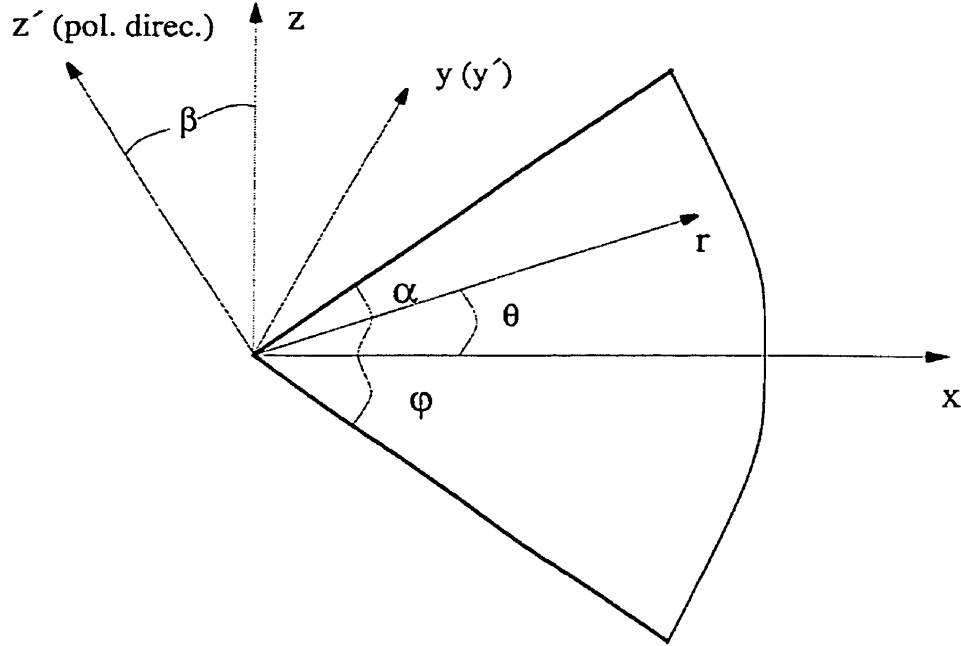


Figure 5.1: A piezoelectric wedge.

where λ is the power of the leading term and $A_n (n = 1, \dots, 6)$ are arbitrary coefficients.

It is convenient to introduce a polar coordinate system (r, θ) as shown in Figure 5.1 for the present class of problems. The following solutions for the complete electroelastic fields (displacement u_i , electrical potential ϕ , stress σ_{ij} , electric displacement D_i and electric field E_i) can be obtained by using eqn (5.2) and basic relations in piezoelectricity (Parton and Kudryavtsev 1988).

$$\begin{aligned}
 u_r &= \lambda \sum_{n=1}^6 A_n H_{1n} r_n^{\lambda-1}; & u_\theta &= \lambda \sum_{n=1}^6 A_n H_{2n} r_n^{\lambda-1}; & \phi &= \lambda \sum_{n=1}^6 A_n H_{3n} r_n^{\lambda-1} \\
 \sigma_{rr} &= \lambda(\lambda-1) \sum_{n=1}^6 A_n H_{7n} r_n^{\lambda-2}; & \sigma_{r\theta} &= \frac{1}{r} \lambda(\lambda-1) \sum_{n=1}^6 A_n H_{4n} r_n^{\lambda-1} \\
 \sigma_{\theta\theta} &= \frac{1}{r} \lambda(\lambda-1) \sum_{n=1}^6 A_n H_{5n} r_n^{\lambda-1} \\
 D_r &= \lambda(\lambda-1) \sum_{n=1}^6 A_n H_{8n} r_n^{\lambda-2}; & D_\theta &= \frac{1}{r} \lambda(\lambda-1) \sum_{n=1}^6 A_n H_{6n} r_n^{\lambda-1} \\
 E_r &= -\frac{1}{r} \lambda(\lambda-1) \sum_{n=1}^6 A_n H_{3n} r_n^{\lambda-1}; & E_\theta &= \lambda(\lambda-1) \sum_{n=1}^6 A_n H_{3n} H_{4n} r_n^{\lambda-2} \quad (5.3)
 \end{aligned}$$

where $r_n = r(\cos \theta + \mu_n \sin \theta)$, μ_n are roots of eqn (2.6), p_n , q_n and s_n are defined under eqn (2.10), and

$$\begin{aligned} H_{1n} &= p_n \cos \theta + q_n \sin \theta; & H_{2n} &= -p_n \sin \theta + q_n \cos \theta; & H_{3n} &= s_n \\ H_{4n} &= \sin \theta - \mu_n \cos \theta; & H_{5n} &= \cos \theta + \mu_n \sin \theta; & H_{6n} &= -\delta_n \\ H_{7n} &= (\mu_n \cos \theta - \sin \theta)^2; & H_{8n} &= \delta_n (\mu_n \cos \theta - \sin \theta) \end{aligned} \quad (5.4)$$

It is worth mentioning that eqn (5.4) can also be obtained by utilizing the correspondence between plane piezoelectricity and generalized plane strain in elasticity established recently by Chen and Lai (1997). For example, the equations for the displacements and stresses of an anisotropic elastic wedge developed by Ting (1986) could be used to derive eqn (5.4) by following Chen and Lai (1997).

Elastic field and electrical field are decoupled in the case of elastic composites or electrodes, thus the elasticity theory is separated from electrostatics. Polymer based composites are anisotropic and non-conducting materials, therefore, the elastic fields are obtained by setting the coefficients $b_{ij} = d_{ij} = 0$ in eqn (2.3). The general solutions for displacements are

$$u_r = \lambda \sum_{n=1}^4 B_n H'_{1n} r'^{\lambda-1}; \quad u_\theta = \lambda \sum_{n=1}^4 B_n H'_{2n} r'^{\lambda-1} \quad (5.5)$$

where $r'_n = r(\cos \theta + \mu'_n \sin \theta)$, B_n are arbitrary coefficients, and μ'_n ($n = 1, \dots, 4$) are the roots of the following equation,

$$a_{11}\mu_n'^4 - 2a_{13}\mu_n'^3 + (2a_{12} + a_{33})\mu_n'^2 - 2a_{23}\mu_n' + a_{22} = 0 \quad (5.6)$$

and

$$H'_{1n} = p'_n \cos \theta + q'_n \sin \theta; \quad H'_{2n} = -p'_n \sin \theta + q'_n \cos \theta \quad (5.7)$$

where

$$p'_n = a_{11}\mu_n'^2 + a_{12} - a_{13}\mu_n'; \quad q'_n = (a_{12}\mu_n'^2 + a_{22} - a_{23}\mu_n')/\mu_n'$$

Most conductors used in the adaptive structures are elastic isotropic. The electric field inside an ideal conductor is zero leading to a constant potential (Cheston, 1964). The general solutions for isotropic elasticity for the present class of problems are (Williams, 1952),

$$\begin{aligned} u_r &= \frac{r^{\lambda-1}}{2\mu_0(\lambda-1)} [C_1 \cos \lambda\theta - C_2 \sin \lambda\theta - C_3(\lambda-4k) \cos(2-\lambda)\theta - C_4(\lambda-4k) \sin(2-\lambda)\theta] \\ u_\theta &= \frac{r^{\lambda-1}}{2\mu_0(\lambda-1)} [-C_1 \sin \lambda\theta - C_2 \cos \lambda\theta + (2-\lambda-4k)(C_3 \sin(2-\lambda)\theta - C_4 \cos(2-\lambda)\theta)] \end{aligned} \quad (5.8)$$

Table 5.1: Admissible basic boundary conditions on edge surfaces.

case	Mechanical	Electric
1	traction free ($\sigma_{\theta\theta} = \sigma_{r\theta} = 0$)	electrically open ($D_\theta = 0$)
2	traction free ($\sigma_{\theta\theta} = \sigma_{r\theta} = 0$)	electrically closed ($\phi = 0$)
3	clamped ($u_r = u_\theta = 0$)	electrically open ($D_\theta = 0$)
4	clamped ($u_r = u_\theta = 0$)	electrically closed ($\phi = 0$)

where λ_0 and μ_0 are Lamé's constants, $k = (\lambda_0 + 2\mu_0)/2(\lambda_0 + \mu_0)$ and $C_n (n = 1, \dots, 4)$ are arbitrary coefficients.

Examination of the above general solutions for piezoelectrics, anisotropic composites and ideal conductors reveals that singular fields exist only if the real part of λ is less than two. Furthermore, the boundedness of displacement or electric potential at the corner of a wedge requires the real part of λ must be greater than one. Therefore, admissible values of λ are in the range of

$$1 < Re(\lambda) < 2 \quad (5.9)$$

5.2 Characteristic equations

In this section, the characteristic equations for composite wedges and junctions are established to determine the admissible values of λ . Consider a piezoelectric wedge as shown in Fig. 5.1. Possible boundary conditions on two radial edges are traction free ($\sigma_{\theta\theta} = \sigma_{r\theta} = 0$) or clamped ($u_r = u_\theta = 0$) combined with electrically open ($D_i n_i = 0$ or $D_\theta = 0$) or closed ($\phi = 0$ or $E_r = 0$). Electrically open case corresponds to an adjoining medium with zero (or negligible) dielectric constants (e.g. vacuum or air), whereas electrically closed case corresponds to an adjoining ideal conducting medium (Kuo and Barnett, 1991). As shown in Table 5.1, four basic types of boundary conditions can be considered for a boundary of a piezoelectric medium. The boundary conditions for an elastic medium are traction free ($\sigma_{\theta\theta} = \sigma_{r\theta} = 0$) or clamped ($u_r = u_\theta = 0$). The continuities of the tangential component of

the electric field and the normal component of the electric displacement are demanded at a piezoelectric material interface.

5.2.1 Piezoelectric wedges

There are altogether ten possible combinations of boundary conditions for the two edges of a piezoelectric wedge. For example, traction free and electrically open on both edges (Figure 5.1) yield

$$\sigma_{\theta\theta}(\alpha) = \sigma_{r\theta}(\alpha) = D_{\theta}(\alpha) = 0; \quad \sigma_{\theta\theta}(\varphi) = \sigma_{r\theta}(\varphi) = D_{\theta}(\varphi) = 0 \quad (5.10)$$

Using eqn (5.3) and eqn (5.10) or any other admissible boundary conditions, the following 6×6 homogeneous equation system can be established.

$$[K]\{A\} = \{0\} \quad (5.11)$$

where $\{A\} = \{A_1, A_2, \dots, A_6\}^T$ is the vector of unknown coefficients in eqn (5.3), $[K]$ is the coefficient matrix whose elements are functions of λ .

A non-trivial solution for eqn (5.11) exists if,

$$\det[K(\lambda)] = 0 \quad (5.12)$$

The determination of admissible values of λ from the above characteristic equation is usually done using a numerical algorithm although analytical solutions can be obtained for a few special cases as shown in a subsequent section.

5.2.2 Piezoelectrics – conductor/composite wedges and junctions

Referring to Figure 5.2, material 1 is assumed to be piezoelectric and material 2 an isotropic elastic ideal conductor. The following continuity conditions can be established at the material interface.

$$\begin{aligned} u_r^p(0) - u_r^e(0) &= 0; & u_{\theta}^p(0) - u_{\theta}^e(0) &= 0; & \phi^p(0) &= 0 \\ \sigma_{\theta\theta}^p(0) - \sigma_{\theta\theta}^e(0) &= 0; & \sigma_{r\theta}^p(0) - \sigma_{r\theta}^e(0) &= 0 \end{aligned} \quad (5.13)$$

where superscript p denotes a piezoelectric medium, and e denotes an elastic conductor. In addition, a set of admissible boundary conditions on the two outside edges has to be considered (Table 5.1). For example, the following boundary conditions can be considered on the two outer edges.

$$\sigma_{\theta\theta}^p(\varphi) = \sigma_{r\theta}^p(\varphi) = D_{\theta}^p(\varphi) = 0; \quad \sigma_{\theta\theta}^e(\alpha) = \sigma_{r\theta}^e(\alpha) = 0 \quad (5.14)$$

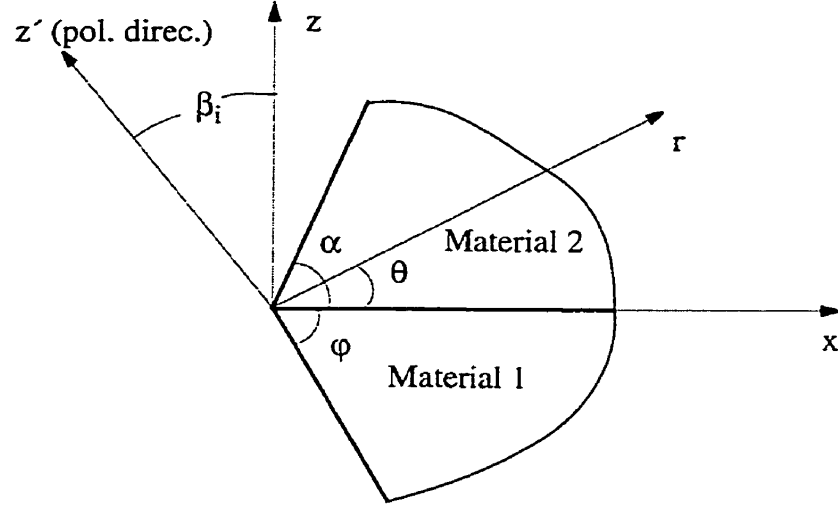


Figure 5.2: A bi-material system.

Substitution of eqns (5.3) and (5.8) in eqns (5.13) and (5.14) results in a homogeneous system of equations similar to eqn (5.11) for the ten coefficients $A_n (n = 1, 2, \dots, 6)$ and $C_n (n = 1, \dots, 4)$. The admissible values of λ is obtained from the corresponding characteristic equation. In the case of a bi-material junction, the eqn (5.14) is replaced by a set of interface conditions similar to eqn (5.13) corresponding to the other interface.

In the case of piezoelectric/elastic composite wedges and junctions, the condition $\phi^p = 0$ is replaced by $D_\theta^p = 0$ in eqn (5.13) to ensure that the bi-material interface is electrically impermeable.

5.2.3 Two piezoelectric material wedge

Consider the case of a wedge consisting of two piezoelectric materials as shown in Fig. 5.2. The two outer edges are assumed to be traction free and electrically impermeable. The interface and boundary conditions can be expressed as,

$$\begin{aligned}
 u_r^{p_1}(0) - u_r^{p_2}(0) &= 0; & u_\theta^{p_1}(0) - u_\theta^{p_2}(0) &= 0; & E_r^{p_1}(0) - E_r^{p_2}(0) &= 0; \\
 \sigma_{\theta\theta}^{p_1}(0) - \sigma_{\theta\theta}^{p_2}(0) &= 0; & \sigma_{r\theta}^{p_1}(0) - \sigma_{r\theta}^{p_2}(0) &= 0; & D_\theta^{p_1}(0) - D_\theta^{p_2}(0) &= 0 \\
 \sigma_{\theta\theta}^{p_1}(\varphi) &= 0; & \sigma_{r\theta}^{p_1}(\varphi) &= 0; & D_\theta^{p_1}(\varphi) &= 0 \\
 \sigma_{\theta\theta}^{p_2}(\alpha) &= 0; & \sigma_{r\theta}^{p_2}(\alpha) &= 0; & D_\theta^{p_2}(\alpha) &= 0
 \end{aligned} \tag{5.15}$$

where superscripts p_1 and p_2 denotes the piezoelectric medium one and two, respectively.

The substitution of eqn (5.3) in eqn (5.15) yields a system of homogeneous equations similar to eqn (5.11) for the twelve unknown coefficients $A_n^{p1}(n = 1, 2, \dots, 6)$ and $A_n^{p2}(n = 1, 2, \dots, 6)$. The admissible values of λ are obtained by solving the corresponding characteristic equation. The above methodology can be directly extended to consider piezoelectric bi-material junctions.

5.2.4 Multi-material system

The general procedure to determine the admissible values of λ for multi-material wedges and junctions is identical to the bi-material case except for the presence of more than one interface. The order of the final equation system [eqn (5.11)] is determined by the number and type (elastic, piezoelectric) of the materials. For example, in the case of a three-material wedge with one medium being piezoelectric and the rest elastic materials, a 14×14 homogeneous equation system is obtained.

5.3 Special cases of half plane and crack

The special cases of piezoelectric half planes and semi-infinite cracks are analytically examined in this section.

The geometry of a wedge is defined by two angles α and φ (Fig. 5.1). A half plane can be defined by $(\gamma, \gamma \pm \pi)$, and a semi-infinite crack by $(\gamma + \pi, \gamma - \pi)$, where the angle γ can be arbitrary. To study the effect of polarization orientation on the singularities of half planes and cracks, the angle β can be fixed while keeping γ arbitrary. β is set to zero without loss of generality. Eqn (5.3) can be rewritten in the matrix form as,

$$\mathbf{u}(\theta) = \lambda \sum_{n=1}^6 A_n \mathbf{h}$$

in Table 5.1, it is found that combinations 1-1, 2-2, 3-3 and 4-4 all result in the following characteristic equation.

$$\sin\lambda\pi = 0 \quad (5.17)$$

Apparently, no root of eqn (5.17) satisfies the requirement $1 < \text{Re}(\lambda) < 2$. Therefore, for piezoelectric half planes, no singularities are found for the homogeneous boundary conditions.

A semi-infinite crack $(\pi, -\pi)$ in a piezoelectric medium with a polarization angle 0° is considered without loss of generality. Consider four homogeneous boundary condition combinations of 1-1, 2-2, 3-3 and 4-4. They all lead to the following characteristic equation.

$$\sin 2\lambda\pi = 0 \quad (5.18)$$

Only one root, $\lambda = 1.5$, satisfies eqn (5.18) resulting in the classical inverse square root type singularity. Kuo and Barnett (1991) employed Stroh's formulation (1962) and obtained the same result for a semi-infinite crack in a piezoelectric medium.

Based on the results by Ting (1986) for general anisotropic elastic wedges, the above conclusions can also be drawn by following the correspondence between plane piezoelectricity and generalized plane strain in elasticity (Chen and Lai, 1997). In the case of free-clamped boundary condition combination for elastic wedges, Ting (1986) showed that, if δ is an order of singularity for a half plane, then $\delta/2$ and $(\delta - 1)/2$ are orders of singularities for a semi-infinite crack. It can be easily shown that this conclusion is also applicable to any admissible boundary condition combinations for piezoelectric half planes and semi-infinite cracks.

5.4 Numerical results and discussion

Two polarized piezoceramics, namely PZT-4 and PZT-5, graphite/epoxy composite, and two isotropic conductors, aluminum and nickel, are used in the numerical study. The material properties of PZT-4 and PZT-5 are given in the Appendix A, and the material properties of the composite and conductors are given below.

Aluminum (Young's modulus E and Poisson's ratio ν): $E = 68.9\text{GPa}$, $\nu = 0.25$

Nickel: $E = 210\text{GPa}$, $\nu = 0.31$

Graphite/epoxy composite (G is the shear modulus):

$$E_{xx} = 132.8\text{GPa}, \quad E_{zz} = 10.76\text{GPa}, \quad E_{yy} = 10.96\text{GPa}$$

$$G_{zy} = 3.61GPa, \quad G_{xy} = 5.65GPa, \quad G_{xz} = 5.65GPa$$

$$v_{xz} = 0.24, \quad v_{xy} = 0.24, \quad v_{zy} = 0.49$$

The characteristic equation for a wedge/junction is transcendental and has infinite number of roots. The root λ can be real or a complex quantity. Numerical experiments show that the roots are generally complex for composite systems and real roots exist for some cases of piezoelectric wedges. The order of electroelastic singularity is governed by the real part of $(\lambda - 2)$. The root of primary interest is the one with the smallest positive real part between one and two. The existence of a non-vanishing imaginary part of $(\lambda - 2)$ leads to oscillatory singularity (Suo, 1990). All roots meeting the requirement in eqn (11) are presented in the numerical study in order to present a complete picture of the nature of singularities in composite piezoelectric wedges/junctions. Plain strain conditions are assumed throughout the computations. A numerical procedure based on Müller's method (Müller, 1956) is used to search for admissible values of λ .

To verify the accuracy of the numerical procedure, the solutions for piezoelectric bi-material wedges are compared with those for isotropic bi-material wedges given by Hein and Erdogan (1971) through a limiting process. Referring to Figure 5.2, consider Material 1 and Material 2 as isotropic ideal elastic materials with Young's moduli $E_1/E_2 = 10/31$ and Poisson's ratios $v_1 = 0.22$, $v_2 = 0.30$. Hein and Erdogan (1971) presented the solutions for two wedges, *i.e.* $\alpha = -\varphi = 90^\circ$ and $\alpha = 90^\circ$, $\varphi = -180^\circ$. To simulate the above isotropic elastic bi-material wedges, set $s_{11} = 3.23 \times 10^{-1}m^2/N$, $s_{33} = 3.23 \times 10^{-1}m^2/N$, $s_{12} = -0.97 \times 10^{-1}m^2/N$, $s_{13} = -0.97 \times 10^{-1}m^2/N$, $s_{44} = 8.39 \times 10^{-1}m^2/N$ as elastic constants of Material 1; $s_{11} = 10 \times 10^{-1}m^2/N$, $s_{33} = 10 \times 10^{-1}m^2/N$, $s_{12} = -2.2 \times 10^{-1}m^2/N$, $s_{13} = -2.2 \times 10^{-1}m^2/N$, $s_{44} = 24.4 \times 10^{-1}m^2/N$ as elastic constants of Material 2. The piezoelectric constants g_{ij} of the two materials are set to negligible values ($g_{ij} \rightarrow 0$) in order to simulate ideal elastic behaviour. The solutions are compared in Table 5.2 and good agreement is observed.

5.4.1 Piezoelectric wedges

Consider a PZT-4 wedge with polarization direction along the z -axis ($\beta = 0$ in Fig. 5.1). Without loss of generality, set $\varphi = -\alpha$ in the numerical study. Figures 5.3a and 5.3b show the variation of the order of singularity with the wedge angle 2α for the homogeneous boundary condition combinations 1-1 and 4-4 in Table 5.1, respectively. It is found that all roots are real. The two cases considered have singularities only for reentrant wedges, *i.e.* wedge angles between 180° and 360° . Two roots exist for all wedge angles between 180° and

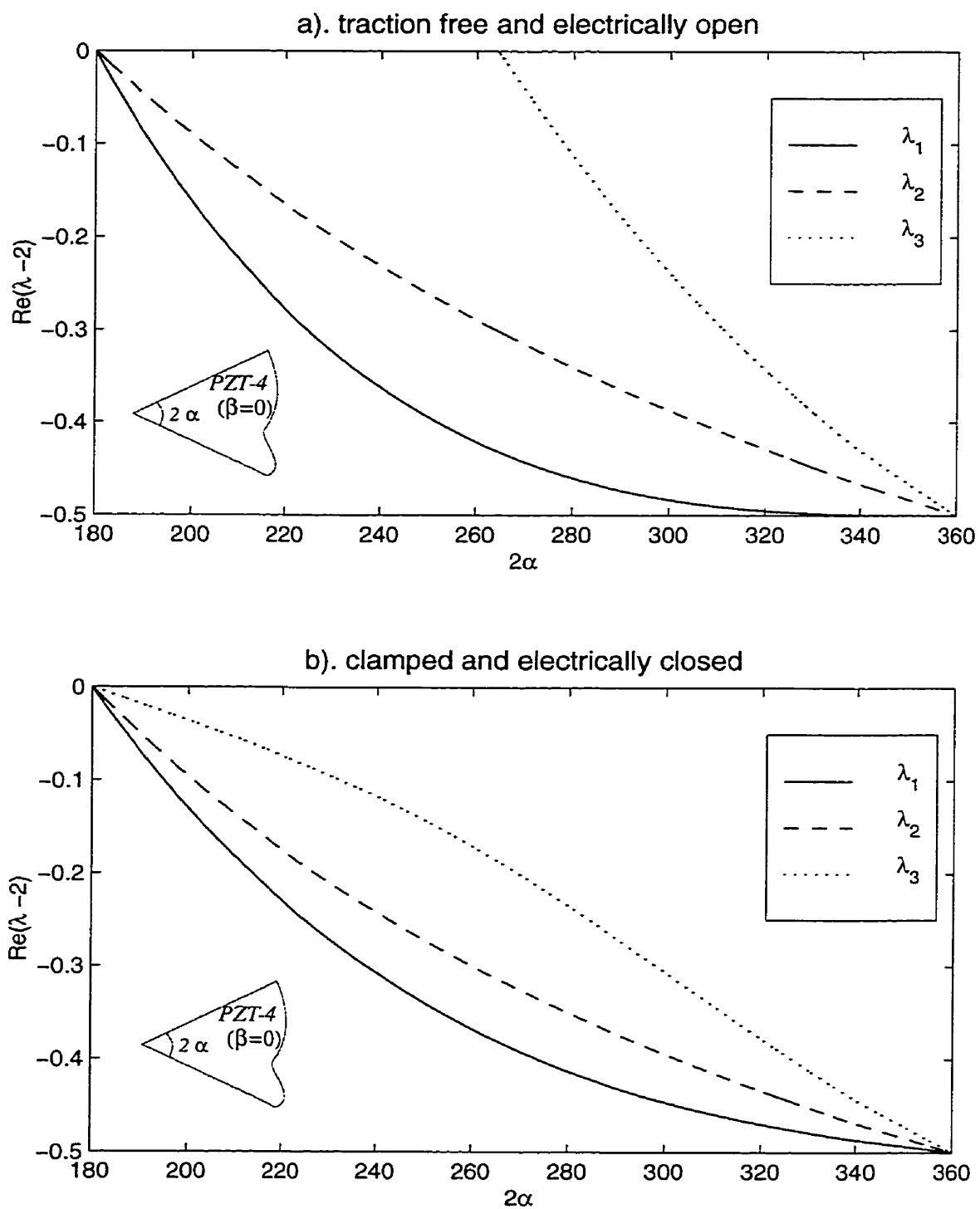


Figure 5.3: Variation of the order of singularity with the wedge angle.

Table 5.2: Comparison of roots λ for isotropic bi-material wedges (Figure 5.2).

Geometry	Present study	Hein & Erdogan (1971)
$\alpha = 90^\circ$ $\varphi = -90^\circ$	1.9494	1.949
	$2.8402 \pm 0.2801i$	$2.840 \pm 0.280i$
	$3.8056 \pm 0.8125i$	$3.800 \pm 0.800i$
	$4.8462 \pm 0.8687i$	$4.850 \pm 0.850i$
	$5.8450 \pm 1.1679i$	$5.900 \pm 1.150i$
$\alpha = 90^\circ$ $\varphi = -180^\circ$	1.6474	1.650
	1.9751	1.977
	$2.7332 \pm 0.2857i$	$2.733 \pm 0.286i$
	$3.0780 \pm 0.2225i$	$3.080 \pm 0.220i$
	$3.9988 \pm 0.1296i$	$4.000 \pm 0.130i$
	$4.8453 \pm 0.8707i$	$4.850 \pm 0.950i$
	$5.0015 \pm 0.1598i$	$5.000 \pm 0.130i$
	$5.9997 \pm 0.1384i$	$6.000 \pm 0.130i$
	1.6388, 2.3526	
	3.6474, 4.3526	
5.6474		

360° while a third root appears between 270° and 360° , and 180° and 360° for boundary condition combinations 1-1 and 4-4 respectively. An increase in the order of singularity is noted with increasing wedge angle. For the limiting case of a semi-infinite crack, two of the roots approach the classical value of -0.5. An investigation of wedges with mixed boundary conditions in Table 5.1 (e.g. 1-4) shows roots for wedge angles less than 180° , and the presence of more than three roots. According to the study of elastic wedges by Mantič *et al* (1997), there are in general two roots for traction free B.C. on both edge surfaces, while present study shows combinations 1-1, 2-2 and 1-2 have three roots. Therefore, piezoelectric wedges generally have one or more extra admissible roots compared to the corresponding elastic case.

Three special cases of wedges, namely a right angle ($2\alpha = 90^\circ$), a half plane ($2\alpha = 180^\circ$) and a semi-infinite crack ($2\alpha = 360^\circ$) are of interest in engineering. The eqn (5.12) is numerically unstable for $2\alpha = 360^\circ$, and $2\alpha = 359.99^\circ$ was used in the computations. Table 5.3 shows the order of singularities ($\lambda - 2$) corresponding to the ten possible boundary condition combinations based on Table 5.1. Numerical results agree with the analytical solution presented earlier for boundary condition combinations 1-1, 2-2, 3-3 and 4-4 for a

Table 5.3: Order of singularities for a right angle wedge, half plane and crack ($\beta = 0$).

B. C. combinations	special wedges		
	right angle	half plane	crack
1-1 (2-2, 3-3, 4-4)	/	/	-0.5000
1-2	-0.0731	-0.5000	-0.7500, -0.5000 -0.2500
1-3	-0.2176	$-0.5000 \pm 0.14395i$	-0.5000 $-0.7500 \pm 0.07197i$ $-0.2500 \pm 0.07197i$
1-4	-0.4855	-0.6261 -0.5000 -0.3739	-0.8131, -0.6869 -0.3131, -0.2500 -0.1869, -0.7500
2-3	-0.3445	-0.5000 $-0.5000 \pm 0.22991i$	-0.7500, -0.2500 $-0.7500 \pm 0.11495i$ $-0.2500 \pm 0.11495i$
2-4	-0.3442	$-0.5000 \pm 0.04309i$	-0.5000 $-0.7500 \pm 0.02154i$ $-0.2500 \pm 0.02154i$
3-4	-0.0416	-0.5000	-0.7500, -0.5000 -0.2500

half plane and a crack. The roots for half planes and cracks in Table 5.3 are valid for all possible polarization angles β in view of the earlier finding that roots are invariant with β . Table 5.3 also shows roots for mixed boundary conditions, such as those considered by Kuo and Barnett (1991), on the two edge surfaces. The order of singularity for semi-infinite cracks is stronger than the classical inverse square root singularity and oscillatory type singularities exist for mixed boundary conditions. In addition, up to six admissible roots may exist for some mixed boundary conditions. At least one of the singularities is of inverse square root type for half planes with mixed boundary conditions and oscillatory singularities exist for some cases. Note that the relation between columns 3 and 4 confirms the conclusion given earlier, *i.e.*, if δ is an order of singularity for a piezoelectric half plane, then $\delta/2$ and $(\delta - 1)/2$ are orders of singularities for a semi-infinite crack with identical boundary conditions. The comparison of results between boundary condition combinations in Table 5.3 indicates that electrical boundary conditions have a significant influence on the order of singularities. In the case of a right angle wedge, singularities exist only for mixed boundary conditions. One admissible root was found and the singularity is normally weaker than that corresponding to a half plane or a crack. No oscillatory type singularities are found.

Figures 5.4 and 5.5 show the effect of polarization orientation (β) on the order of singularities for PZT-4 wedges. In Fig. 5.4, the dependence of the order of singularity on β is examined for two wedge angles 240° , 300° under traction free and electrically open boundary conditions on both edges. Note under the assumed boundary conditions, singularities exist only for wedge angles greater than 180° . The singularities are identical for orientations β and $-\beta$ showing symmetry about $\beta = 0$. The singularity corresponding to $\beta = \pm 90^\circ$ is slightly stronger than that corresponding to $\beta = 0$ indicating a weak dependence on the polarization orientation. Oscillatory type singularities are not found. The results for right angle wedges ($2\alpha = 90^\circ$) with traction free boundary conditions on one edge surface, *i.e.* combinations 1-3, 1-4, 2-3 and 2-4 in Table 5.1, are shown in Figure 5.5. Oscillatory type singularities exist only in the case of combination 2-3. A strong dependence on the polarization orientation is observed for all boundary condition combinations except for 2-4 and the roots are symmetric about $\beta = 0^\circ$. The combination 1-4 shows two roots for $|\beta| > 45^\circ$ and the strongest or weakest singularity exists when the poling direction is along the z - or x -axis. An exception occurs for the combination 2-3 resulting in the weakest singularity for $\beta \simeq \pm 50^\circ$.

A study of PZT-5 wedges show that singularities follow trends similar to those in Figs.

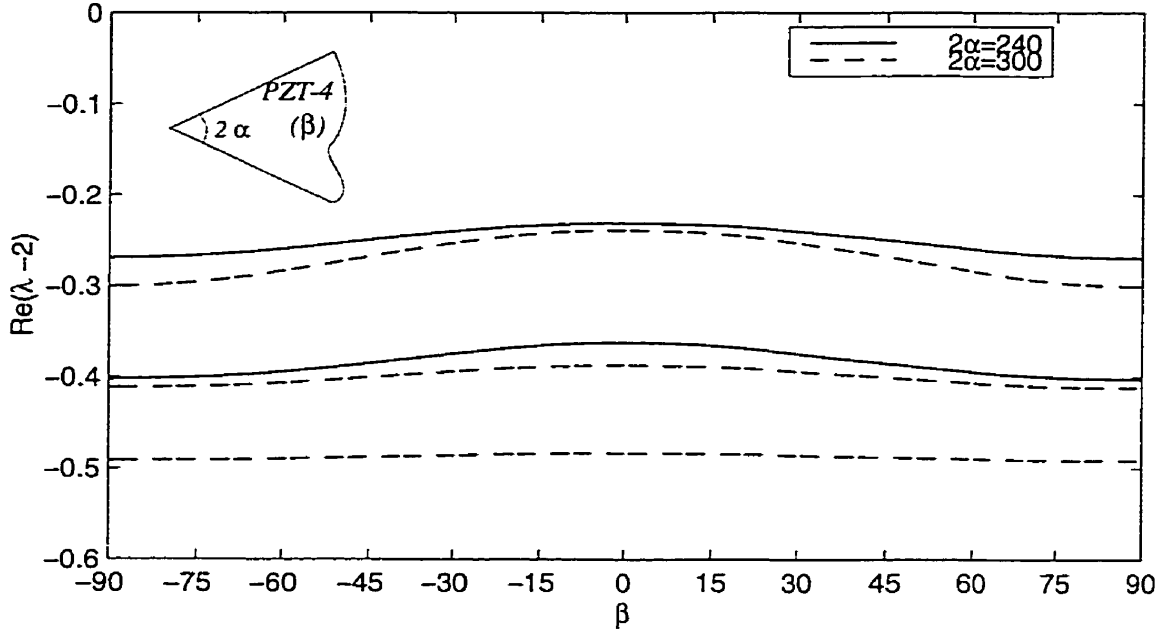


Figure 5.4: Variation of the order of singularity with the polarization angle for traction free and electrically open wedges.

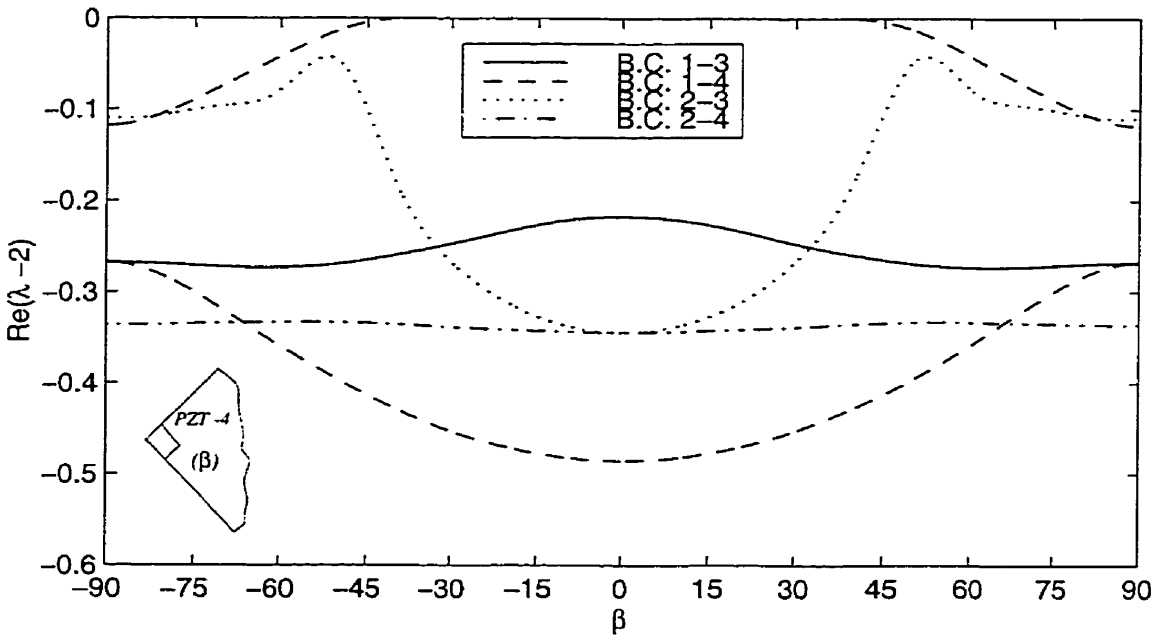


Figure 5.5: Variation of the order of singularity with the polarization angle for right angle wedges.

5.3-5.5 and Table 5.3, and the magnitude of roots are also nearly identical.

5.4.2 Piezoelectric – conductor wedges and junctions

The results for PZT-4 – aluminum/nickel wedges and junctions are presented in Figures 5.6 and 5.7. The first case considered (Fig. 5.6a) involves aluminum or nickel (treated as an ideal conductor) quarter plane bonded to a PZT-4 quarter plane. The edges of the PZT quarter planes are traction free and electrically open, and traction free for conductors. Interface conditions are given by eqn (5.13). The polarization orientation β is varied from 180° to -180° . Only one root is observed for aluminum and two for nickel. The singularity in nickel – PZT wedge is stronger than that in aluminum – PZT wedge. The latter system has a very weak singularity with less dependence on β . The influence of poling direction is more significant in the case of nickel – PZT wedges with $\beta = -45^\circ, 135^\circ$ showing the strongest singularities. In general, the singularity is weaker than the classical inverse square root singularity. An aluminum or nickel wedge bonded to a PZT-4 half plane is considered in Figure 5.6b. Setting polarization orientation angle $\beta = 0$, the effect of wedge angle α is investigated. Three roots exist for both nickel and aluminum, and the singularities become more severe as the wedge angle α increases. The case of an interface crack is obtained when $\alpha = 180^\circ$ and the singularity is found to be stronger than the classical inverse square root singularity for both bi-material systems.

A fully bonded PZT-4 – aluminum or nickel junction is considered in Figure 5.7a for varying angle α and three poling directions ($\beta = 0^\circ, 90^\circ, 180^\circ$). The results for $\beta = 0^\circ$ are identical to that for $\beta = 180^\circ$. No singularity exists when α is less than 180° for both aluminum and nickel. When α is larger than 180° , a very weak singularity is noted for aluminum – PZT system only for $\beta = 90^\circ$. The root corresponding to nickel – PZT system increases rapidly until α is closer to 240° for the three poling directions. An additional root for this system exists for α closer to 270° when $\beta = 90^\circ$. The singularities are weaker than the classical inverse square root singularity. Consider the same bi-material systems except that the interface defined by angle α is fully debonded and electrically open, as shown in Fig. 5.7b. Three roots are found for aluminum, and four for nickel. Singularities exists for all values of α considered and are more stronger for both nickel – PZT and aluminum – PZT systems when compared to the fully bonded case in Fig. 5.7a. The singularity is also stronger than the classical inverse square root singularity for most α in the case of nickel. Based on the results shown in Figs. 5.6 and 5.7, it can be concluded that aluminum-PZT systems have weaker singularities in most cases when compared to nickel-PZT systems. The

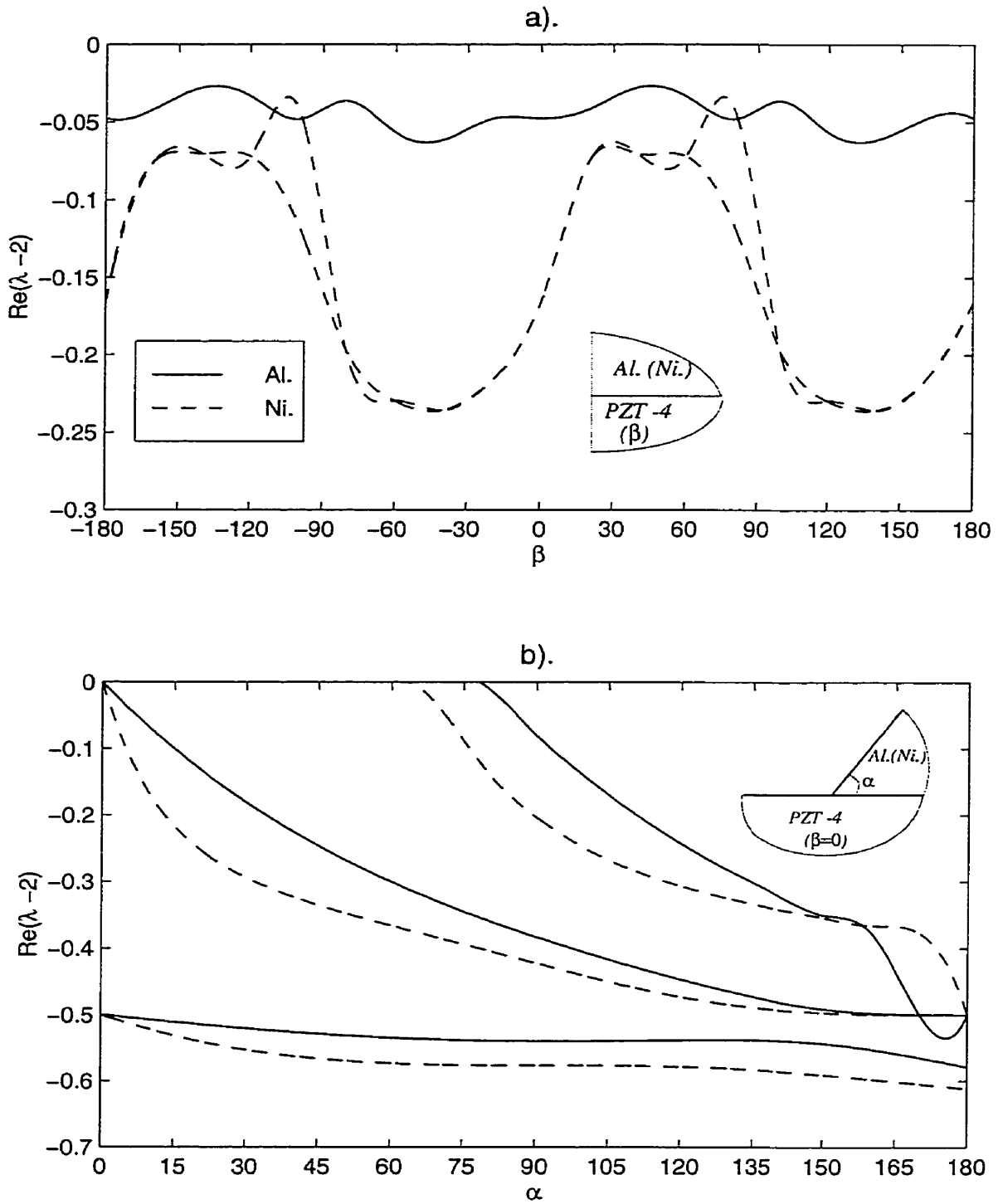


Figure 5.6: Variation of the order of singularity for PZT-4 - aluminum (nickel) wedges.

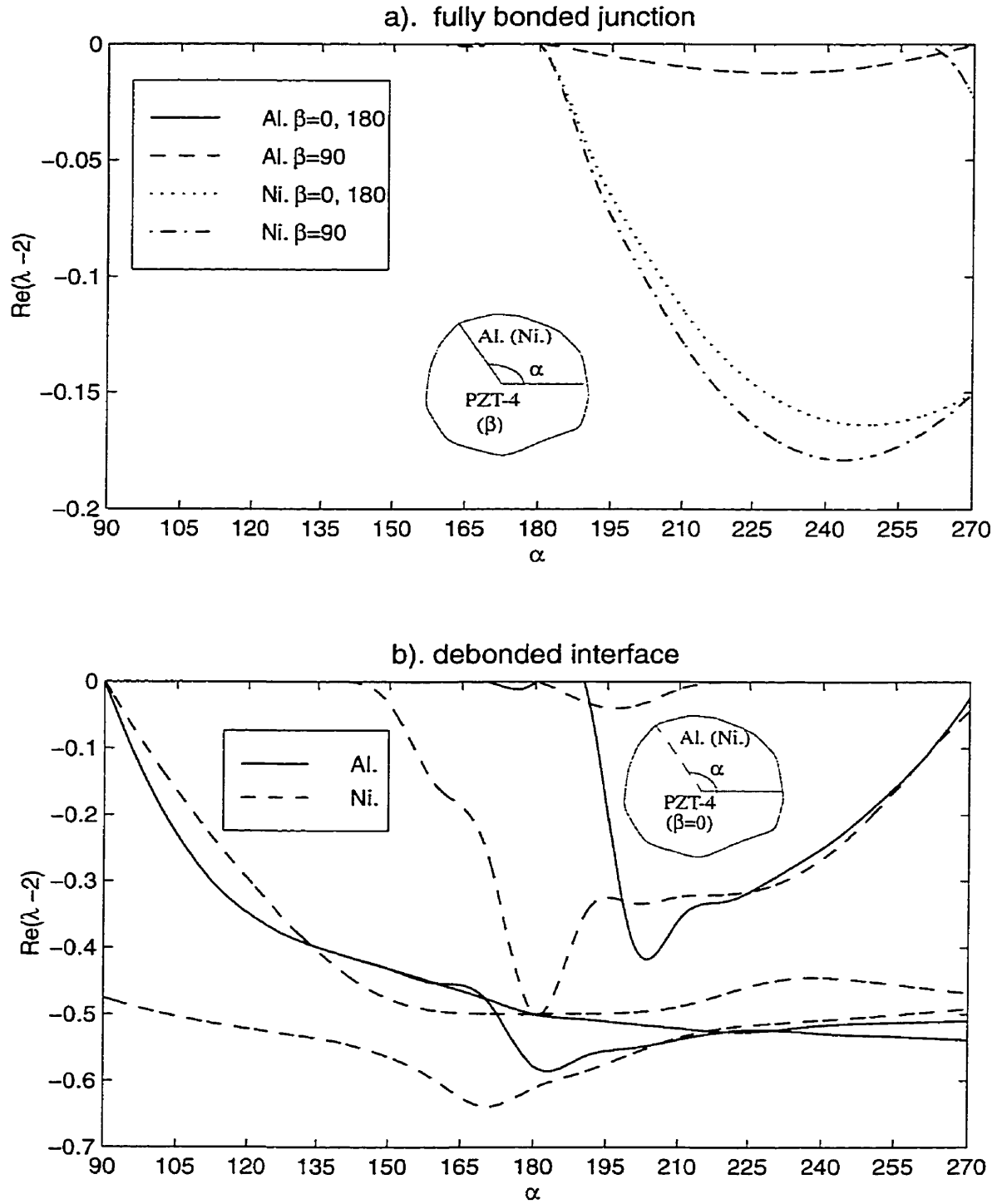


Figure 5.7: Variation of the order of singularity for PZT-4 – aluminum (nickel) junctions.

same systems are considered with electrically closed boundary conditions on the debonded interface and the results are found to follow trends quite similar to Fig. 5.7b with some difference in the magnitude.

5.4.3 Piezoelectric – graphite/epoxy wedges and junctions:

The roots of a PZT – Gr./Ep. wedge with traction free and electrically open outer edges are shown in Fig. 5.8a. The interface is fully bonded and electrically impermeable. The influence of wedge angle α on the order of singularity is investigated, while the polarization β is set to zero. Generally two roots exist with one over the full range of α , while another exists only for α larger than 80° . The singularities become stronger as the wedge angle α increases for both PZT-4 and PZT-5. The roots show negligible dependence on the type of piezoelectric material. The case of an interface crack between PZT and Gr./Ep. is obtained when $\alpha = 180^\circ$, and the singularity is identical to the classical inverse square root singularity. A piezoelectric-graphite/epoxy wedge similar to that shown in Fig. 5.6a is also considered and the singularities are found very weak (weaker than -0.06) for the range of β shown in Fig. 5.6a.

A completely bonded PZT – Gr./Ep. composite junction similar to that shown in Figure 5.7a is examined in the numerical study, no singularities are found for the considered range of α . A PZT – Gr/Ep. bi-material junction with a fully debonded and electrically impermeable interface is examined in Fig. 5.8b. The polarization of PZT is set to 0° with the debonded interface varied from 90° to 270° . Two roots exist for PZT-5 and three for PZT-4. The roots are symmetric about $\alpha = 180^\circ$ and show strong dependence on α . When α is 180° (interface crack), the classical inverse square root type singularity is observed for both piezoelectric materials. The nonexistence of singularities for a fully bonded bi-material junction and the presence of strong singularities for a debonded junction indicate the importance of interface conditions on the stress field near a sharp corner.

5.4.4 Piezoelectric bi-material systems:

Bi-material junctions involving PZT-4 and PZT-5 with a debonded interface defined by angle α are considered in Figure 5.9. Traction free and electrically open boundary conditions are assumed along the debonded interface and full continuity (mechanical and electrical) conditions are assumed on the other interface. The influence of α on the singularities is investigated for three different polarization orientations (β_1) of PZT-4 and for $\beta_2 = 0^\circ$. Three modes of singularities are generally observed and the significance of poling direction

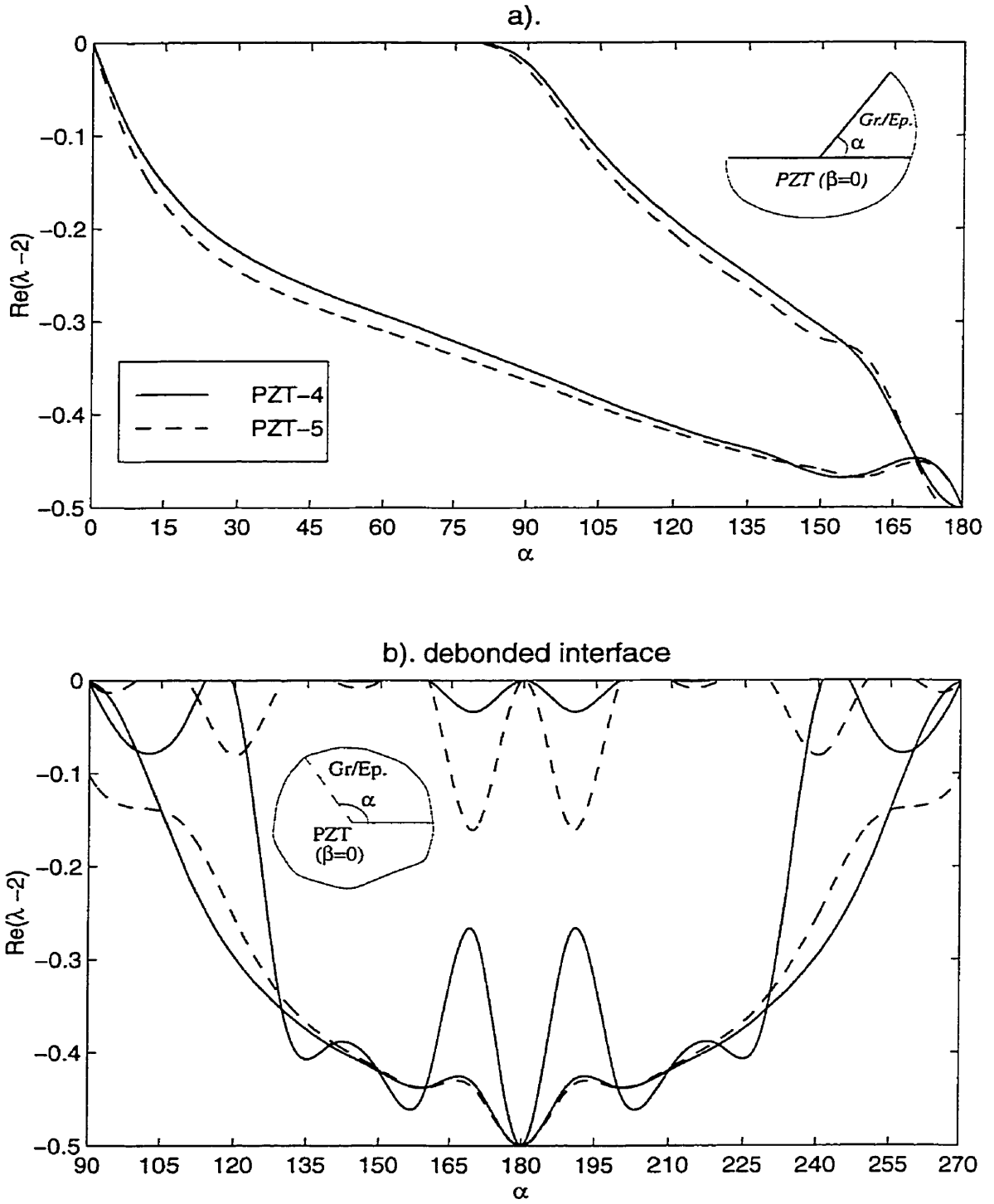


Figure 5.8: Variation of the order of singularity for PZT-4 – graphite/epoxy systems.

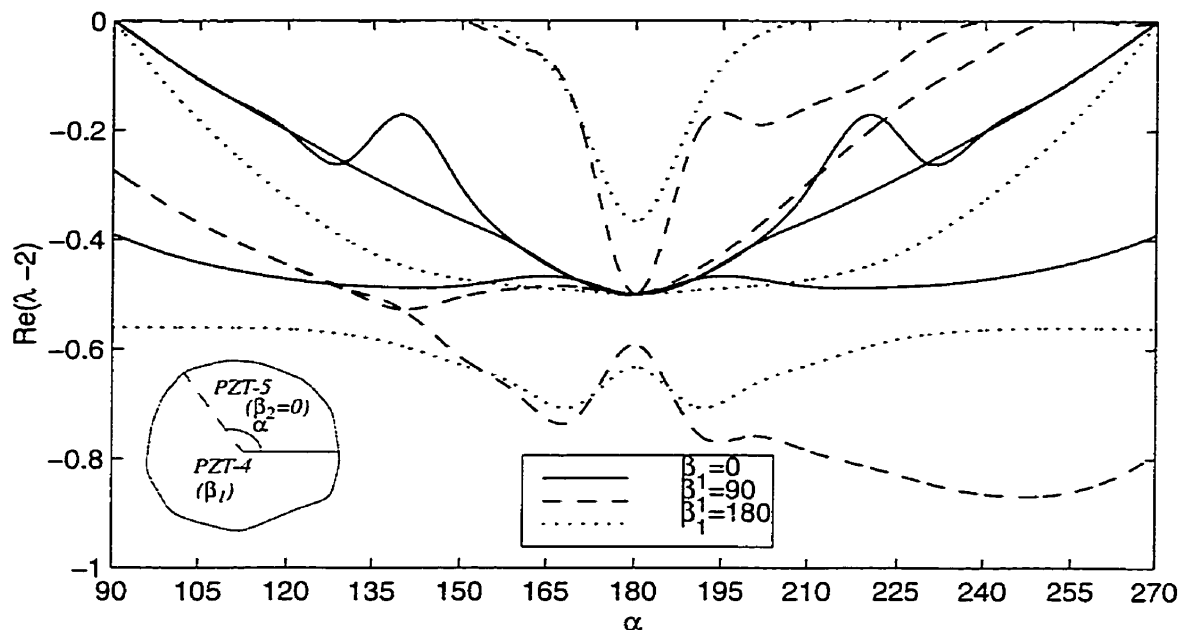


Figure 5.9: Variation of the order of singularity for PZT-4 – PZT-5 junctions with debonded interface.

β_1 is clearly noted. The singularities are stronger than any of the previously considered cases. It is also interesting to note that roots for $\beta_1 = 0^\circ$ are not identical for $\beta_1 = 180^\circ$. The strongest singularity is noted when the two materials are polarized perpendicular to each other and α is greater than 180° . The singularity is relatively weaker when the two materials are polarized in the same direction when compared to opposite directions. Furthermore, the singularities are symmetric about $\alpha = 180^\circ$ when the materials are polarized in the same or opposite directions. The present case can be considered as a general case of a horizontal bi-material crack considered by Kuo and Barnett (1991). It is seen from Fig. 5.9 that for a horizontal interface crack ($\alpha = 180^\circ$), the strongest singularity is obtained when the two piezoelectric materials are polarized in opposite directions. Therefore the polarization orientations of both materials have a significant influence on singular field near the tip of an interface crack between two piezoelectric materials. Other admissible homogeneous boundary conditions can be considered on the debonded interface and the results are not presented here for brevity.

5.4.5 Three material systems

Finally, the singularities in three dissimilar material systems, namely PZT, nickel and Gr./Ep. composite, are considered. Such material systems are encountered in adaptive structures, stack actuators, etc. The results are presented in Fig. 5.10 for two systems involving three materials. The direction of polarization is assumed to be along the z -axis. The system shown in Fig. 5.10a has a fully bonded interface between nickel and graphite/epoxy. Nickel – PZT and PZT – graphite/epoxy interfaces are both fully mechanically bonded, and electrically closed and impermeable respectively. A crack is assumed in PZT-4 along the plane measured by the angle α . The crack faces have traction free and electrically open boundary conditions. The numerical results show two to four roots depending on the angle α . The singularities are very strong. The singularities corresponding this system in the absence of a crack is also shown in Fig. 5.10a. Note the singularities become severe due to the presence of the crack. Figure 5.10b shows results for a similar system involving PZT-4, PZT-5 and nickel. The crack is assumed to exist in one of the piezoelectric materials and $\alpha = 180^\circ$ corresponds to a debonded interface between PZT-4 and PZT-5. Three roots are found for the debonded PZT-4/PZT-5 interface case. One to four roots exist when the crack is inside the piezoelectric medium depending on the angle α . Note the singularities are discontinuous across the interface of PZT-4 and PZT-5. Again, the singularities are very strong. In the case of fully bonded junction without a crack, the singularity is very weak (-0.0078), as shown in the Figure 5.10b.

5.5 Conclusions

A general method of obtaining electroelastic singularities in piezoelectric wedges and composite piezoelectric wedges/junctions is successfully developed by extending Williams' eigenfunction expansion for elastic solids. The formulation is valid for an arbitrary polarization orientation. The characteristic equation governing the order of singularity is transcendental and the Müller's numerical method (1956) can be used to determine the roots accurately.

Compared to the corresponding elastic cases, piezoelectric wedges generally have one or more extra admissible roots. Electric boundary conditions show a significant effect on the order of singularities. The singularities of piezoelectric half planes and semi-infinite cracks are found to be invariant with respect to the directions of polarization. The polarization orientation has a negligible influence on singularities of piezoelectric wedges with identical boundary conditions on both surfaces. However, for different boundary conditions on the

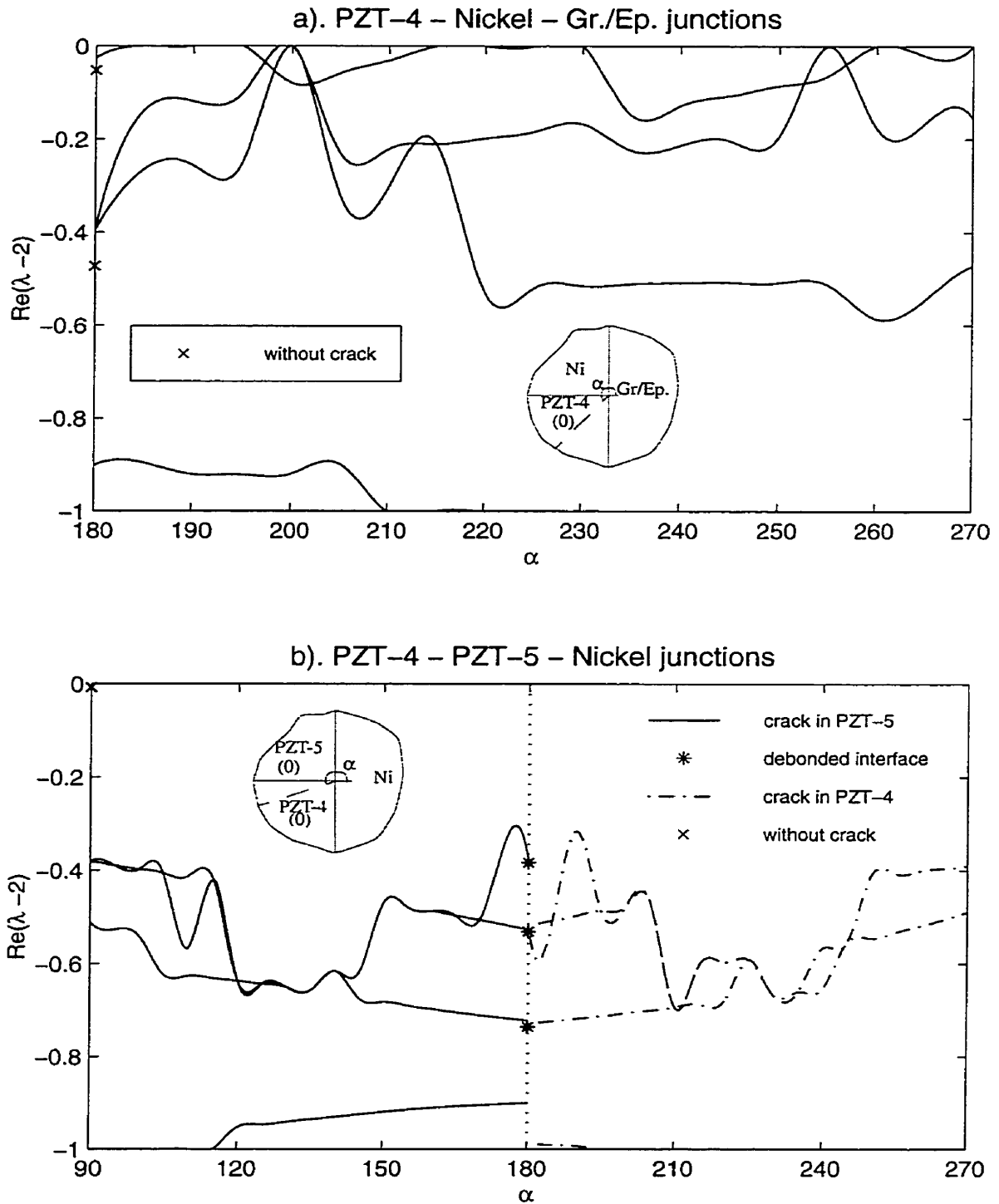


Figure 5.10: Variation of the order of singularity for three material systems with a crack in piezoelectrics.

edges, the order of singularities show strong dependence on the polarization angle.

The singularities are weaker for PZT – aluminum systems when compared to PZT – nickel systems. The strongest singularities of PZT – graphite/epoxy systems are -0.5, which corresponds to the case of a horizontal bi-material crack. Fully bonded PZT-graphite/epoxy junctions do not show any singularities. Bi-material systems of two piezoelectrics have stronger singularities that also depend significantly on the polarization direction. Two piezoelectrics polarized in the same or opposite directions show weaker singularities when compared to bi-material systems with polarizations perpendicular to each other. Three material systems with a crack inside a piezoelectric medium have singularities more stronger than the classical inverse square root singularity. The presence of a crack or a debonded interface result in a much severe singularity for both two and three material systems. The results presented in this Chapter are useful in material selection, optimum design and failure analysis of adaptive structures and piezoelectric actuators. The present results are also useful to the development of special finite and boundary elements for accurate simulation of electroelastic fields at crack tips and sharp corners.

Chapter 6

Conclusions and Recommendations

6.1 Major Findings

The main conclusions of this thesis are summarized in this Chapter. Separate detailed conclusions are given at the end of Chapters 2-5 based on the analysis and numerical results presented in those Chapters. Following are the major conclusions and findings of the present study.

1. The extended Lekhnitskii's formalism can be successfully applied to study piezoelectric plane problems with an arbitrarily oriented defect (elliptical void or crack). The analytical solutions for electroelastic field around an impermeable void and a permeable void can be derived in a remarkably compact form. By mathematically reducing an elliptical void to a crack, the analytical solutions for electroelastic field at the crack tip as well as fracture parameters can be obtained for impermeable and conducting cracks. The present results can be reduced to special cases of defect orientation reported previously, namely defects parallel or perpendicular to the direction of polarization.
2. It is found that the void orientation has a significant effect on the electroelastic field. The solutions for special cases, namely voids that are either parallel or perpendicular to the direction of polarization, cannot always be considered as the critical case. Numerical results indicate that the impermeable void model is applicable to most practical situations, whereas the more complex permeable void model (exact solution) should be used when the medium is subjected to electric loading and the void geometry ratio (b/a) is larger than 1000.
3. The orientation of a crack is found to have a negligible influence on the crack-tip

hoop stress under remote mechanical loading. However, a significant influence of crack orientation is observed under electrical loading or combined loading with larger electric to mechanical load ratio. Crack closure may happen depending on the direction of applied electric loading and the ratio of electric to mechanical loading. The influence of an applied electric displacement normal to an impermeable crack is analogous to that of an applied electric field tangential to a conducting crack.

For cracks containing air or vacuum in plane piezoelectric media, a unified formulation accounting for three existing electric boundary conditions, namely the impermeable crack model, the permeable crack model and the Hao & Shen type crack model, can be developed. The three types of cracks practically have identical response under pure mechanical loading. Under applied electric loading, the permeable crack model leads to the conclusion that electric loading has no influence on crack problems. The Hao & Shen type electric boundary conditions reduce to impermeable or permeable boundary conditions under practical situations. It is shown that the applicability of reducing the exact void solution to the exact crack solution is questionable. Such a reduction results in the solution for a permeable crack instead of a solution corresponding to the exact electric boundary condition for a crack as previously claimed by others.

4. The method of continuously distributed generalized dislocations and Lekhnitskii's complex potentials can be successfully applied for analysis of branched crack problems. The problems of an impermeable branched crack and an impermeable bifurcated crack can be reduced to the solution of a system of singular integral equations. It is found that branch closure may happen depending on branch length, branch angle and loading condition. The ranges of branch angles within which a branch is open are quite larger for mechanical loading than for electric loading. The length of a branch has negligible influence on branch closure under electric loading.

In the case of mechanical loading, a deviated branch plays a shielding effect on Mode I stress and electric displacement intensity factors, compared to self-similar crack extension. In the case of positive electric loading, a shielding effect is also observed for the electric displacement intensity factor. In general, the asymptotic electroelastic fields at the branch tip have a complex dependence on branch length, branch angle, crack orientation and the type of loading. The influence of applied electric loading is more complicated and significant than the influence of mechanical loading. The trends of field intensity factors of a symmetrically branched crack are similar to those of a single-branched crack, but a symmetrically branched crack has a narrower range

of branched angles within which the crack remains open. The numerical results for an asymmetrically branched crack indicate that, if a fracture criterion based on stress intensity factors is used, it is unlikely that the two branches can simultaneously grow when a bifurcated crack is subjected to remote tension.

5. A new stress-based criterion and two energy-based criteria, namely the criterion of modified hoop stress intensity factor, modified strain energy release rate and modified total energy release rate, are proposed to predict potential propagation of an impermeable crack. The salient features of proposed criteria are the consideration of fracture toughness anisotropy and removal of self-similar crack extension assumption. A simple model is developed to describe the fracture toughness anisotropy in piezoelectrics, based on available experimental results.

Numerical results show that distinctly different propagation directions are predicted if isotropic fracture toughness is used for both stress and energy based criteria. The modified hoop stress intensity factor and the modified strain energy release rate criteria indicate that a crack may branch off from a straight path even under symmetric loading and geometry, which qualitatively agrees with previously reported experimental findings. Under applied mechanical loading, the criteria of modified strain energy release rate and modified total energy release rate are virtually equivalent, and the two energy-based criteria and the stress-based criterion predict similar crack propagation paths. Under applied electrical loading, however, the predicted propagation paths by the stress-based criterion are significantly different from those by the energy-based criteria. Based on the criterion of strain energy release rate, a crack tends to branch off from a straight path regardless of the polarization angle. Under combined mechanical and electric loading, an electric field can either promote or retard crack propagation depending on the branching angle, the direction of polarization and the direction of applied electric field.

6. A general method of obtaining electroelastic singularities in piezoelectric wedges and composite piezoelectric wedges/junctions is successfully developed as a precursor to the analysis of fracture problems involving multi-material systems. Analytical solutions for piezoelectric half-planes and cracks can be obtained for some special boundary conditions. The solutions for general cases involving multi-material systems can be obtained numerically.

Piezoelectric wedges generally have one or more extra types of singularities, compared

to the corresponding elastic cases. Electric boundary conditions show a significant effect on the order of singularities. The singularities of piezoelectric half planes and semi-infinite cracks are found to be invariant with respect to the direction of polarization. The polarization orientation has a negligible influence on singularities of piezoelectric wedges with identical boundary conditions on both surfaces. However, for different boundary conditions on the edges, the order of singularities shows strong dependence on the polarization angle.

The singularities are weaker for PZT/aluminum wedges when compared to PZT/nickel wedges. A fully bonded PZT-graphite/epoxy junction does not show any singularity. Bi-material systems of two piezoelectrics have stronger singularities which also depend significantly on the polarization direction. Two piezoelectrics polarized in the same or opposite directions show weaker singularities when compared to bi-material systems with polarizations perpendicular to each other. The presence of a crack or a debonded interface results in a higher order singularity for two and three material systems.

6.2 Recommendations for future work

The following recommendations are made for future work.

1. Nonlinear effects associated with domain switching at the crack tip should be examined. The switched domains induce incompatible strain under the constraint of unswitched material, and consequently alter the stress distribution near the crack. The fracture toughness may vary considerably due to domain switching. The consideration of poly-domain systems in modelling is also important. Research in this direction may explain the basis for some conflicting views reported in the literature. Furthermore, the residual stresses, which are developed during the poling process, need to be considered.
2. Coordinated experimental studies are needed to understand the real electric boundary conditions on crack faces.
3. The exact nature of fracture toughness anisotropy should be determined. This requires both experimental studies and complementary theoretical work. The proposed fracture criteria should be experimentally validated.

Reference

- Azhdari, A. and Nemat-Nasser, S. (1996), Energy-release rate and crack kinking in anisotropic brittle solids, *Journal of the Mechanics and Physics of Solids*, 44, 929-951.
- Azhdari, A. and Nemat-Nasser, S. (1998), Experimental and computational study of fracturing in an anisotropic brittle solid, *Mechanics of Materials*, 28, 247-262.
- Barsoum, R.G.S. (1997), Active materials and adaptive structures. *Smart Materials and Structures*, 6, 117-122.
- Berlincourt, D. A., Curran, D. R. and Jaffe, H. (1964), Piezoelectric and piezoceramic materials and their function in transducers, *Physical Acoustics* (Edited by Mason, W. P., Vol. I-A.), Academic Press, New York.
- Bogy, D. B. (1968), Edge-bonded dissimilar orthogonal elastic wedge under normal and shear loading, *Transactions of the ASME, Journal of Applied Mechanics*, 35, 460-466.
- Bogy, D. B. (1970), On the problem of edge-bonded elastic quarter-plane loaded at the boundary, *International Journal of Solids and Structures*, 6, 1287-1313.
- Bottcher, C.J.F. (1973), *Theory of Electric Polarization*, Second edition, Vol. 1.
- Calderon-Moreno, J. M., Guiu, F., Meredith, M. and Reece, M. J. (1997), Fracture toughness anisotropy of PZT, *Materials Science and Engineering*, A234-236, 1062-1066.
- Chen, P. C. and Chopra, I. (1997), Hover testing of smart rotor with induced-strain actuation of blade twist, *AIAA*, 35, 6-16.
- Chen, T. and Lai, D. (1997), An exact correspondence between plane piezoelectricity and generalized plane strain in elasticity, *Proceeding of the Royal Society, London Series A*, 453, 2689-2713.
- Chen, W., Lupascu, D. and Lynch, C. S. (1999), Fracture behavior of ferroelectric ceramics, *Proceedings of SPIE, Conference of Smart Structures and Materials*, 3667, 145.

- Cheston, Warren B. (1964), *Elementary Theory of Electric and Magnetic Fields*, John Wiley & Sons, Inc.
- Deeg, W. F. (1980), The analysis of dislocation, crack and inclusion problems in piezoelectric solids, *Ph.D. Thesis*, Stanford University, USA.
- Delale, F. (1984), Stress singularities in bonded anisotropic materials, *International Journal of Solids and Structures*, 20, 31-40.
- Dempsey, J. P. and Sinclair, G. B. (1979), On the stress singular behaviour at the vertex of a bi-material wedge, *Journal of Elasticity*, 9, 373-391.
- Dunn, M.L. (1994), The effects of crack face boundary conditions on the fracture mechanics of piezoelectric solids. *Engng. Frac. Mech.*, 48, 25-39.
- Gao, C.-F. and Fan, W.-X. (1999), Exact solutions for the plane problem in piezoelectric materials with an elliptic or a crack, *International Journal of Solids and Structures*, 36, 2527-2540.
- Gerasoulis, A. (1982), The use of piecewise quadratic polynomials for the solution of singular integral equations of Cauchy type, *Computational Mathematics with Applications*, 8, 15.
- Gross, D. (1982), Spannungintensitätsfaktoren von ribsystemen (stress intensity factor of systems of cracks), *Ing Arch*, 51, 301-310.
- Hao, T.-H. and Shen, Z.-Y. (1994), A new electric boundary condition of electric fracture mechanics and its applications, *Engineering Fracture Mechanics*, 47, 793-802.
- Hein, V. L. and Erdogan, F. (1971), Stress singularities in a two-material wedge, *International Journal of Fracture*, 7, 317-330.
- Hill, L. S. (1997), Three-dimensional piezoelectric boundary elements, *Ph.D. Thesis*, Purdue University, USA.
- Irwin, G. R. (1957), Analysis of stresses and strains near the end of a crack traversing a plate, *Journal of Applied Mechanics*, 24, 361-364.
- Jain, A. K. and Sirkis, J. S. (1994), Continuum Damage Mechanics in Piezoelectric Ceramics, *ASME 1994 International Mechanical Engineering Congress and Exposition, Chicago, Illinois*, 47-58.
- Kamada, T., Fujita, T., Hatayama, T., Arikabe, T., Murai, N., Aizawa, S and Tohyama, K. (1997), Active vibration control of frame structures with smart structures using piezoelectric actuators: Vibration control by control of bending moments of columns, *Smart Mat Struct*,

6, 448-456.

Karihaloo, B. L. and Anderson, J. H. (1998), Two practical applications of crack kinking, *Mechanics of Materials*, 28, 263-270.

Kumar, S. and Singh, R. N. (1996), Crack propagation in piezoelectric materials under combined mechanical and electrical loadings, *Acta Materialia*, 44, 173-200.

Kumar, S. and Singh, R. N. (1997a), Energy release rate and crack propagation in piezoelectric materials. Part I: mechanical/electrical load, *Acta Materialia*, 45, 849-857.

Kumar, S. and Singh, R. N. (1997b), Energy release rate and crack propagation in piezoelectric materials. Part II: combined mechanical and electrical loads, *Acta Materialia*, 45, 859-868.

Kuo, C. M. and Barnett, D. M. (1991), Stress singularities of interfacial cracks in bonded piezoelectric half-spaces, *Modern Theory of Anisotropic Elasticity and Applications* (Edited by Wu, J. J., Ting, T. C. T. and Barnett, D. M., SIAM, Philadelphia, 33-50.

Lekhnitskii, S.G. (1963), *Theory of Elasticity of an Anisotropic Elastic Body*, Holden-Day, New York.

Lynch, C. S., Yang, W., Collier, L., Suo, Z. and McMeeking, R. M. (1995), Electric field induced cracking in ferroelectric ceramics, *Ferroelectrics*, 166, 11-30.

Mantič, V. , París, F. and Cañas, J. (1997), Stress singularities in 2D orthotropic corners, *International Journal of Fracture*, 83, 67-90.

McHenry, K.D. and Koepke, B.G. (1983), Electric fields effects on subcritical crack growth in PZT-4. In *Fracture Mechanics of Ceramics*, (Edited by R.C. Bradt, D.P. Hasselman and F.F. Lange), Vol. 5, 337-352.

Mikhailov, G.K. and Parton, V.Z. (1990), *Electromagnetoelasticity*, Hemisphere, New York.

Miller, G. R. and Stock, W. L. (1989), Analysis of branched interface cracks between dissimilar anisotropic media, *Journal of Applied Mechanics*, 56, 844-849.

Müller, D. E. (1956), A method for solving algebraic equations using an automatic computer, *Mathematical Tables and Aids to Computation*, 10, 208-215.

Nemat-Nasser, S. and Hori, M. (1993), *Micromechanics: overall properties of heterogeneous materials*, North-Holland.

Obata, M., Nemat-Nasser, S. and Goto, Y. (1989), Branched cracks in anisotropic elastic

- solids, *J. Appl. Mech.*, 56, 858-864.
- Pak, Y.E. (1990), Crack extension force in a piezoelectric material, *J. Appl. Mech.*, 57, 647-653.
- Pak, Y. E. (1992), Linear electro-elastic fracture mechanics of piezoelectric materials, *International Journal of Fracture*, 54, 79-100.
- Park, S. B. and Carman, G. P. (1997), Tailoring the properties of piezoelectric ceramics: analytical, *International Journal of Solids and Structures*, 34, 3385-3399.
- Park, S. B.; Park, S. S.; Carman, G. P.; Hahn, H. T. (1998), Measuring strain distribution during mesoscopic domain reorientation in ferroelectric material, *Journal of Engineering Materials and Technology, Transactions of ASME*, 120, 1-6.
- Park, S. B. and Sun, C. T. (1995a), Effect of electric fields on fracture of piezoelectric ceramics, *International Journal of Fracture*, 70, 203-216.
- Park, S. B. and Sun, C. T. (1995b), Fracture criteria for piezoelectric ceramics, *Journal of the American Ceramic Society*, 78, 1475-1480. And correction (1996).
- Parton, V.Z. (1976). Fracture mechanics of piezoelectric materials, *Acta Astronaut.*, 3, 671-683.
- Parton, V.Z. and Kudryavtsev, B.A. (1988), *Electromagnetoelasticity*, Gordon and Breach Science Publishers, New York.
- Pisarenko, G.G., Chushko, V.M. and Kovalev, S. P. (1985), *Journal of the American Ceramic Society*, 68, 259.
- Polovinkina, I.B. and Ulitko, A.F. (1978), On the equilibrium of piezoceramic bodies containing cracks, *TN*, 18, 10-17.
- Rao, S. S. and Sunar, M. (1994), Piezoelectricity and its use in disturbance sensing and control of flexible structures: A survey, *Applied Mechanics Review*, 47, 113-123.
- Schmidt, I. and Gross, D. (1997), Equilibrium shape of an elastically inhomogeneous inclusion, *Journal of the Mechanics and Physics of Solids*, 45, 1521-1549.
- Seelig, Th. and Gross, D. (1997), Analysis of dynamic crack propagation using a time-domain boundary integral equation method, *International Journal of Solids and Structures*, 34, 2087-2103.
- Singh, R. N. and Wang, H. (1995), *Adaptive Materials Systems*, ed. G. P. Carman, C. Lynch

- and N. R. Scottos, Proc. of AMD-vol. 206/MD-vol. 58, ASME, 85-95.
- Sosa, H. A. and Pak, Y. E. (1990), Three-dimensional eigenfunction analysis of a crack in a piezoelectric material, *International Journal of Solids and Structures*, 26, 1-15.
- Sosa, H. A. (1991), Plane problems in piezoelectric media with defects, *International Journal of Solids and Structures*, 28, 491-505.
- Sosa, H. A. (1992), On the fracture mechanics of piezoelectric solids, *International Journal of Solids and Structures*, 28, 2613-2622.
- Sosa, H. and Khutoryansky, N. (1996), New developments concerning piezoelectric materials with defects, *International Journal of Solids and Structures*, 33, 3399-3414.
- Stroh, A. N. (1962), Steady state problems in anisotropic elasticity, *Journal of Mathematics and Physics*, 41, 77-103.
- Sunar, M. and Rao, S. S. (1999), Recent advances in sensing and control of flexible structures via piezoelectric materials technology, *Appl Mech Rev*, 52, 1-16.
- Suo, Z. (1990), Singularities, interfaces and cracks in dissimilar anisotropic media, *Proceeding of the Royal Society, London Series A*, 427, 331-358.
- Suo, Z., Kuo, C. M., Barnett, D. M. and Willis, J. R. (1992), Fracture mechanics for piezoelectric ceramics, *Journal of the Mechanics and Physics of Solids*, 40, 739-765.
- Tani, J., Takagi, T. and Qiu, J. (1998), Intelligent material systems: Application of function materials, *Appl Mech Rev*, 51, 505-521.
- Theocaris, P. S. (1972), Complex stress-intensity factors at bifurcated cracks, *Journal of Applied Mathematics and Physics*, 20, 265-279.
- Theocaris, P. S. and Ioakimidis, N. (1976), The symmetrically branched crack in an infinite elastic medium, *Journal of Applied Mathematics and Physics*, 27, 801-814.
- Ting, T. C. T. (1986), Explicit solution and invariance of the singularities at an interface crack in anisotropic composites, *International Journal of Solids and Structures*, 22, 965-983.
- Williams, M.L. (1952), Stress singularities resulting from various boundary conditions in angular corners of plates in extension, *Transactions of the ASME, Journal of Applied Mechanics*, 19, 526-528.
- Williams, M.L. (1956), The complex-variable approach to stress singularities-II, *Transactions of the ASME, Journal of Applied Mechanics*, 23, 477-478.

- Xu, X.-L. and Rajapakse, R.K.N.D. (1998), Boundary element analysis of piezoelectric solids with defects, *Composites B*, 29, 655-669.
- Zhang, Ch. and Gross, D. (1994), Ductile crack analysis by a cohesive damage zone model, *Engineering Fracture Mechanics* 47, 237-248.
- Zhang, T.-Y., Qian, C.-F. and Tong, P. (1998), Linear electro-elastic analysis of a cavity or a crack in a piezoelectric material, *International Journal of Solids and Structures*, 35, 2121-2149.
- Zhang, T.-Y. and Tong, P. (1996), Fracture mechanics for a mode III crack in a piezoelectric material, *International Journal of Solids and Structures*, 33, 343-359.
- Zhu, T. and Yang, W. (1999), Crack kinking in a piezoelectric solid, *International Journal of Solids and Structures*, 36, 5013-5027.

Appendix A

Material properties

The properties of three piezoceramics, namely PZT-4 (PZT-4a and PZT-4b), PZT-5 and PZT-5H, used in this thesis are given here. PZT-4a and PZT-5H are used in Chapters 2-4, and their properties are given in the form of eqn (2.2). PZT-4b and PZT-5 are used in Chapter 5, and their properties are given in the form of eqn (2.1). Note that PZT-4a and PZT-4b are from different sources, and their properties are slightly different.

PZT-4a (Park and Sun, 1995b):

$$\begin{aligned}c_{11} &= 13.9 \times 10^{10} N/m^2, & c_{12} &= 7.78 \times 10^{10} N/m^2, & c_{13} &= 7.43 \times 10^{10} N/m^2 \\c_{33} &= 11.3 \times 10^{10} N/m^2, & c_{44} &= 2.56 \times 10^{10} N/m^2 \\e_{31} &= -6.98 C/m^2, & e_{33} &= 13.84 C/m^2, & e_{15} &= 13.44 C/m^2 \\ \epsilon_{11} &= 6.00 \times 10^{-9} CV/m, & \epsilon_{33} &= 5.47 \times 10^{-9} CV/m\end{aligned}$$

PZT-4b (Berlincourt *et al*, 1964):

$$\begin{aligned}s_{11} &= 10.9 \times 10^{-12} m^2/N, & s_{33} &= 7.90 \times 10^{-12} m^2/N, & s_{12} &= -5.42 \times 10^{-12} m^2/N \\s_{13} &= -2.10 \times 10^{-12} m^2/N, & s_{44} &= 19.3 \times 10^{-12} m^2/N \\g_{31} &= -11.1 \times 10^{-3} Vm/N, & g_{33} &= 26.1 \times 10^{-3} Vm/N, & g_{15} &= 39.4 \times 10^{-3} Vm/N \\ \beta_{11} &= 7.66 \times 10^7 V^2/N, & \beta_{33} &= 8.69 \times 10^7 V^2/N\end{aligned}$$

PZT-5 (Berlincourt *et al*, 1964):

$$\begin{aligned}s_{11} &= 14.4 \times 10^{-12} m^2/N, & s_{33} &= 9.46 \times 10^{-12} m^2/N, & s_{12} &= -7.71 \times 10^{-12} m^2/N \\s_{13} &= -2.98 \times 10^{-12} m^2/N, & s_{44} &= 25.2 \times 10^{-12} m^2/N \\g_{31} &= -11.4 \times 10^{-3} Vm/N, & g_{33} &= 24.8 \times 10^{-3} Vm/N, & g_{15} &= 38.2 \times 10^{-3} Vm/N \\ \beta_{11} &= 6.53 \times 10^7 V^2/N, & \beta_{33} &= 6.65 \times 10^7 V^2/N\end{aligned}$$

PZT-5H (Pak, 1992):

$$c_{11} = 12.6 \times 10^{10} N/m^2, \quad c_{12} = 5.5 \times 10^{10} N/m^2, \quad c_{13} = 5.3 \times 10^{10} N/m^2$$

$$c_{33} = 11.7 \times 10^{10} N/m^2, \quad c_{44} = 3.53 \times 10^{10} N/m^2$$

$$e_{31} = -6.5 C/m^2, \quad e_{33} = 23.3 C/m^2, \quad e_{15} = 17.0 C/m^2$$

$$\epsilon_{11} = 151 \times 10^{-10} CV/m, \quad \epsilon_{33} = 130 \times 10^{-10} CV/m$$

Appendix B

Constants Associated with Branched Cracks

The constants k_{ni} ($n, i = 1, 2, 3$) appearing in eqn (3.3) are

$$\begin{aligned} k_{11} &= \frac{g_{22}g_{33} - g_{23}g_{32}}{\Delta_2}; & k_{12} &= \frac{g_{12}g_{33} - g_{13}g_{32}}{-\Delta_2}; & k_{13} &= \frac{g_{12}g_{23} - g_{22}g_{13}}{\Delta_2} \\ k_{21} &= \frac{g_{21}g_{33} - g_{31}g_{23}}{-\Delta_2}; & k_{22} &= \frac{g_{11}g_{33} - g_{31}g_{13}}{\Delta_2}; & k_{23} &= \frac{g_{11}g_{23} - g_{21}g_{13}}{-\Delta_2} \\ k_{31} &= \frac{g_{21}g_{32} - g_{31}g_{22}}{\Delta_2}; & k_{32} &= \frac{g_{11}g_{32} - g_{31}g_{12}}{-\Delta_2}; & k_{33} &= \frac{g_{11}g_{22} - g_{12}g_{21}}{\Delta_2} \end{aligned} \quad (\text{B.1})$$

where

$$g_{1n} = p_n + \bar{p}_i f_{in}; \quad g_{2n} = q_n + \bar{q}_i f_{in}; \quad g_{3n} = s_n + \bar{s}_i f_{in} \quad (\text{B.2})$$

$$\Delta_2 = g_{11}(g_{22}g_{33} - g_{23}g_{32}) - g_{12}(g_{21}g_{33} - g_{23}g_{31}) + g_{13}(g_{21}g_{32} - g_{22}g_{31}) \quad (\text{B.3})$$

$$f_{1n} = (\bar{\mu}_3 \bar{\delta}_2 - \bar{\mu}_2 \bar{\delta}_3 + \mu_n \bar{\delta}_3 - \mu_n \bar{\delta}_2 - \delta_n \bar{\mu}_3 + \delta_n \bar{\mu}_2) / \Delta_1$$

$$f_{2n} = (\bar{\mu}_1 \bar{\delta}_3 - \bar{\mu}_3 \bar{\delta}_1 - \mu_n \bar{\delta}_3 + \mu_n \bar{\delta}_1 - \delta_n \bar{\mu}_1 + \delta_n \bar{\mu}_3) / \Delta_1$$

$$f_{3n} = (\bar{\mu}_2 \bar{\delta}_1 - \bar{\mu}_1 \bar{\delta}_2 - \mu_n \bar{\delta}_1 + \mu_n \bar{\delta}_2 - \delta_n \bar{\mu}_2 + \delta_n \bar{\mu}_1) / \Delta_1 \quad (\text{B.4})$$

$$\Delta_1 = \bar{\mu}_1(\bar{\delta}_2 - \bar{\delta}_3) + \bar{\mu}_2(\bar{\delta}_3 - \bar{\delta}_1) + \bar{\mu}_3(\bar{\delta}_1 - \bar{\delta}_2) \quad (\text{B.5})$$

and an overbar denotes the complex conjugate of a complex-valued quantity.

The constants q_{ij} ($i, j = 1, 2, 3$) appearing in eqn (3.8) are

$$\begin{aligned} q_{11} &= \frac{s_{22}s_{33} - s_{23}s_{32}}{\Delta_3}; & q_{12} &= \frac{s_{12}s_{33} - s_{13}s_{32}}{-\Delta_3}; & q_{13} &= \frac{s_{12}s_{23} - s_{22}s_{13}}{\Delta_3} \\ q_{21} &= \frac{s_{21}s_{33} - s_{31}s_{23}}{-\Delta_3}; & q_{22} &= \frac{s_{11}s_{33} - s_{13}s_{31}}{\Delta_3}; & q_{23} &= \frac{s_{11}s_{23} - s_{21}s_{13}}{-\Delta_3} \\ q_{31} &= \frac{s_{21}s_{32} - s_{31}s_{22}}{\Delta_3}; & q_{32} &= \frac{s_{11}s_{32} - s_{12}s_{31}}{-\Delta_3}; & q_{33} &= \frac{s_{11}s_{22} - s_{12}s_{21}}{\Delta_3} \end{aligned} \quad (\text{B.6})$$

where

$$s_{1j} = \text{Im} \sum_{n=1}^3 k_{nj}; \quad s_{2j} = -\text{Im} \sum_{n=1}^3 \mu_n k_{nj}; \quad s_{3j} = -\text{Im} \sum_{n=1}^3 \delta_n k_{nj} \quad (\text{B.7})$$

$$\Delta_3 = s_{11}(s_{22}s_{33} - s_{23}s_{32}) - s_{12}(s_{21}s_{33} - s_{23}s_{31}) + s_{13}(s_{21}s_{32} - s_{22}s_{31}) \quad (\text{B.8})$$

The constants J_{ij} ($i, j = 1, 2, 3$) in eqn (3.21) are

$$\begin{aligned} J_{11} &= \frac{h_{22}h_{33} - h_{23}h_{32}}{\Delta_4}; & J_{12} &= \frac{h_{12}h_{33} - h_{13}h_{32}}{-\Delta_4}; & J_{13} &= \frac{h_{12}h_{23} - h_{22}h_{13}}{\Delta_4} \\ J_{21} &= \frac{h_{21}h_{33} - h_{31}h_{23}}{-\Delta_4}; & J_{22} &= \frac{h_{11}h_{33} - h_{13}h_{31}}{\Delta_4}; & J_{23} &= \frac{h_{11}h_{23} - h_{21}h_{13}}{-\Delta_4} \\ J_{31} &= \frac{h_{21}h_{32} - h_{31}h_{22}}{\Delta_4}; & J_{32} &= \frac{h_{11}h_{32} - h_{12}h_{31}}{-\Delta_4}; & J_{33} &= \frac{h_{11}h_{22} - h_{12}h_{21}}{\Delta_4} \end{aligned} \quad (\text{B.9})$$

where

$$h_{1j} = s_{1j}; \quad h_{2j} = -s_{2j}; \quad h_{3j} = -s_{3j} \quad (\text{B.10})$$

$$\Delta_4 = h_{11}(h_{22}h_{33} - h_{23}h_{32}) - h_{12}(h_{21}h_{33} - h_{23}h_{31}) + h_{13}(h_{21}h_{32} - h_{22}h_{31}) \quad (\text{B.11})$$